DOCTORAL THESIS

Theory of edge induced quantum critical phenomena in strongly correlated system

強相関電子系における 表面誘起量子臨界現象の理論

February 16 2022

Department of Physics, Nagoya University

Material Science (Physics)

Condensed-Matter Theory Group (Sc)

Shun Matsubara

Contents

1 Introduction **4**
- 1.1 BCS theory . . . 4
- 1.2 Strongly Correlated Electron Systems . . . 5
  - 1.2.1 Cuprate superconductors . . . 5
  - 1.2.2 Iron-based superconductors . . . 6
- 1.3 Effect of Real-Space structure in Strongly Correlated Electron Systems . . . 7
- 1.4 Andreev Bound State . . . 9
- 1.5 Singlet and Triplet Superconductivity . . . 10
- 1.6 Odd-frequency superconductivity . . . 12
- 1.7 The contents of this thesis . . . 13

2 Model **15**
- 2.1 Cluster Hubbard model with edge . . . 15
- 2.2 Nambu Green function in the bulk d-wave SC state . . . 16
- 2.3 LDOS . . . 17
- 2.4 Random Phase Approximation (RPA) in the real space . . . 17
- 2.5 Fluctuation Exchange approximation (FLEX) in the real space . . . 18
- 2.6 Modified FLEX (GV^I-FLEX) approximation . . . 19
- 2.7 Nambu representation for coexisting SC state in (k_x, y, y')-representation . . . 20
- 2.8 linearized triplet gap equation . . . 21

3 Edge-induced Strongly Correlated Electronic States in the normal state **23**
- 3.1 Introduction . . . 23
- 3.2 Model and Theoretical Method . . . 23
- 3.3 Site-dependent spin susceptibilities . . . 24
- 3.4 FLEX results . . . 25
- 3.5 Site-dependent damping and mass-enhancement . . . 26
- 3.6 T-dependences of the electronic states . . . 27
- 3.7 Summary . . . 28

4 Emergence of edge-induced strong ferromagnetic fluctuations caused by the Andreev bound state in d-wave superconductors **29**
- 4.1 Introduction . . . 29
- 4.2 Model . . . 29
- 4.3 Numerical result of $\hat{\chi}$ and α_S by the RPA in real space . . . 29
- 4.4 FLEX analysis . . . 32
  - 4.4.1 GV^I-FLEX . . . 32
  - 4.4.2 Numerical result of $\hat{\chi}$ and α_S in real space . . . 33
- 4.5 Effect of the finite d-wave coherence length on the edge-induced spin fluctuations 34
- 4.6 Summary . . . 36

5 Edge-induced $d \pm ip$-wave superconducting state mediated by Andreev-bound-state-driven ferromagnetic fluctuations in d-wave superconductors 38
5.1 Introduction . . . 38
5.2 Theoretical method of triplet gap equation . . . 39
5.3 Numerical result of triplet gap equation . . . 41
5.3.1 $d \pm ip$-wave SC state . . . 42
5.3.2 Temperature-dependence of λ . . . 43
5.3.3 Result of the GV^I-FLEX approximation . . . 44
5.3.4 Effect of finite d-wave coherence length on edge-induced triplet superconductivity . . . 45
5.4 Cancellation of edge supercurrent in $d \pm ip$-wave SC state . . . 46
5.5 Summary . . . 48

6 Generation of edge-induced odd-frequency superconductivity with spontaneous spin current due to zero-energy Andreev-bound-state 49
6.1 Introduction . . . 49
6.2 Model and Theoretical Method . . . 49
6.3 Numerical Results . . . 50
6.3.1 $s^{\rm odd}$-wave SC state . . . 51
6.3.2 $s^{\rm odd}$ wave SC state dominates $p^{\rm even}$ wave SC state . . . 52
6.3.3 Edge Super Current . . . 53
6.4 Relationship between ϕ and ϕ^+ . . . 56
6.5 Analysis of gap equation without linearization . . . 57
6.6 Evaluation of Free energy by Luttinger-Ward theory . . . 59
6.7 Summary . . . 60

7 Nematic state of FeSe 61
7.1 Introduction . . . 61
7.2 Model . . . 62
7.3 Numerical Results of DW equation . . . 64
7.4 Temperature dependence . . . 66
7.5 Physical meaning of Relative Phase between $\Delta\Sigma_{22}$ and $\Delta\Sigma_{44}$ . . . 66
7.6 Linearized DW equation based on FLEX approximation . . . 67
7.7 DW equation based on FLEX approximation . . . 68
7.8 Summary . . . 71

8 Summary 72

9 Acknowledgement 74

A Filling dependence in the normal state 75
A.1 Filling dependence in LSCO TB model . . . 75
A.2 Filling dependence in YBCO TB model . . . 75

B The origin of the minor peak in the LDOS **77**

C Relation between enhanced FM fluctuations and odd-frequency superconductivity **78**

D LDOS in the $d \pm ip$-wave SC state **81**

E k_x-dependence of $s^{\mathbf{odd}}$ gap **82**

F Analysis by modified FLEX approximation **82**

1 Introduction

1.1 BCS theory

Superconductivity is an interesting phenomenon in condensed matter physics. In the superconducting (SC) state below critical temperature T_c, the resistivity becomes zero. At the same time, the magnetic field is rejected from the material. It is called the Meissner effect. Superconductivity was found by Kamerlingh Onnes in 1911. However, its microscopic mechanism had not been clarified for a long time until the BCS theory is proposed in 1957 by Bardeen, Cooper, and Schrieffer.

Here, we explain the outline of the BCS theory. In the BCS theory, we consider the following Hamiltonian:

$$H = \sum_k \varepsilon_k c^\dagger_{k,\sigma} c_{k,\sigma} + \sum_{k,k'} V_{k,k'} c^\dagger_{k,\uparrow} c^\dagger_{-k,\downarrow} c_{-k',\downarrow} c_{k',\uparrow}, \tag{1}$$

where $c^\dagger_{k,\sigma}$ ($c_{k,\sigma}$) is the creation (annihilation) operator for electron with wave vector k and spin σ. The second term is the attractive electron-electron interaction. In BCS superconductors, the origin of attractive interaction is the electron-phonon interaction. Because the electron and crystal lattice have negative and attractive charges, respectively, two electron-phonon interactions can be an effective electron-electron attractive interaction. If an attractive interaction exists, the two electrons with $(k,\uparrow)$ and $(-k,\downarrow)$ near the Fermi level form a pair irrespective of the origin of the attractive interaction. This pair is called the Cooper pair and the expectation value

$$\Delta_k = \sum_{k'} V_{k,k'} < c_{k'\uparrow} c_{-k'\downarrow} > \tag{2}$$

becomes finite. Here, Δ_k is called gap function, which is the order parameter of the SC. The Cooper pair can be regarded as a boson because it consists of two fermions. Thus, Cooper pairs can condense like bosons in low temperature. The coherent behavior of the condensed Cooper pairs is the origin of the zero resistivity. Next, we can obtain BCS Hamiltonian by performing the mean-field approximation

$$\begin{aligned} H &= \sum_k \varepsilon_k c^\dagger_{k,\sigma} c_{k,\sigma} + \sum_k \left(\Delta_k c^\dagger_{k,\uparrow} c^\dagger_{-k,\downarrow} + \Delta^*_k c_{-k,\downarrow} c_{k,\uparrow} \right) \\ &= \sum_k (c^\dagger_{k,\uparrow}, c_{-k,\downarrow}) \begin{pmatrix} \varepsilon_k & \Delta_k \\ \Delta^*_k & -\varepsilon_{-k} \end{pmatrix} \begin{pmatrix} c_{k,\uparrow} \\ c^\dagger_{-k,\downarrow} \end{pmatrix}, \end{aligned} \tag{3}$$

The second line is called Nambu representation, which is useful to analyze the superconducting state. By performing diagonalization of the second line, we obtain the excitation energy

$$E_k = \sqrt{\varepsilon_k^2 + |\Delta_k|^2} \tag{4}$$

Therefore, finite energy Δ_k is at least needed to excite the ground state. Furthermore, by considering the effect of finite temperature, the gap function satisfies

$$\Delta_k(T) = -\frac{1}{2}\sum_{k'} V_{k,k'} \frac{\Delta_{k'}}{\sqrt{\varepsilon_{k'}^2 + |\Delta_{k'}(T)|^2}} \tanh\left(\frac{\sqrt{\varepsilon_{k'}^2 + |\Delta_{k'}(T)|^2}}{2k_B T}\right). \tag{5}$$

For the electron-phonon interaction, we can ignore the k,k'-dependence of V and considering the Debye frequency ω_D,

$$\Delta = 2\hbar\omega_D \exp\left(-\frac{1}{\rho V}\right), \tag{6}$$

where ρ is the density of states at the Fermi level. Thus, large ρ and V make the superconducting gap larger. The superconducting gap is s-wave in BCS superconductors because the electron-phonon interaction is isotropic in the wave vector space. The transition temperature T_c is evaluated as

$$k_B T_c \approx 1.13\hbar\omega_D \exp\left(-\frac{1}{\rho V}\right) \tag{7}$$

T-dependence of gap function is obtained as

$$\Delta^d(T) = \Delta_0^d \tanh\left(1.74\sqrt{\frac{T_{cd}}{T} - 1}\right). \tag{8}$$

By using (6) and (7) the relation between the size of gap function at zero-temperature and T_c is obtained as follows

$$\frac{2\Delta}{T_c} \approx 3.52 \tag{9}$$

this coefficient is universal in all materials. In addition, the observed jump in heat capacity at T_c can be explained. In the BCS theory, the upper limit of the critical temperature T_c is about 40K. However, in 1986, cuprate superconductors that have a higher T_c than the BCS limit were found and the mechanism of the unconventional superconductivity became an important issue in condensed matter physics.

1.2 Strongly Correlated Electron Systems

1.2.1 Cuprate superconductors

In the cuprate superconductors, the spin fluctuations mediate the d-wave superconductivity. Figure 1 shows the schematic diagram of the antiferromagnetic fluctuations in cuprate superconductors. By doping carrier in the antiferromagnetic (AFM) Mott insulator, AFM order is suppressed, Eventually, the magnetic order vanishes even at $T = 0$. This point is called the magnetic quantum critical point (QCP). Near the QCP, the normal state with

strong magnetic fluctuations is realized. In strongly correlated electron systems, various unconventional superconductivity is induced near QCP. The origin of this AFM fluctuations is the nesting of the Fermi surface. These AFM fluctuations work as an effective repulsive interaction between electrons with wave vector k and $k+q$. Thus, the gap function $\Delta(k)$ and $\Delta(k+q)$ has the opposite sign, and the d-wave SC gap is realized. [1–6].

On the other hand, below T^*, pseudo-gap (PG) is observed as the Fermi arc [7–10], which is the vanishing of the part of Fermi surface. The mechanism of pseudo-gap is an important unsolved problem.

In addition, in the normal state of cuprate superconductors, the non-Fermi liquid phenomena such as the T-linear resistivity above the pseudo-gap temperature T^* is explained by the effect of the strong spin fluctuations. [11–14]. Furthermore, the spin fluctuation-driven quasiparticle scattering strongly increases the Hall coefficient and magnetoresistance [15–17].

In recent years, the axial and uniform charge-density-wave (CDW) is observed in various optimally- and under-doped cuprate superconductors [18–21]. The mechanism of the CDW attracts a lot of attention in the field of strongly correlated electron systems. To explain the CDW mechanism, spin-fluctuation-driven CDW mechanisms have been proposed [22–33]

Because various interesting phenomena are induced by spin fluctuations, it is significant to clarify how the spin fluctuations are affected by the real-space structures. However, theoretical studies have been limited because of its huge numerical calculation cost.

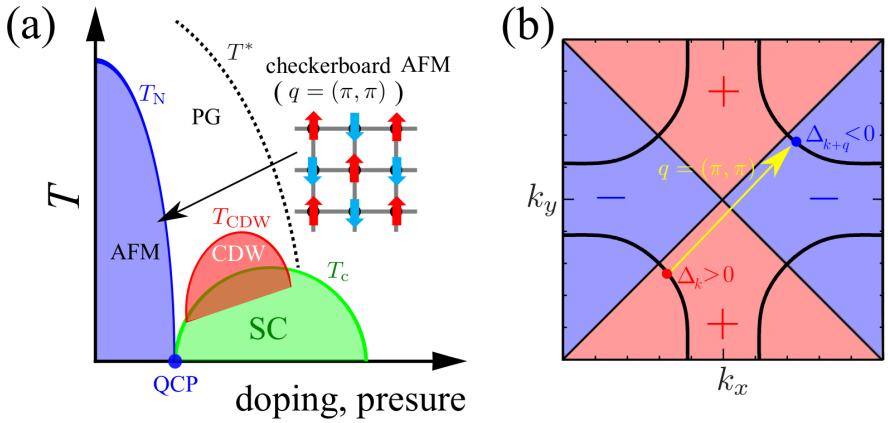

Figure 1: (a) Antiferromagnetic fluctuations developing in cuprate superconductors. (b) Schematic diagram of d-wave SC. In the area painted in red (blue), the sign of the gap function is positive (negative). The yellow arrow represents the AFM fluctuations, which work as a repulsive interaction between k and $k+q$. The black curve is the Fermi surface.

1.2.2 Iron-based superconductors

The iron-based superconductor was found in 2008. It has been attracting a lot of attention because superconductivity is not expected in Fe compounds. To date, many compounds were found such as LaFeAsO [34], $BaFe_2As_2$, LiFeAs, and FeSe. The crystal structure consists of a block layer and a 2-dimensional conducting layer. The conducting layer is composed of

Fe and pnictogen. In iron-based superconductors, the band structure near the Fermi level consists of multiple Fe 3d orbitals. Thus, we must treat them as a multi-orbital system, while cuprate superconductors can be treated as a single orbital system. Figure 2 shows the phase diagram of typical iron-based superconductors [35–39]. The blue region below $T_{\rm s}$ is the nematic state, where the rotational symmetry broken from C_4 to C_2. To explain the nematic order, orbital order due to the interference between the spin fluctuations is proposed [22, 30, 31]. In almost iron-based superconductors, the stripe antiferromagnetic order emerges below T_N, while FeSe does not have a magnetic phase. Therefore, FeSe is a favorable system to clarify the relation between superconductivity and nematic order. In the green region in Fig. 2, superconductivity is realized. The mechanism and symmetry of superconductivity has been studied actively. The spin fluctuation mediated $s_{\pm}$-wave [40–43] and orbital fluctuation mediated s_{++} wave [44] are proposed.

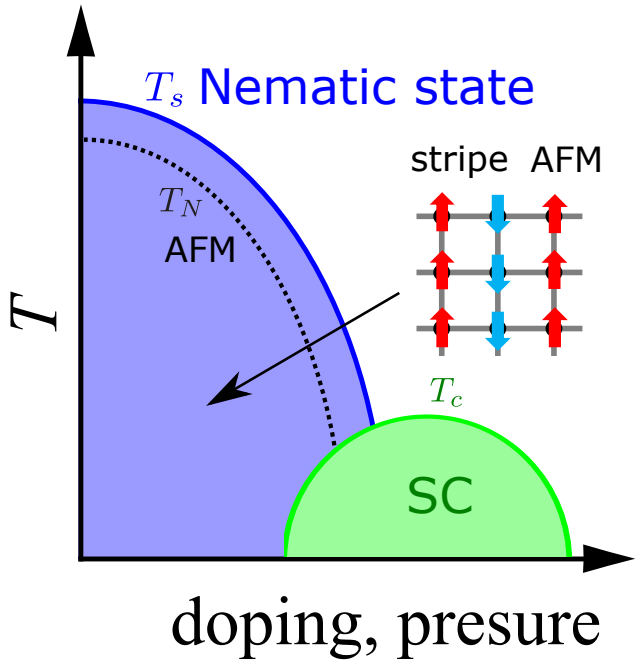

Figure 2: Schematic phase diagram of typical iron-based superconductors. In the blue region below $T_{\rm s}$, nematic order is realized. Below $T_{\rm N}$, stripe type AFM order is realized. In the green region, superconductivity is realized.

1.3 Effect of Real-Space structure in Strongly Correlated Electron Systems

In strongly correlated electron systems, real-space structures such as the surface and impurity drastically modify the many-body electronic states, and various quantum phenomena are expected. It is the main theme in this study. For example, the development of local magnetic moment ($\sim 1\mu_{\rm B}$) around the impurity is observed in cuprate superconductors $YBa_2Cu_3O_{7-x}$ (YBCO) [45,46] and $La_{2-\delta}Sr_{\delta}CuO_4$ (LSCO) [47]. By the NMR experiments [48–50], strongly

enhancement of the local and the staggered spin susceptibilities are observed around the impurity site. In addition, dilute nonmagnetic impurities cause huge residual resistivity beyond the s-wave unitary scattering limit in cuprate superconductors [51] and heavy-fermion systems [52, 53]. Thus, the system approaches the magnetic quantum-critical point (QCP) by introducing dilute point defects. [54].

To examine the exotic electronic state created by the impurities, it is important to construct theoretical methods of analyzing the strongly correlated metals without translational symmetry. Many theoretical studies on the effects of point impurity in cuprates have been performed [55–61]. In the random-phase-approximation (RPA), enhancement of the antiferromagnetic spin susceptibility near a defect is reproduced for nonlocal impurity site, while spin susceptibility is suppressed for local impurity [59–61]. By considering the site-dependent self-energy based on the GV^I method, impurity-induced enhancement of AFM fluctuations is obtained even if the impurity potential is local [54].

Next, we explain the intuitive physical picture of impurity-induced strongly correlated states. Due to the Friedel oscillation, the local density of states (LDOS) is modified around an impurity, and the LDOS increases at some sites as shown by the red circle in Fig. 3 (b). In these sites, strong electron correlation is realized. These results indicate that the open edge of the cluster Hubbard model strongly enhances the AFM fluctuations because the edge can be regarded as the aligned impurity sites in a straight line. The effect of the nonmagnetic impurities and open edges in graphene have been discussed in Refs. [62, 63]. However, detail behavior of spin fluctuations in the "open edge cluster Hubbard model" have not been analyzed yet.

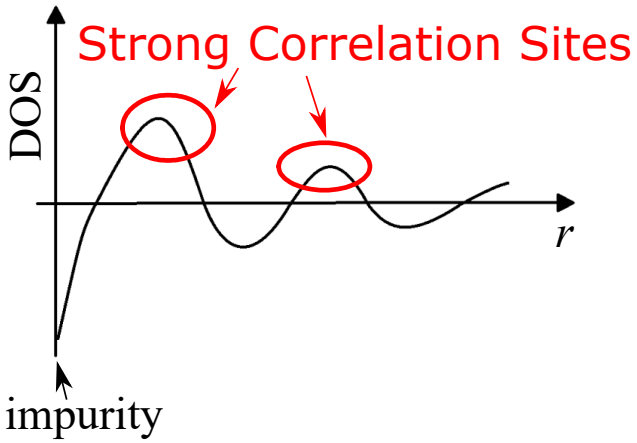

Figure 3: Strong correlation sites created by the Friedel oscillation around an impurity The red circle represents strong correlation sites, which is driven by the increase of LDOS.

1.4 Andreev Bound State

In the superconducting state surfaces or interfaces cause various interesting phenomena. For example, the surface Andreev bound state (ABS) is a drastic phenomenon peculiar in the

anisotropic superconductor. It is originated from the sign change in the bulk superconducting gap. In $d_{x^2-y^2}$-wave superconductors, the ABS is formed at the $(1,1)$ edge or interface. [64–69]. The ABS is formed when the quasiparticle feels sign change of gap function before and after the reflection by the edge as shown in Figure 4. $(1,1)$ edge is the most favorable direction for the formation of the ABS. On the other hand, ABS completely vanishes for $(1,0)$ edge, because the quasiparticle feels the same sign through the reflection process. For $d_{x^2-y^2}$-wave superconductors, ABS has flat dispersion at zero energy. Thus, the LDOS increases at the Fermi level near the edge. The ABS is observed by scanning tunneling spectroscopy (STS) experiments as the zero-bias conductance peak [71–75] Because of the large increase in the LDOS, enhancement of the electron correlation is expected. However, the effects of ABS on the electron correlation have not been clarified yet. Furthermore, time-reversal symmetry breaking (TRSB) SC state can be induced by the real space structure such as a surface or an interface. For example, emergence of $d \pm is$-wave SC is predicted at the $(1,1)$ edge of a d-wave superconductor [76–78]. In this case, the edge-induced s-wave gap has non-zero phase difference $\pi/2$ measured from the bulk d-wave gap. The real-space structure induced TRSB SC state has been studied in polycrystalline YBCO [79] or twined iron-based superconductor FeSe in the nematic phase [80]. However, the origin of the pairing interaction of edge-induced SC is not evaluated microscopically. To understand such surface or interface-induced SC, we have to study the effect of the ABS on the spin fluctuations, which can work as the pairing interaction of surface-induced SC.

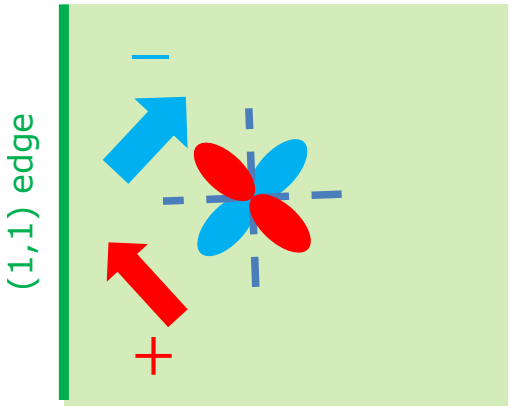

Figure 4: Andreev bound state of d-wave superconductor. The red and blue arrows represent the injection and reflection direction of quasiparticle, respectively. The bulk d-wave gap works as the positive (negative) potential to the injection (reflection) quasiparticle.

1.5 Singlet and Triplet Superconductivity

Superconductivity is realized by the condensation of cooper pairs. The Cooper pair consists of two electrons. The possible total spin of the Cooper pair is $S = 0$ or $S = 1$ as shown in Figure 5. $S = 0$ case is called spin singlet superconductivity and $S = 1$ case is called spin triplet superconductivity.

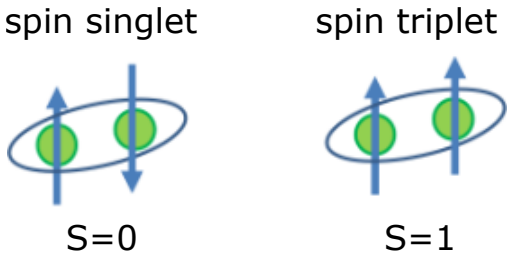

Figure 5: Spin singlet and triplet Cooper pairs. Singlet gap is odd for exchange of spins, while triplet gap is even for exchange of spins.

The order parameter of the superconductivity is called gap function. It is represented as $\Delta_{\sigma\rho}(k) \approx V < c_{k\sigma}c_{-k\rho} >$, where $c_{k\sigma}$ is the annihilation operator. V is the pairing interaction. σ and ρ are the spin index. Due to the Fermion anticommutation relation, all type of gap functions satisfy

$$\Delta_{\sigma\rho}(k) = -\Delta_{\rho\sigma}(-k) \tag{10}$$

The definition of the singlet superconductivity is

$$\Delta^{\text{singlet}}_{\sigma\rho}(k) = -\Delta^{\text{singlet}}_{\rho\sigma}(k). \tag{11}$$

From (10) and , the singlet gap is even parity in the space.

$$\Delta^{\text{singlet}}_{\sigma\rho}(k) = +\Delta^{\text{singlet}}_{\sigma\rho}(-k) \tag{12}$$

Thus, singlet s-wave, d-wave, $\cdots$ are allowed as the singlet superconductivity. On the other hand, the definition of the triplet superconductivity is

$$\Delta^{\text{triplet}}_{\sigma\rho}(k) = +\Delta^{\text{triplet}}_{\rho\sigma}(k). \tag{13}$$

From (13) and (14), the triplet gap is odd parity in the space

$$\Delta^{\text{triplet}}_{\sigma\rho}(k) = -\Delta^{\text{triplet}}_{\sigma\rho}(-k). \tag{14}$$

Thus, triplet p-wave, f-wave, $\cdots$ are allowed as the triplet superconductivity. Above relations are summarized in table 2. In the BCS theory, phonon mediates the spin singlet s-wave superconductivity. d-wave superconductivity in cuprate is also spin singlet superconductivity. On the other hand, spin triplet superconductivity is rare. In the superfluidity of ^{3}He, spin triplet state is realized. Also, UPt_3 are the candidates of the spin triplet superconductivity.

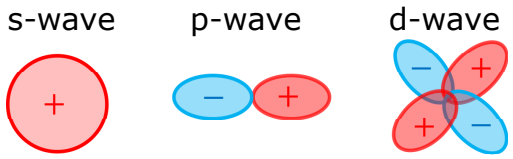

Figure 6: Various k-dependence of superconducting gap function. s and d-wave gap have even parity for $k \to -k$, while p-wave gap has odd parity.

Table 1: Difference between singlet and triplet superconductivity.

	Singlet	Triplet
Spin $\sigma \leftrightarrow \rho$	$\Delta_{\sigma\rho}(k) = -\Delta_{\rho\sigma}(k)$ Odd	$\Delta_{\sigma\rho}(k) = +\Delta_{\rho\sigma}(k)$ Even
Wave number $k \leftrightarrow -k$	$\Delta_{\sigma\rho}(k) = +\Delta_{\sigma\rho}(-k)$ Even	$\Delta_{\sigma\rho}(k) = -\Delta_{\sigma\rho}(-k)$ Odd
Fermion anticommutation relation	$\Delta_{\sigma\rho}(k) = -\Delta_{\sigma\rho}(-k)$ Odd	

In strongly correlated electron systems, spin and charge fluctuations can be the effective interaction of the superconductivity [81]. For singlet superconductivity, they work as

$$V^{\text{singlet}}(q) = \left(\frac{3}{2}\chi^s(q) - \frac{1}{2}\chi^c(q)\right). \tag{15}$$

For triplet superconductivity, they work as

$$V^{\text{triplet}}(q) = \left(-\frac{1}{2}\chi^s(q) - \frac{1}{2}\chi^c(q)\right). \tag{16}$$

The sign and coefficient of spin susceptibility in V are different in singlet and triplet cases. When strong spin fluctuations develop at wave vector q, the gap equation is approximately represented as

$$\Delta(k) \propto -\Delta(k+q)V(q). \tag{17}$$

For large ferromagnetic fluctuations, $V^{\text{singlet}} \approx \frac{3}{2}\chi^s(q=0)$ works as repulsive interaction. It suppresses the singlet superconductivity. $\Delta^{\text{singlet}}(k) \propto -\Delta^{\text{singlet}}(k)\chi^s(q=0)$ However, for the the triplet superconductivity V is works as an attractive interaction $\Delta^{\text{triplet}}(k) \propto +\Delta^{\text{triplet}}(k)\chi^s(q=0)$ Therefore, when the strong ferromagnetic (FM) fluctuations develop, the triplet superconductivity can be realized [82–86].

1.6 Odd-frequency superconductivity

In the previous subsection, we implicitly assumed that the gap function is even for frequency $i\varepsilon_n$. However, the gap function with odd-frequency dependence is not prohibited by the fermion anticommutation relation. This odd-frequency gap function is also odd function for relative time between paring electrons. As shown in Figure 7, Cooper pair is formed only for non-zero relative time t, while superconducting correlation vanishes at $t = 0$. Table 2 shows the possible superconductivity including the frequency. To satisfy the fermion anti-commutation relation, four combinations are allowed. The mechanisms and properties of the odd-frequency SC states have been actively discussed by many theorists [87–99].

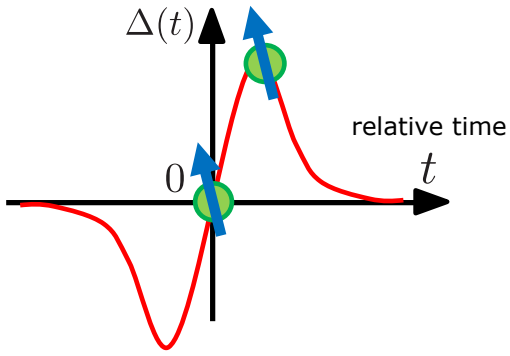

Figure 7: Time-dependence of odd-frequency gap function. t is the relative time between two electrons. The red line represents odd-frequency gap function in t-representation $\Delta(t)$.

Theoretically, it is proposed that the FM (AFM) spin fluctuations can be a pairing interaction of odd-frequency s wave triplet (p wave singlet) SC [96, 100–104]. However, if we assume Hermite odd-frequency gap, bulk odd-frequency SC state is inevitably unstable due to the "paramagnetic Meissner (para-Meissner) effect" [88, 89, 105]. Because of the difference in the sign of the Meissner kernel, the magnetic field is infinitely taken into the inside of the bulk off-frequency superconductor. To overcome this problem, inhomogeneous SC states with large center of mass momentum of the gap function have been considered [106]. In contrast, a homogeneous non-Hermite odd-frequency gap function with usual Meissner has been proposed [97–99]. However, coexistence between Hermite and non-Hermite odd-frequency "pair amplitudes" yields unphysical imaginary part of Josephson current and superfluid density [94]. At present, the essential properties of the odd-frequency gap function has not been revealed yet. To address this unsolved problem, study on the coexisting states of the odd-frequency and "well-known" even-frequency gap functions should be valuable.

It is known that odd-frequency pair amplitude can be induced from conventional even-frequency superconducting gap by introducing external symmetry breaking. In superconductor/ferromagnet junction, the breaking in spin-rotational symmetry induces the odd-frequency spin-triplet s-wave pairing from conventional spin-singlet one. [107–118]. On the other hand, odd-frequency pair amplitude is also induced from bulk even-frequency superconducting gap by introducing translational symmetry breaking [91, 119–122]. In this case, spin-singlet odd-parity (spin-triplet even-parity) pairing can be generated from spin-singlet even-parity (spin-triplet odd-parity) bulk superconductors [91, 119–122]. In these cases, the anomalous proximity [123, 124] and para-Meissner effects [125–130] are induced even if the $s^{\rm odd}$ wave gap function is zero. In particular, the odd-frequency amplitude is enlarged by the zero-energy surface Andreev bound state (SABS), and it can induce the $s^{\rm odd}$ wave gap function through the enhancement of electron correlation effect in this study. In this thesis, we study the edge-induced odd-frequency superconducting gap function in the paramagnetic state, mediated by strong FM fluctuations.

Table 2: Possible superconductivity including parity of frequency

	Singlet Even-f	Singlet Odd-f	Triplet Even-f	Triplet Odd-f
Spin $\sigma \leftrightarrow \rho$	Odd		Even	
Wave number $k \leftrightarrow -k$	Even	Odd	Odd	Even
Frequency $i\varepsilon_n \leftrightarrow -i\varepsilon_n$	Even	Odd	Even	Odd
Fermion anticommutation relation	Odd $\Delta_{\sigma\rho}(k, i\varepsilon_n) = -\Delta_{\rho\sigma}(-k, -i\varepsilon_n)$			

1.7 The contents of this thesis

To construct a theory of edge induced strong correlation and predict exotic phenomena, we study the cluster Hubbard model with open edge.

In section 2, we explain the formalism used in this thesis. The detail of the cluster Hubbard model Hamiltonian with the open edge is introduced here. Next, we explain the real space random phase approximation and fluctuation exchange approximation, which is necessary to analyze the open edge model. Then, to analyze the edge induced superconductivity, we introduce the linearized gap equation in the presence of bulk d-wave SC gap.

In section 3, we explain the edge-induced quantum critical phenomena in the normal state. By introducing the edge, spin susceptibility is enhanced near the edge, especially for the (1,1) edge. The mass-enhancement factor and the damping are also enhanced near the edge.

In section 4, we explain the Andreev bound state induced quantum critical phenomena. To examine the electron correlation near the edge, we perform the real space RPA in the presence of the bulk d-wave SC gap. The ABS plays an important role in the development of the ferromagnetic fluctuations near the edge. It is a favorable situation for the emergence of triplet superconductivity.

For the possible edge-induced triplet superconductivity, both even-f and odd-f superconductivity have to be considered. In section 5, we discuss the edge-induced even frequency triplet superconductivity. We analyze the linearized gap equation, and time-reversal symmetry breaking $d + ip$ wave SC state is obtained

In section 6, we discuss the edge-induced odd frequency triplet superconductivity. By analyzing the linearized gap equation, we obtain the odd-frequency SC gap localized at the edge. In the $d + s^{\mathrm{odd}}$-wave state, spin current flows along the edge. In addition, we explain the Hermite relation is the correct relation for the triplet superconductivity.

In section 7, we study the nematic state of iron-based superconductor FeSe. We analyze the DW equation for d_{xz}, d_{yz}, and d_{xy} orbitals, and the orbital polarization d_{xz} between d_{yz} and d-wave bond order for d_{xy} are obtained. In this case, the Y electron pocket vanished in the nematic state, and the observed Fermi surface is reproduced.

2 Model

2.1 Cluster Hubbard model with edge

In this study, we consider following cluster Hubbard model Hamiltonian

$$\mathcal{H} = \sum_{i,j,\sigma} t_{i,j} c^{\dagger}_{i\sigma} c_{j\sigma} + U \sum_{i} n_{i\uparrow} n_{i\downarrow} + \sum_{i,j} \Delta^{d}_{i,j} \left(c^{\dagger}_{i\uparrow} c^{\dagger}_{j\downarrow} + \text{h.c} \right), \tag{18}$$

where U is the on-site Coulomb interaction. $n_{i\sigma} = c^{\dagger}_{i\sigma} c_{i\sigma}$ is the number operator of electron at site i. $t_{i,j}$ denotes the hopping integral between sites i and j. In this study, we set $(t_1, t_2, t_3) = (-1, 1/6, -1/5)$, where t_n is the n-th nearest neighbor hopping integral and this set of values correspond to $YBa_2Cu_3O_{7-x}$ (YBCO) model [14, 131–133]. In this study, we set $|t_1|$ as the energy unit, which corresponds to ~ 0.4eV in cuprate superconductors without renormalization. The Fermi surface (FS) in the periodic system is shown in Fig. 8 (b). $\Delta^{d}_{i,j}$ is the bulk d_{xy} wave ($=d_{X^2-Y^2}$ wave) SC gap function given as $\Delta^{d}_{i,j} = (\Delta^{d}/4)(\delta_{\boldsymbol{r}_i - \boldsymbol{r}_j, \pm\hat{\boldsymbol{X}}} - \delta_{\boldsymbol{r}_i - \boldsymbol{r}_j, \pm\hat{\boldsymbol{Y}}})$. Similar bulk d wave gap function is microscopically obtained based on spin-fluctuation theories. Considering this fact, we introduce Δ^{d} as the model parameter to simplify the analysis. In the following numerical study, we set the filling as $n = 0.95$. The numerical results are essentially unchanged for $n = 0.8$–1.2.

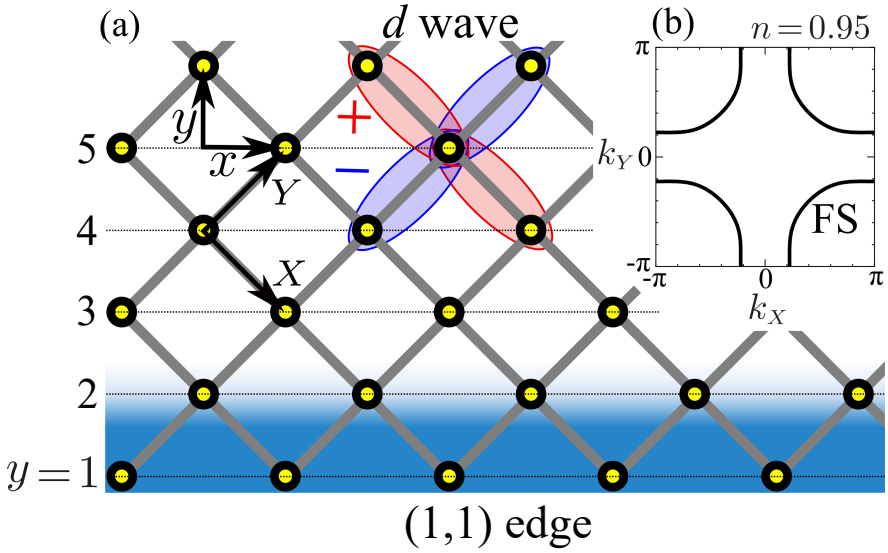

Figure 8: (a) Cluster Hubbard model with (1,1) edge. The orthogonal unit vectors ($\hat{\boldsymbol{x}}$, $\hat{\boldsymbol{y}}$) and ($\hat{\boldsymbol{X}}, \hat{\boldsymbol{Y}}$) are illustrated. (b) Bulk Fermi surface in the normal state.

To examine the temperature dependence of the system, we suppose that $\Delta^{d}(T)$ obeys the BCS-like T-dependence:

$$\Delta^{d}(T) = \Delta^{d}_{0} \tanh \left(1.74 \sqrt{\frac{T_{cd}}{T} - 1} \right), \tag{19}$$

where $\Delta_0^d \equiv \Delta_0^d(T=0)$.

Near the edge layer ($y = 1$), $\Delta_{i,j}^d$ should be suppressed in the range of $1 \le y \le \xi_d$, where ξ_d is the coherence length of the d-wave gap. In order to take into account this suppression, we multiply $\Delta_{i,j}^d$ by the suppression factor $(1 - \exp[(y_i + y_j - 2)/2\xi_d])$ [133]. For $\xi_d = 10$, we illustrated $|\Delta_{i,j}^d|$ for $i = (x, y)$ and $j = (x+1, y+1)$ in Fig. 9. Based on the experiments [134–137], the coherence length in the a-b plane of YBCO is evaluated as 1nm for $T \ll T_{cd}$ Therefore, $\xi_d = 10$ is reasonable value.

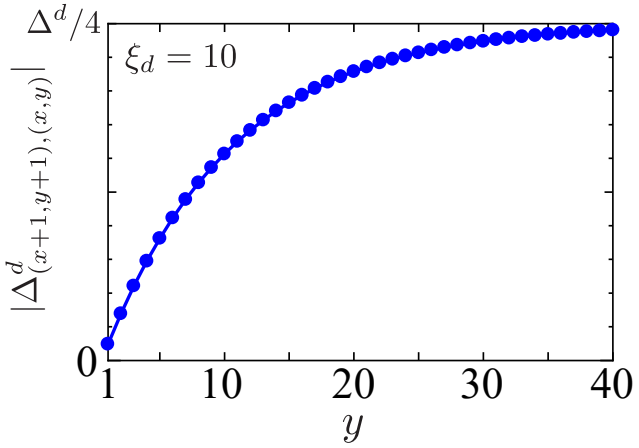

Figure 9: $|\Delta_{i,j}^d|$ for $i = (x, y)$ and $j = (x+1, y+1)$ for $\xi_d = 10$.

2.2 Nambu Green function in the bulk d-wave SC state

In this study, we introduce the $2N_y \times 2N_y$ Nambu Green function in the presence of the bulk d wave gap $\Delta_{y,y'}^d(k_x) \equiv \Delta^{d\uparrow\downarrow}_{y,y'}(k_x)$. To simplify the analysis, we assume that $\Delta_{i,j}^d$ is real. Thus, $\left\{\Delta_{y',y}^d(k_x)\right\}^* = \Delta_{y,y'}^d(k_x)$ is satisfied. The Nambu Hamiltonian is given as follows [132, 133]:

$$\mathcal{H}_d = \sum_{k_x} \left({}^t\hat{c}^\dagger_{k_x,\uparrow}, {}^t\hat{c}_{-k_x,\downarrow} \right) \begin{pmatrix} \hat{H}^0(k_x) & \hat{\Delta}^d(k_x) \\ \hat{\Delta}^d(k_x) & -{}^t\hat{H}^0(-k_x) \end{pmatrix} \begin{pmatrix} \hat{c}_{k_x,\uparrow} \\ \hat{c}^\dagger_{-k_x,\downarrow} \end{pmatrix}, \tag{20}$$

where $\hat{c}_{k_x,\uparrow}$ and $\hat{c}^\dagger_{-k_x,\downarrow}$ represent the N_y-component column vector of sites. Next, the Green functions in the bulk d wave SC state are defined as follows:

$$\begin{pmatrix} \hat{G}_d(k_x, i\epsilon_n) & \hat{F}_d(k_x, i\epsilon_n) \\ \hat{F}^\dagger_d(k_x, i\epsilon_n) & -{}^t\hat{G}_d(-k_x, -i\epsilon_n) \end{pmatrix} = \begin{pmatrix} i\epsilon_n\hat{1} - \hat{H}^0(k_x) & -\hat{\Delta}^d(k_x) \\ -\hat{\Delta}^d(k_x) & i\epsilon_n\hat{1} + {}^t\hat{H}^0(-k_x) \end{pmatrix}^{-1}, \tag{21}$$

where $\varepsilon_n = (2n+1)\pi T$ represents the fermion Matsubara frequency. F and $F^\dagger$ are the anomalous Green functions, which are finite only in the superconducting state. The Green functions G and F are $N_y \times N_y$ matrix of sites.

2.3 LDOS

To demonstrate the emergence of the ABS in the present $(1,1)$ edge TB model in the bulk d-wave SC state, we evaluate the LDOS using the Green function G as follows:

$$D_y(\epsilon) = \frac{1}{2\pi^2}\int_{-\pi}^{\pi} dk_x \mathrm{Im} G_{y,y}(k_x, \epsilon - i\delta). \tag{22}$$

Figure 10 shows the obtained LDOS for $\Delta^d(T) = 0.08$ by setting $\delta = 0.01$. For simplicity, we ignore the suppression of the bulk d-wave gap near the edge. There is a large peak at the Fermi level ($\epsilon = 0$), at the edge layer ($y = 1$), due to the ABS. In the bulk ($y = 300 = N_y/2$), LDOS is suppressed around the Fermi level due to the d-wave SC gap, and exhibits a V-shape ϵ-dependence. The height of the zero-energy peak is proportional to the size of bulk d-wave gap [77]. In the present model, a secondary minor peak emerges at $\varepsilon = 0.1$. It is originated from a superconducting surface state that is different from the surface ABS. We explain it in Appendix B.

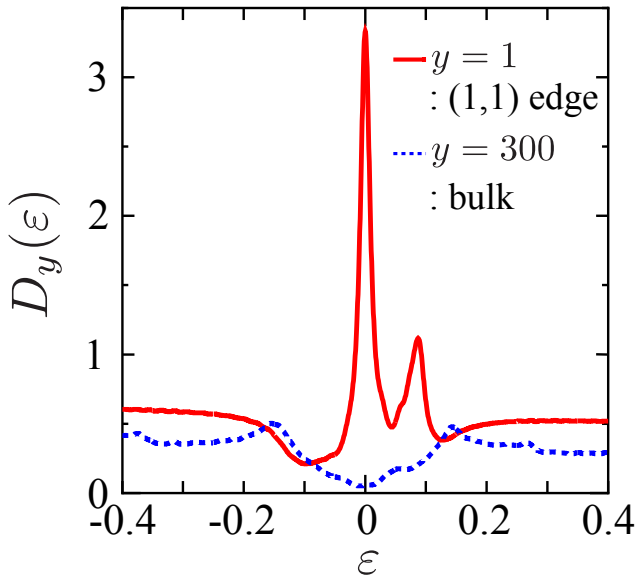

Figure 10: LDOS in the $(1,1)$ edge cluster Hubbard model in the d-wave SC state for $\Delta^d = 0.08$. The unit of energy is $|t| = 1$. $y = 1$ and $y = 300$ correspond to the $(1,1)$ edge and bulk, respectively. For convenience, we set $\delta = 0.01$.

2.4 Random Phase Approximation (RPA) in the real space

To evaluate the enhancement of the electron correlation near the edge, we calculate the site-dependent spin susceptibility $\chi^s_{y,y'}(q_x, i\omega_l)$ using the real-space random-phase-approximation (RPA). Here, we adopt the k_x representation by considering the translational symmetry in the x direction, and $\omega_l = 2\pi T l$ represents the boson Matsubara frequency. The irreducible

susceptibilities are given by $\hat{G}_d$, $\hat{F}_d$, and $\hat{F}_d^\dagger$ as

$$\chi^0_{y,y'}(q_x, i\omega_l) = -T\sum_{k_x,n} G_{dy,y'}(q_x + k_x, i\omega_l + i\epsilon_n) \tag{23}$$

$$\varphi^0_{y,y'}(q_x, i\omega_l) = -T\sum_{k_x,n} F_{dy,y'}(q_x + k_x, i\omega_l + i\epsilon_n) F^\dagger_{d y',y}(k_x, i\epsilon_n). \tag{24}$$

φ^0 is finite only in the SC state. The Feynman diagram of χ^0 and φ^0 are represented by bubble diagram illustrated in Figure 11.

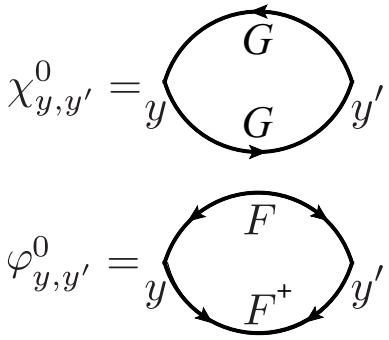

Figure 11: Diagram of the irreducible susceptibility, χ^0 or φ^0, in the (k_x, y, y') representation. The line with an arrow is G. The line with two arrows is F or $F^\dagger$.

The $N_y \times N_y$ matrix of the spin (charge) susceptibility $\hat{\chi}^{s(c)}$ is calculated using $\hat{\chi}^0$ and $\hat{\varphi}^0$ as

$$\hat{\chi}^{0s(c)}(q_x, i\omega_l) = \hat{\chi}^0(q_x, i\omega_l) + (-)\hat{\varphi}^0(q_x, i\omega_l), \tag{25}$$

$$\hat{\chi}^{s(c)}(q_x, i\omega_l) = \hat{\chi}^{0s(c)}(q_x, i\omega_l)\left\{\hat{1} - (+)U\hat{\chi}^{0s(c)}(q_x, i\omega_l)\right\}^{-1}. \tag{26}$$

The spin Stoner factor is the largest eigenvalue of $U\hat{\chi}^{0s}(q_x, i\omega_l)$ at $\omega_l = 0$. The magnetic order is realized when $\alpha_S \geq 1$. The spin and charge fluctuations can mediate superconductivity and the pairing interaction for triplet SC is given by

$$\hat{V}(q_x, i\omega_l) = U^2\left(-\frac{1}{2}\hat{\chi}^s(q_x, i\omega_l) - \frac{1}{2}\hat{\chi}^c(q_x, i\omega_l)\right). \tag{27}$$

2.5 Fluctuation Exchange approximation (FLEX) in the real space

In the FLEX approximation, the self-energy effect due to the spin and charge fluctuations is considered self-consistently. The self-energy is given by

$$\Sigma_{y,y'}(k_x, \epsilon_n) = T\sum_{q_x,l} G_{y,y'}(k_x + q_x, \epsilon_n + \omega_l) V_{y,y'}(q_x, \omega_l), \tag{28}$$

where $\hat{V}^{\rm FLEX}(q_y,\omega_l) = U^2\left(\frac{3}{2}\hat{\chi}^s(q_y,\omega_l) + \frac{1}{2}\hat{\chi}^c(q_y,\omega_l) - \hat{\chi}^0(q_y,\omega_l)\right)$. Figure 12 shows the diagram of self-energy $\Sigma_{x,x'}(k_y,\epsilon_n)$. In this real-space analysis, the FLEX self-energy also has site dependence. In the FLEX approximation, we solve Eqs. (23)-(28) self-consistently.

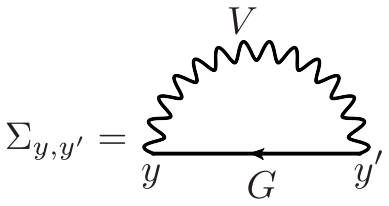

Figure 12: Diagram of the FLEX self-energy $\Sigma_{y,y'}(k_x,\epsilon_n)$. The line with an arrow is Green function G. The wavy curve corresponds to $V^{\rm FLEX}$.

Based on the FLEX self-energy, we can evaluate the site-dependent mass-enhancement factor Z and quesiparticle damping γ as follows.

$$\gamma_x = \frac{1}{2\pi}\int_{-\pi}^{\pi} dk_x {\rm Im}\Sigma_{y,y}(k_x, 0-i\delta) \tag{29}$$

$$Z_y = 1 - \frac{1}{2\pi}\int_{-\pi}^{\pi} dk_x \frac{\partial}{\partial\epsilon}{\rm Re}\Sigma_{y,y}(k_x,\epsilon-i\delta)|_{\epsilon=0}, \tag{30}$$

When the strong electron correlation develops, Z_y increases from 1, while $Z_y = 1$ for $U = 0$. The self-energy also renormalizes the bulk d-wave gap. In this approximation, we evaluated the renormalized bulk d-wave gap by $\Delta_0^{d*} = \Delta_0^d/Z_{\rm bulk}$, where $Z_{\rm bulk}$ is the on-site mass-enhancement factor in the bulk.

2.6 Modified FLEX (GV^I-FLEX) approximation

Next, we explain the modified FLEX (GV^I-FLEX) approximation developed in Ref. [54]. In the conventional FLEX approximation, the negative feedback effect of self-energy on $\hat{\chi}$ is overestimated near the impurity due to the absence of vertex corrections. In fact, vertex corrections suppresses the negative feedback effect of the FLEX self-energy near the impurity [54]. In the modified FLEX, the cancellation between negative feedback and vertex corrections is assumed, and then enhancement of spin susceptibility is reproduced for single impurity problem [54].

To perform the modified FLEX in the present model, we first calculate the self-energy in the periodic system without the edge, $\Sigma^0(k_x,k_y,i\varepsilon_n)$, using the conventional FLEX approximation. Then, its (k_x,y,y')-representation $\Sigma^0(k_x,y,y',i\varepsilon_n) = \Sigma^0(k_x,y-y',i\varepsilon_n)$ is obtained by Fourier transformation in y-direction, Next, the Green functions are calculated by using

$(1,1)$ edge model hamiltonian $\hat{H}^0(k_x)$ and self-energy $\Sigma^0(k_x, y, y', i\varepsilon_n)$ as follows:

$$\begin{pmatrix} \hat{G}^I(k_x,\epsilon_n) & \hat{F}^I(k_x,\epsilon_n) \\ \hat{F}^{I\dagger}(k_x,\epsilon_n) & -\hat{G}^I(k_x,-\epsilon_n) \end{pmatrix} = \begin{pmatrix} \epsilon_n\hat{1} - \hat{H}^0(k_x) - \hat{\Sigma}^0(k_x,i\varepsilon_n) & -\hat{\Delta}^d(k_x) \\ -\hat{\Delta}^d(k_x) & \epsilon_n\hat{1} + \hat{H}^0(k_x) + \hat{\Sigma}^0(k_x,-i\varepsilon_n) \end{pmatrix}^{-1}. \tag{31}$$

The spin susceptibility is calculated using $\hat{G}^I$, $\hat{F}^I$, and $\hat{F}^{I\dagger}$ instead of $\hat{G}$, $\hat{F}$, and $\hat{F}^\dagger$ in Eqs.(23)–(26) in the GV^I-FLEX.

2.7 Nambu representation for coexisting SC state in (k_x, y, y')-representation

In this subsection, we explain the Nambu representation in the coexisting SC state to analyze the edge-induced superconducting state. When the bulk d-wave gap $\Delta_{y,y'}(k_x) \equiv \Delta^{\uparrow\downarrow}_{y,y'}(k_x)$ defined in (48) and the edge triplet gap $\phi_{y,y'}(k_x) \equiv \phi^{\uparrow\downarrow}_{y,y'}(k_x)$ are both finite, Hamiltonian is given by

$$H = \sum_{k,y,y',\sigma} H^0_{y,y'}(k_x) c^\dagger_{k_x,y,\sigma} c_{k_x,y,\sigma} + \frac{1}{2}\sum_{k_x,y,y',\sigma\rho} \left\{ D^{\sigma\rho}_{y,y'}(k_x) c^\dagger_{k_x,y,\sigma} c^\dagger_{-k_x,y',\rho} + h.c. \right\}, \tag{32}$$

where $D^{\sigma\rho}_{y,y'}(k_x)$ is the total gap function, which includes both singlet d-wave gap and triplet gap. σ and ρ represent the spin index. In this study, we ignore the spin orbit interaction for simplicity. Thus, we can set the d-vector as $\hat{\boldsymbol{d}}(k_x) = (0, 0, \hat{\phi}(k_x))$, where hat means $N_y \times N_y$ matrix of sites. Then, the total gap is given by

$$\begin{aligned} \hat{D}(k_x) &= i\hat{d}_0(k_x)\sigma_2 + i\hat{\boldsymbol{d}}(k_x)\cdot\boldsymbol{\sigma}\sigma_2 \\ &= \begin{pmatrix} 0 & \hat{\Delta}(k_x) + \hat{\phi}(k_x) \\ -\hat{\Delta}(k_x) + \hat{\phi}(k_x) & 0 \end{pmatrix}, \end{aligned} \tag{33}$$

where $\boldsymbol{\sigma} = (\sigma_1, \sigma_2, \sigma_3)$ is the Pauli matrix for spin space. Then, the $2N_y \times 2N_y$ Nambu representation is obtained as follows:

$$H = \sum_{k_x} \left({}^t\hat{c}^\dagger_{k_x,\uparrow}, {}^t\hat{c}_{-k_x,\downarrow} \right) \begin{pmatrix} \hat{H}^0(k_x) & \hat{D}^{\uparrow\downarrow}(k_x) \\ \left\{\hat{D}^{\uparrow\downarrow}(k_x)\right\}^\dagger & -\hat{H}^0(-k_x) \end{pmatrix} \begin{pmatrix} \hat{c}_{k_x,\uparrow} \\ \hat{c}^\dagger_{-k_x,\downarrow} \end{pmatrix}, \tag{34}$$

where $\hat{c}_{k_x,\uparrow}$ and $\hat{c}^\dagger_{-k_x,\downarrow}$ represent the N_y-component column vector of sites. The corresponding Nambu Green function is given as

$$\begin{pmatrix} \hat{\mathcal{G}}^{\uparrow\uparrow}(k_x,\varepsilon_n) & \hat{\mathcal{F}}^{\uparrow\downarrow}(k_x,\varepsilon_n) \\ \hat{\mathcal{F}}^{\dagger\uparrow\downarrow}(k_x,\varepsilon_n) & -{}^t\hat{\mathcal{G}}^{\downarrow\downarrow}(-k_x,-\varepsilon_n) \end{pmatrix} = \begin{pmatrix} i\varepsilon_n - \hat{H}^0(k_x) & -\hat{D}^{\uparrow\downarrow}(k_x) \\ -\left\{\hat{D}^{\uparrow\downarrow}(k_x)\right\}^\dagger & i\varepsilon_n + {}^t\hat{H}^0(-k_x) \end{pmatrix}^{-1}. \tag{35}$$

$\hat{\mathcal{G}}$, $\hat{\mathcal{F}}$, and $\hat{\mathcal{F}}^\dagger$ are the $N_y \times N_y$ Green function in the coexisting SC state. The Green function in the band representation G_b in section 5 is obtained by usingthe unitary matrix $\hat{U}$ on (73).

2.8 linearized triplet gap equation

In the coexisting SC state, the total gap is represented by the anomalous Green function as follows:

$$D^{\uparrow\downarrow}_{y,y'}(k_x, i\varepsilon_n) = T\sum_{k'_x,n',\sigma} V^{\uparrow\downarrow\sigma\bar{\sigma}}_{y,y'}(k_x - k'_x, i\varepsilon_n - i\varepsilon'_n)\mathcal{F}^{\sigma\bar{\sigma}}_{y,y'}(k'_x, i\varepsilon'_n), \tag{36}$$

where $V^{\rm triplet}_{y,y'}(q_x, i\omega_n)$ is the pairing interaction (76). $\bar{\sigma}$ represents the opposite spin to σ. Because of the large calculation cost of eq. 36, the linearized equation is useful for numerical analysis. Thus we derive the linearized triplet gap equation in the presence of the bulk d-wave gap.

First, we extract the triplet component $\phi_{y,y'}(k_x)$ from (36) by considering the relation $\phi_{y,y'}(k_x) = \{D^{\uparrow\downarrow}_{y,y'}(k_x) + D^{\downarrow\uparrow}_{y,y'}(k_x)\}/2$ Then, we obtain the equation for the triplet gap $\phi_{y,y'}(k_x)$ as follows:

$$\phi_{y,y'}(k_x) = T\sum_{k'_x,n} V^{\rm triplet}_{y,y'}(k_x - k'_x, i\varepsilon_n - i\varepsilon_0)F^{\rm triplet}_{y,y'}(k'_x, i\varepsilon_n) \tag{37}$$

where $F^{\rm triplet}_{y,y'}(k_x, i\varepsilon_n) \equiv \{\mathcal{F}^{\uparrow\downarrow}_{y,y'}(k_x, i\varepsilon_n) + \mathcal{F}^{\downarrow\uparrow}_{y,y'}(k_x, i\varepsilon_n)\}/2$ is triplet part of anomalous Green function in the coexisting SC state. $V^{\rm triplet}_{y,y'}(q_x, i\omega_n) \equiv V^{\uparrow\downarrow\uparrow\downarrow}_{y,y'}(q_x, i\omega_n) + V^{\uparrow\downarrow\downarrow\uparrow}_{y,y'}(q_x, i\omega_n)$ is the pairing interaction for triplet SC, which corresponds to (76). Here, we derive the linearized triplet gap equation in the presence of finite d-wave gap from (37). We expand the full Nambu Green function in (73) with respect to $\hat{\phi}$ and $\hat{\phi}^\dagger$, using the following identity:

$$\begin{aligned}
(73) &= \left\{ \begin{pmatrix} \hat{G} & \hat{F} \\ \hat{F}^\dagger & -\hat{\bar{G}} \end{pmatrix}^{-1} - \begin{pmatrix} 0 & \hat{\phi} \\ \hat{\phi}^\dagger & 0 \end{pmatrix} \right\}^{-1} \\
&= \begin{pmatrix} \hat{G} & \hat{F} \\ \hat{F}^\dagger & -\hat{\bar{G}} \end{pmatrix} \\
&+ \begin{pmatrix} \hat{G}\hat{\phi}\hat{F}^\dagger + \hat{F}\hat{\phi}^\dagger\hat{G} & -\hat{G}\hat{\phi}\hat{\bar{G}} + \hat{F}\hat{\phi}^\dagger\hat{F} \\ \hat{F}^\dagger\hat{\phi}\hat{F}^\dagger - \hat{\bar{G}}\hat{\phi}^\dagger\hat{G} & -\hat{F}^\dagger\hat{\phi}\hat{\bar{G}} - \hat{\bar{G}}\hat{\phi}^\dagger\hat{F} \end{pmatrix} \\
&+ \text{higher order terms of } \phi \text{ and } \phi^\dagger.
\end{aligned} \tag{38}$$

where $\hat{G} \equiv \hat{G}(k_x, i\varepsilon_n)$, $\hat{F} \equiv \hat{F}(k_x, i\varepsilon_n)$, $\hat{F}^\dagger \equiv \hat{F}^\dagger(k_x, i\varepsilon_n)$, $\hat{\bar{G}} \equiv {}^t\hat{G}(-k_x, -i\varepsilon_n)$ are the Green function in the pure d-wave SC state introduced in (54). The second term in the right-hand-side of (38) is the first order terms of $\hat{\phi}$ and $\hat{\phi}^\dagger$. Because $\hat{F}$ satisfies the relation in (55), we obtain the relation $\hat{F}^{\rm triplet} = -\hat{G}\hat{\phi}\hat{\bar{G}} + \hat{F}\hat{\phi}^\dagger\hat{F}$. By substituting it into (37), we obtain the linearized triplet gap equation in the presence of bulk d-wave gap, equation (74).

$$\begin{aligned}
\lambda^{\rm edge}\phi_{y,y'}(k_x, i\epsilon_n) &= -T\sum_{k'_x,Y,Y',m} V_{y,y'}(k_x - k'_x, i\epsilon_n - i\epsilon_m) \\
&\times \{G_{y,Y}(k'_x, i\epsilon_m)\phi_{Y,Y'}(k'_x, i\epsilon_m)G_{y',Y'}(-k'_x, -i\epsilon_m) \\
&- F_{y,Y}(k'_x, i\epsilon_m)\phi^\dagger_{Y,Y'}(k'_x, i\epsilon_m)F_{Y',y'}(k'_x, i\epsilon_m)\Big\},
\end{aligned} \tag{39}$$

$$\lambda^{\rm edge}\phi^\dagger_{y,y'}(k_x,i\epsilon_n) = -T\sum_{k'_x,Y,Y',m} V_{y,y'}(k_x-k'_x,i\epsilon_n-i\epsilon_m) \times\Big\{G_{Y,y}(-k'_x,-i\epsilon_m)\phi^\dagger_{Y,Y'}(k_x,i\epsilon'_m)G_{Y',y'}(k'_x,i\epsilon_m) - F^\dagger_{y,Y}(k'_x,i\epsilon_m)\phi_{Y,Y'}(k'_x,i\epsilon_m)F^\dagger_{Y',y'}(k'_x,i\epsilon_m)\Big\}. \quad (40)$$

(We did not study the singlet gap equation because FM fluctuations suppress spin-singlet gaps.) The triplet SC state is realized when the eigenvalue λ in eqs. (74) and (75) reaches unity. Because the odd-frequency pairing state $\hat{\phi}(k_x,i\epsilon_n) = -\hat{\phi}(k_x,-i\epsilon_n)$ is not prohibited in principle.

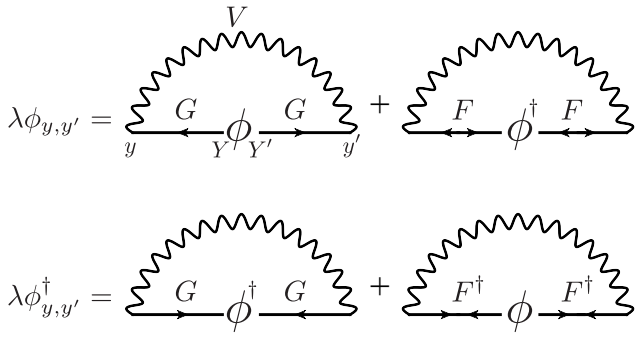

Figure 13: Diagram of the linearized triplet SC gap equation in the presence of the bulk d-wave SC gap. The undulating lines are pairing interactions of the triplet superconductivity. The line with a single arrow represents the Green function $\hat{G}$ and the line with double arrows represents anomalous Green functions $\hat{F}$ and$\hat{F}^\dagger$.

In figure 13 the diagrams of the linearized gap equation (74) and (75) are represented. The pairing interactions V due to spin fluctuations are illustrated by the wavy lines. The GG terms in the diagram correspond to the conventional gap equation in the normal state. In this study, we added the FF terms, which corresponds to the coupling effect between bulk d-wave SC gap and edge-induced triplet gap. Note that we can determine the relative phase between the bulk d-wave gap and edge triplet gap uniquely because mixing of $\hat{\phi}$ and $\hat{\phi}^\dagger$ are included via the effect of the d-wave gap in FF terms. From the view point of the Ginzburg-Landau (GL) theory, the diagrams with GG and those with FF in Fig. 13, respectively correspond to the fourth-order term $|\Delta|^2|\phi|^2$ or Re$\{\Delta^2\phi^{*2}\}$ in the free energy. The latter GL term depends on the relative phase between $\hat{\Delta}$ and $\hat{\phi}$. and the relative phase is determined to minimize the free energy.

3 Edge-induced Strongly Correlated Electronic States in the normal state

3.1 Introduction

In this section, we study the effect of edge on the electron correlation in the normal state by evaluating the site-dependence of spin susceptibility and self-energy based on the RPA and the fluctuation-exchange (FLEX) approximation [1]. In both approximations, the spin fluctuations are enhanced near the open edge. Especially at the $(1,1)$ open edge, prominent FM correlation is developed along the edge. Because of this strong electron correlation, both the mass-enhancement factor ($Z = m^*/m = 1 - \partial\Sigma(\epsilon)/\partial\epsilon|_{\epsilon=0}$) and the quasiparticle damping ($\gamma = \mathrm{Im}\Sigma(-i\delta)$) given by the spin-fluctuation-induced self-energy increase near the open edge. These results can be understood as the emergence of exotic edge electronic states in strongly-correlated metals, like the quantum-critical phenomena, which induce superconductivity, and spin-fluctuation-driven CDW order.

3.2 Model and Theoretical Method

In this section, to understand the exotic electronic state induced at the normal state we study the square-lattice cluster Hubbard model

$$H = \sum_{i,j,\sigma} t_{i,j} c^{\dagger}_{i\sigma} c_{j\sigma} + U \sum_{i} n_{i\uparrow} n_{i\downarrow}, \tag{41}$$

where U is the on-site Coulomb interaction, and $t_{i,j}$ is the hopping integral between sites i and j. We set the nearest, the next nearest, the third-nearest hopping integrals as $(t, t', t'') = (-1, 1/6, -1/5)$ for YBCO tight-binding (TB) model, and $(t, t', t'') = (-1, 1/6, 0)$ for LSCO TB model. Figure 14 (a) shows the Fermi surfaces of YBCO and LSCO TB models for the filling $n = 0.95$ without edges. Figures 14 (b) and (c) show the cluster models with $(1,0)$ and $(1,1)$ open edges, respectively. In both clusters, the layer $y = 1$ or N_y is the edge layer. Both models are periodic along the x direction. The $(1,0)$ edge cluster model is shown in Fig. 14 (b). For the $(1,1)$ edge model, we analyze the one-site unit cell structure shown in the right-hand-side of Fig. 14 (c).

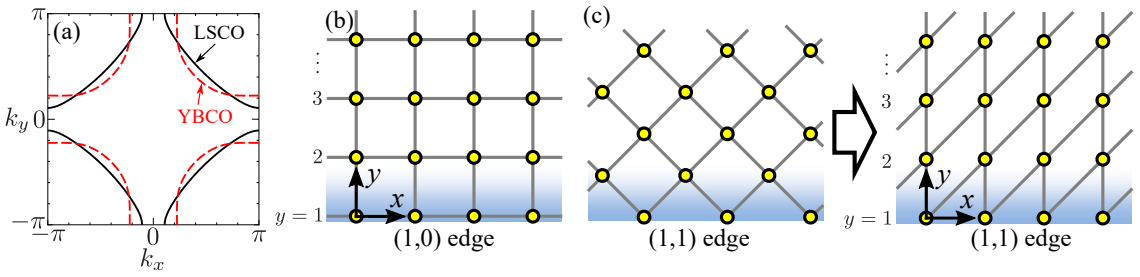

Figure 14: (a) Fermi surfaces in the YBCO and LSCO TB models at filling $n = 0.95$. (b)(c) Cluster models with $(1, 0)$ and $(1, 1)$ open edges, respectively. To simplify the analysis, we modified the original $(1, 1,)$ edge model to the one-site unit cell structure shown in the right-hand-side of (c). In (b) and (c), the solid lines correspond to the nearest-neighbor bonds connected by t.

3.3 Site-dependent spin susceptibilities

Hereafter, we explain the result of the RPA and FLEX analyses for the cluster Hubbard models. The Stoner factor α_S is given as the largest eigenvalue of $U\hat{\chi}^0(q_x, i\omega_l)$ at $i\omega_l = 0$. The magnetic order is realized when $\alpha_S \geq 1$. In both edge models, site number in y-direction is $N_y = 64$, and the models have translational symmetry along x-direction. The number of k_x-meshes is $N_x = 64$, and the number of Matsubara frequencies is 1024. We set the electron filling $n = 0.95$, and the temperature $T = 0.02$. Here, the unit of the energy is $|t|$, which corresponds to ~ 0.4eV in cuprate superconductors without renormalization.

First, we study $\hat{\chi}^s(q_x)$ at $i\omega_l = 0$ using the RPA. Figures 15 (a) and (b) show the static RPA susceptibilities $\chi^s_{y,y}(q_x)$ for the LSCO TB model at $U = 1.39$. The Stoner factor is $\alpha_S = 0.804$ and $\alpha_S = 0.900$ for (a) $(1, 0)$ edge model and (b) $(1, 1)$ edge model, respectively. Both open edge system approaches to the magnetic QCP because $\alpha_S = 0.781$ in the periodic system. In Fig. 15 (a), $\chi^s_{y,y}(q_x)$ in the $(1, 0)$ edge model has the largest peak in the second layer $y = 2$, at the wave vector $q_x = \pi$. Thus, the AFM correlation increases in the second layer. In Fig. 15 (b), $\chi^s_{y,y}(q_x)$ in the $(1, 1)$ edge model has large peak in the first layer $y = 1$ at $q_x = 0$. This result means that strong ferromagnetic (FM) fluctuations develop along the $(1, 1)$ open edge. The obtained FM fluctuations along the edge are consistent with the bulk AFM correlation between next-nearest-neighbor.

Figures 15 (c) and (d) show the static $\chi^s_{y,y}(q_x)$ for the YBCO TB model at $U = 2.13$ for $(1, 0)$ and $(1, 1)$ edge model, respectively. The obtained Stoner factor is $\alpha_S = 0.707$ in the (c) $(1, 0)$ edge model, and $\alpha_S = 0.900$ in the (d) $(1, 1)$ edge model, respectively. Because $\alpha_S = 0.639$ in the periodic system without edge, the spin fluctuations are strongly enlarged near the edge. The obtained spin susceptibility exhibits the essentially similar (q_x, y)-dependence both in the LSCO and YBCO cluster Hubbard model. i(In Fig. 15 (c), $\chi^s_{y,y}(q_x)$ has the largest peak in the first edge layer $y = 1$.) To summarize, strong magnetic fluctuations are generated by introducing the open edge, insensitive to the detail of the TB model parameters.

In Figs. 15 (a)-(d), the y-dependence of $\chi^s_{y,y}(q_x)$ is represented, and it well corresponds to

that Friedel oscillation of the local density-of-states (LDOS), $D_y(\epsilon) = \frac{1}{2\pi^2}\int_{-\pi}^{\pi} dk_x \mathrm{Im}G^0_{y,y}(k_x, \epsilon - i\delta)$, at $\epsilon = 0$. Therefore, the enhancement of the spin-fluctuation is caused by the increment in the LDOS due to the Friedel oscillation by the open edge [54].

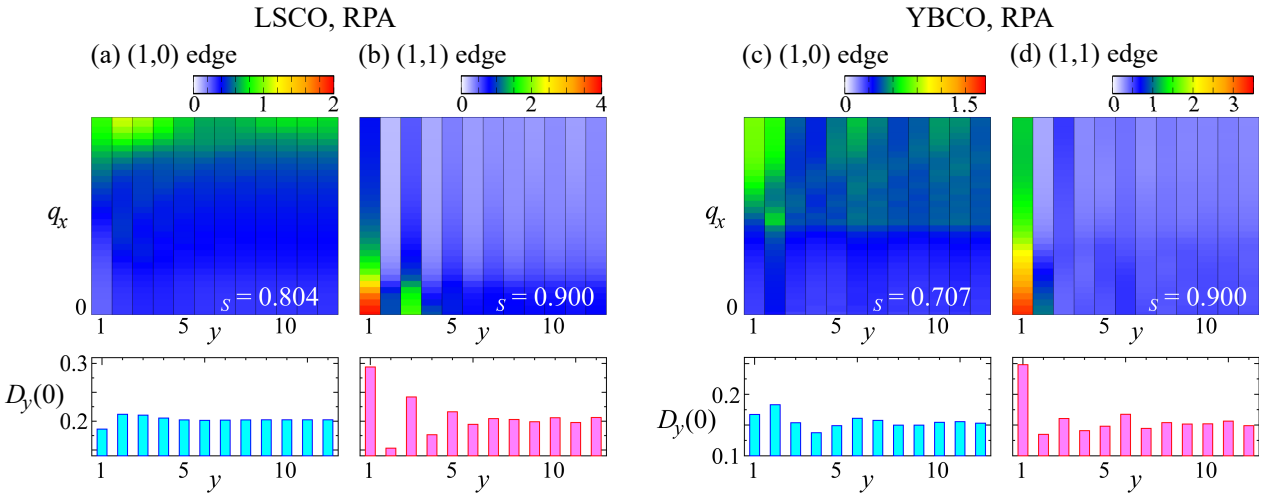

Figure 15: (a) $\chi^s_{y,y}(q_x)$ in the $(1,0)$ edge LSCO model obtained by the RPA (b) LDOS at the Fermi level $D_y(0)$ in the $(1,0)$ edge LSCO model $y = 1$ is the edge layer. (c) $\chi^s_{y,y}(q_x)$ in the $(1,0)$ edge YBCO model obtained by the RPA (d) LDOS at the Fermi level $D_y(0)$ in the $(1,0)$ edge YBCO model

3.4 FLEX results

Next, we explain the result of $\hat{\chi}^s(q_x)$ using the FLEX approximation, in order to consider the negative feedback effect due to the site-dependent self-energy. Figures 16 (a) and (b) show the obtained static $\chi^s_{y,y}(q_x)$ in the LSCO TB model at $U = 1.78$, in the (a) $(1,0)$ edge model and (b) $(1,1)$ edge model. The Stoner factor α_S is 0.900 for both (a) and (b). Note that $\alpha_S = 0.896$ in the periodic system without edges. Figures 16 (c) and (d) show the static $\chi^s_{y,y}(q_x)$ in the YBCO TB model at $U = 3.54$, in the (c) $(1,0)$ edge model ($\alpha_S = 0.880$) and (d) $(1,1)$ edge model ($\alpha_S = 0.900$), respectively. Note that $\alpha_S = 0.836$ in the periodic system.

Therefore, the edge-induced spin-fluctuation enhancement is also obtained by the FLEX approximation. In the YBCO TB model, in the $(1,1)$ edge system, α_S increases from 0.836 (0.641) to 0.900 in the FLEX approximation (RPA). Due to the negative feedback between χ^s and self-energy, the increment of α_S is moderate compared to that in RPA.

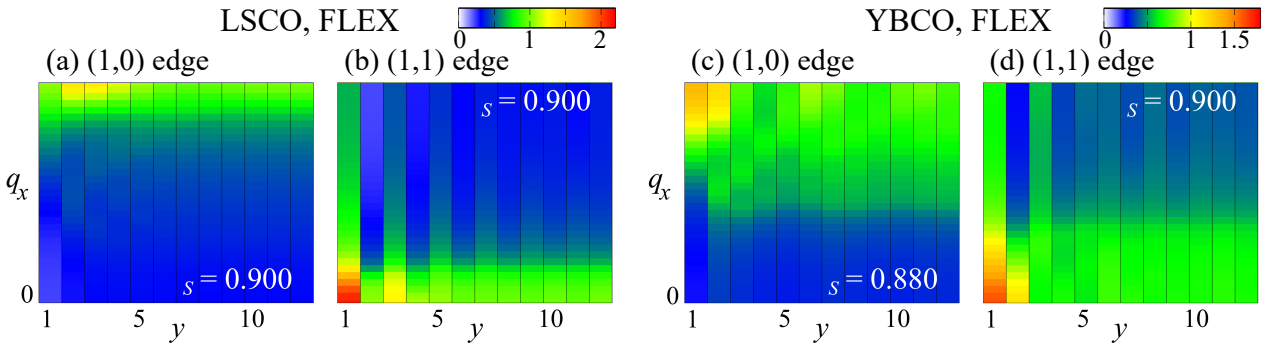

Figure 16: (a)(b) In LSCO TB model: $\chi^s_{y,y}(q_x)$ given by the FLEX approximation (a) $(1,1)$ edge model and (b) $(1,0)$ edge model, respectively. (c)(d) In YBCO TB model: $\chi^s_{y,y}(q_x)$ for the (c) $(1,0)$ edge model and (d) $(1,1)$ edge model, respectively.

3.5 Site-dependent damping and mass-enhancement

Hereafter, we discuss the site-dependence of the self-energy $\hat{\Sigma}(k_y, \epsilon - i\delta)$ given by the FLEX approximation. First, we explain the numerical results in the LSCO TB model. Figure 17 (a) shows the local quasiparticle damping rate at Fermi energy $\gamma_x = \dfrac{1}{2\pi}\displaystyle\int_{-\pi}^{\pi} dk_x \mathrm{Im}\Sigma_{y,y}(k_x, 0 - i\delta)$ in LSCO at $U = 1.78$. In the $(1,0)$ edge model, the site-dependence of γ_y is moderate. In contrast, γ_y at the edge $(y = 1)$ takes large value in the $(1,1)$ edge model, due to the strong spin fluctuations near the edge. Figure 17 (b) shows the local mass-enhancement factor $Z_y = 1 - \dfrac{1}{2\pi}\displaystyle\int_{-\pi}^{\pi} dk_x \frac{\partial}{\partial\epsilon}\mathrm{Re}\Sigma_{y,y}(k_x, \epsilon - i\delta)|_{\epsilon=0}$. In the $(1,0)$ edge model, $Z_y \approx 1.3$ for any y (≥ 1). On the other hand, in the $(1,1)$ edge model, Z_y increases to 1.75 at the edge.

Next, we show the numerical results in the YBCO TB model. Figure 17 (c) shows the obtained γ_y in YBCO at $U = 3.54$. The increase of γ_y is obtained in both $(1,0)$ and $(1,1)$ edge models. In particular for the $(1,1)$ edge model, γ_y drastically increases to 0.022 at the edge layer. Figure 17 (d) shows the obtained Z_y. In the $(1,1)$ edge model, Z_y increases from 2 in the bulk to 3.2 at the edge.

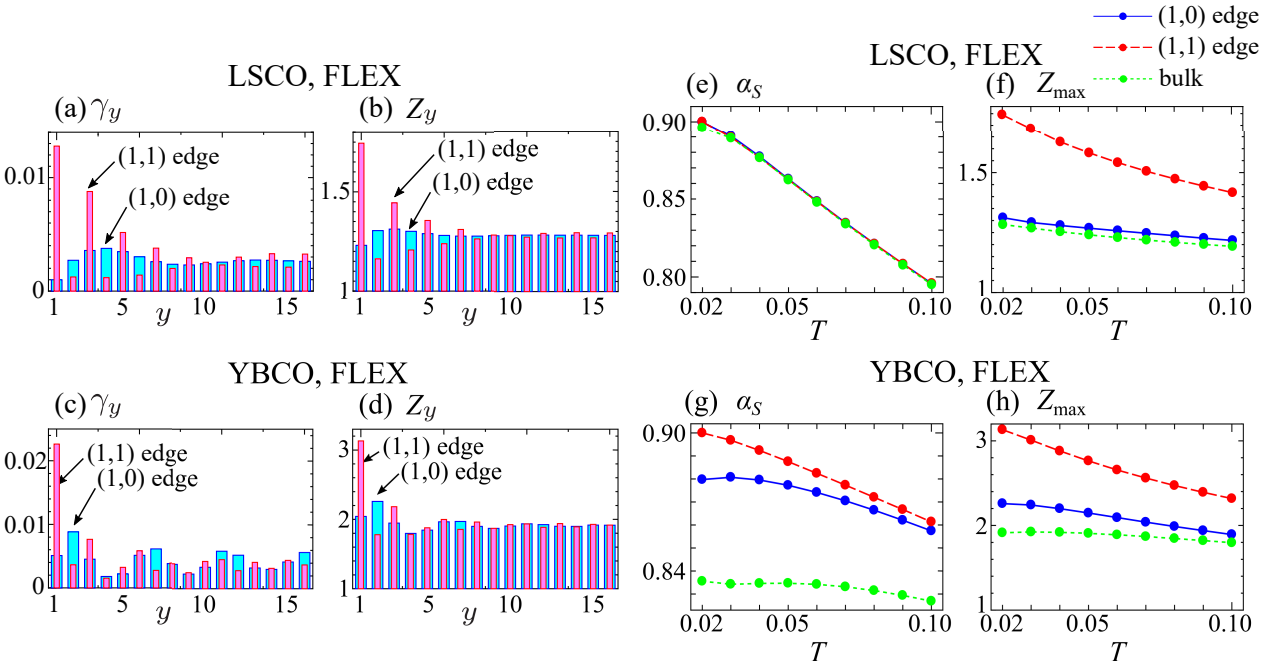

Figure 17: Result of FLEX approximation in the $(1,0)$ edge and $(1,1)$ edge cluster models at $T = 0.02$: (a) Local damping rate γ_y and (b) local mass-enhancement factor Z_y obtained in the LSCO TB model. (c) γ_y and (d) Z_y obtained in the YBCO TB model. T-dependences of the FLEX results in the $(1,0)$ edge and $(1,1)$ edge cluster models, and in the bulk model (without edges). (e) Stoner factor α_S and (f) maximum local mass-enhancement factor $Z_{\max}$ obtained in the LSCO TB model. (g) α_S and (h) $Z_{\max}$ obtained in the YBCO TB model.

Therefore, by introducing the open edge, strong AFM or FM fluctuations are induced near the open edge, even if the bulk AFM fluctuations are moderate ($\alpha_S \sim 0.9$). The induced strong spin fluctuations give rise to huge quasiparticle damping rate and mass enhancement near the open edge. These results indicate that various exotic quantum critical phenomena are expected to emerge near the open edge.

3.6 T-dependences of the electronic states

Finally, we examine the T-dependences of the electronic states in detail based on the FLEX approximation. Figures 17 (e)-(h) show the Stoner factor α_S and the largest local mass-enhancement factor $Z_{\max} = \max_x\{Z_y\}$. The results in LSCO model are shown in Figs. 17 (e) and (f). $Z_{\max}$ strongly increases as T decreases near $(1,1)$ edge by reflecting the large χ^s at the edge layer shown in Fig. 16 (b). In YBCO model, as shown in Figs. 17 (g) and (h), both α_S and $Z_{\max}$ strongly increase as T decreases by introducing the $(1,1)$ edge. Therefore, we predict the edge-induced quantum critical phenomena. In Appendix A we investigate the filling-dependence of the edge-induced quantum critical phenomena by using the FLEX approximation. The enhancement of spin fluctuations is obtained for filling $n = 0.90--1.10$. This information can be a guideline to search the edge-induced quantum criticality in real

materials. We expect that the pseudo-gap behavior due to the large damping is observed experimentally.

3.7 Summary

In this section, we investigated the effect of the edge in the Hubbard model in the normal state. We evaluated the site dependence of the spin susceptibility and self-energy by performing the RPA and FLEX approximation in the real space. The obtained spin susceptibility is modified by the edge and the strong electron correlation is created near the edge layer. Especially, for the $(1, 1)$ edge, ferromagnetic fluctuations drastically develop along the edge. In the FLEX, both the local mass-enhancement factor Z_x and the local quasiparticle damping γ_y given by the spin-fluctuation-induced self-energy becomes huge near the open edge. Thus, interesting edge-induced quantum critical phenomena are predicted by the present study. However, in the framework of the conventional FLEX, the enhancement of χ^s and γ are inevitably underestimated because the vertex corrections to the spin susceptibility are not included [54]. To obtain qualitatively more accurate prediction, the GV^I FLEX is a reliable method because the impurity-enhanced spin fluctuations observed in cuprate are reproduced by this method [54]. Another important future problem is to study the novel edge-induced phenomena because the strong spin fluctuations drive the superconductivity and nematic order proposed in Refs. [22, 24, 30, 33]

4 Emergence of edge-induced strong ferromagnetic fluctuations caused by the Andreev bound state in d-wave superconductors

4.1 Introduction

In this section, we investigate the drastic effects of the ABS on the surface electron correlation. For this purpose, we analyze the two-dimensional cluster Hubbard model with the $(1,1)$ edge in the bulk d-wave SC state, and calculate the site-dependent spin susceptibility by performing random-phase-approximation (RPA) and modified FLEX approximation (GV^I-FLEX) in the real space [54]. In the bulk d-wave SC state, the strong FM fluctuations are induced at the $(1,1)$ edge compared to the normal state without bulk d-wave gap. Furthermore, this strong surface ABS-induced FM fluctuations may drive interesting emerging phenomena, such as edge-induced SC.

4.2 Model

In this analysis, we analyze the square-lattice cluster Hubbard model in the presence of the d-wave SC gap:

$$H = \sum_{i,j,\sigma} t_{i,j} c^\dagger_{i\sigma} c_{j\sigma} + U \sum_i n_{i\uparrow} n_{i\downarrow} + \sum_{i,j} \Delta^d_{i,j} \left(c^\dagger_{i\uparrow} c^\dagger_{j\downarrow} + c_{j\downarrow} c_{i\uparrow} \right), \tag{42}$$

where $t_{i,j}$ is the hopping integral between sites i and j. We set the nearest, next nearest, and third-nearest hopping integrals as $(t, t', t'') = (-1, 1/6, -1/5)$, which correspond to the YBCO tight-binding (TB) model. $c^\dagger_{i\sigma}$ and $c_{i\sigma}$ are the creation and annihilation operators of an electron with spin σ, respectively. U is the on-site Coulomb interaction, and $\Delta^d_{i,j} \equiv \Delta^{d,\uparrow\downarrow}_{i,j}$ is the d-wave SC gap between sites i and j.

4.3 Numerical result of $\hat{\chi}$ and α_S by the RPA in real space

Next, we calculate the site-dependent spin susceptibility by the RPA in real space. We set the number of k_x-meshes as $N_x = 64$, that of sites along the y-direction as $N_y = 64$ and that of Matsubara frequencies as $N_\omega = 1024$. The electron filling, $n = 0.95$. We set the Coulomb interaction as $U = 2.25$ in the RPA. Here, the unit of energy is $|t| = 1$, which corresponds to ~ 0.4eV in cuprate superconductors. We set the transition temperature for the d-wave SC as $T_{cd} = 0.04$. In addition, $\Delta_{\max}$ is defined as the maximum value of the d-wave gap on the Fermi surface. In the present model, $\Delta_{\max} = 1.76\Delta^d_0$ for $n = 0.95$. Experimentally, $4 < 2\Delta_{\max}/T_{cd} < 10$ in YBCO [138, 139]. Therefore, we set $\Delta^d_0 = 0.06$ or 0.09, which corresponds to $2\Delta_{\max}/T_{cd} = 5.28$ or 7.92 for $T_{cd} = 0.04$. By performing this analysis, we show that the FM fluctuations are drastically enhanced by the ABS at the $(1,1)$ edge, and the system rapidly approaches a magnetic-order phase.

First, we explain the site-dependent static spin susceptibility, $\hat{\chi}(q_x, \omega_l = 0)$, in the d-wave SC state using the RPA. Hereafter, $\hat{\chi}^{(n)}$ denotes the spin susceptibility in the normal state. To analyze the origin of the enhancement in the FM fluctuations, we introduce the following susceptibilities:

$$\hat{\chi}' = \hat{\Phi}'(1 - U\hat{\Phi}')^{-1} \quad (\hat{\Phi}' = \hat{\chi}^0), \tag{43}$$

$$\hat{\chi}'' = \hat{\Phi}''(1 - U\hat{\Phi}'')^{-1} \quad (\hat{\Phi}'' = \hat{\chi}^{0(n)} + \hat{\varphi}^0). \tag{44}$$

Here, $\hat{\chi}^0$ and $\hat{\chi}^{0(n)}$ are the irreducible susceptibilities in the bulk d-wave SC and normal states, respectively. In susceptibilities $\hat{\chi}'$ and $\hat{\chi}''$, the effect of d-wave gap in $\hat{\varphi}^0$ and $\hat{\chi}^0$ are dropped, respectively.

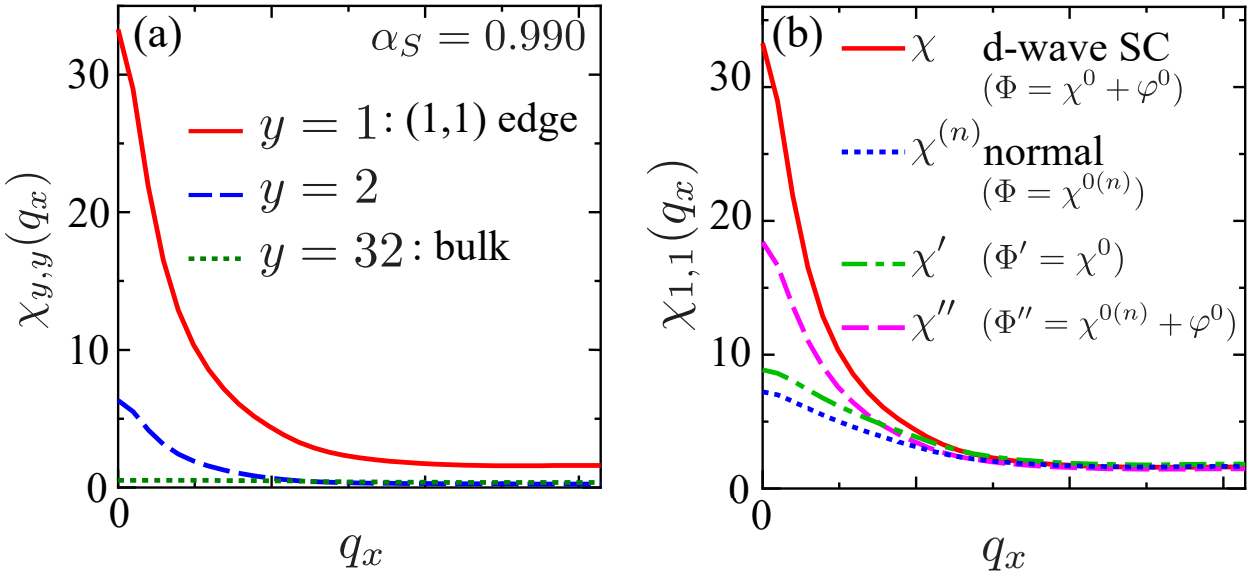

Figure 18: (a)q_x-dependence of $\chi_{y,y}(q_x)$ obtained by the RPA for $\Delta_0^d = 0.09$ at $T = 0.0365$. The value of y corresponds to the depth from the $(1,1)$ edge. $y = 1$ is the $(1,1)$ edge and $y = 32$ corresponds to the bulk. (b)Comparison between $\chi_{1,1}(q_x)$, $\chi_{1,1}^{(n)}(q_x)$, $\chi'_{1,1}(q_x)$, and $\chi''_{1,1}(q_x)$ for $\Delta_0^d = 0.09$ at $T = 0.0365$.

Figure 18 (a) shows the spin susceptibilities for $\Delta_0^d = 0.09$ at $T = 0.0365$. $\chi_{y,y}(q_x)$ represents the correlation between spins in the same layer y at $\omega_l = 0$. $\chi_{y,y}(q_x)$ has a large peak at $q_x = 0$ in the edge layer ($y = 1$). It means that strong FM fluctuations develop along the $(1,1)$ edge layer. The FM correlation in the edge layer is consistent with the next-nearest-neighbor correlation of the bulk AFM correlation.This strong enhancement occurs only for $y = 1$ and $y = 2$. The Stoner factor is $\alpha_S = 0.990$ with the edge, whereas $\alpha_S = 0.673$ in the periodic model. Therefore, this system approaches the magnetic quantum critical point with introduction of the edge.

Next, we compare the d-wave SC and normal state. Figure 18 (b) shows $\chi_{1,1}$ and $\chi_{1,1}^{(n)}$ in the model with edge. The enhancement in the FM fluctuations is much more drastic in the

d-wave SC state compared to that in the normal state discussed in section 3Therefore, this strong enhancement cannot be explained only by the existence of edge.

Furthermore, we examine the contribution from $\hat{\varphi}^0$ and $\hat{\chi}^0$ to the enhancement of total spin susceptibility. In Figure 18 (b), $\chi'_{1,1}(q_x)$ and $\chi''_{1,1}(q_x)$ are represented. The height of the peak of $\hat{\chi}'$ is much smaller than that of $\hat{\chi}$. Although $\hat{\chi}''$ is smaller than $\hat{\chi}$, $\hat{\chi}''$ has a larger and sharper peak at $q_x = 0$ than that of $\hat{\chi}'$. Therefore, increment of $\hat{\chi}$ can be mainly explained by the emergence of $\hat{\varphi}^0$ due to anomalous Green functions. Also $\hat{\chi}^0 - \hat{\chi}^{0(n)}$ gives minor contribution since $\hat{\chi}' > \hat{\chi}^{(n)}$.

Figure 19(a) shows the q_x-dependence of $\hat{\varphi}^0$. In the bulk, $\varphi^0_{32,32}$ is zero because x-axis corresponds to the direction of d-wave gap node. Interestingly, $\varphi^0_{1,1}$ has a peak at $q_x = 0$. This is explained as an effect of the ABS, which corresponds to the odd-frequency SC pairing amplitude induced at the $(1,1)$ edge as discussed in Refs. [91, 119]. We give brief discussion on this issue in Appendix C. In Figure 19(b), we show the q_x-dependence of $\hat{\chi}^0$ and $\hat{\chi}^{0(n)}$. At the edge, $\chi^0_{1,1}$ is slightly larger than $\chi^{0(n)}_{1,1}$ due to the emergence of large ABS peak in the d-wave SC state.

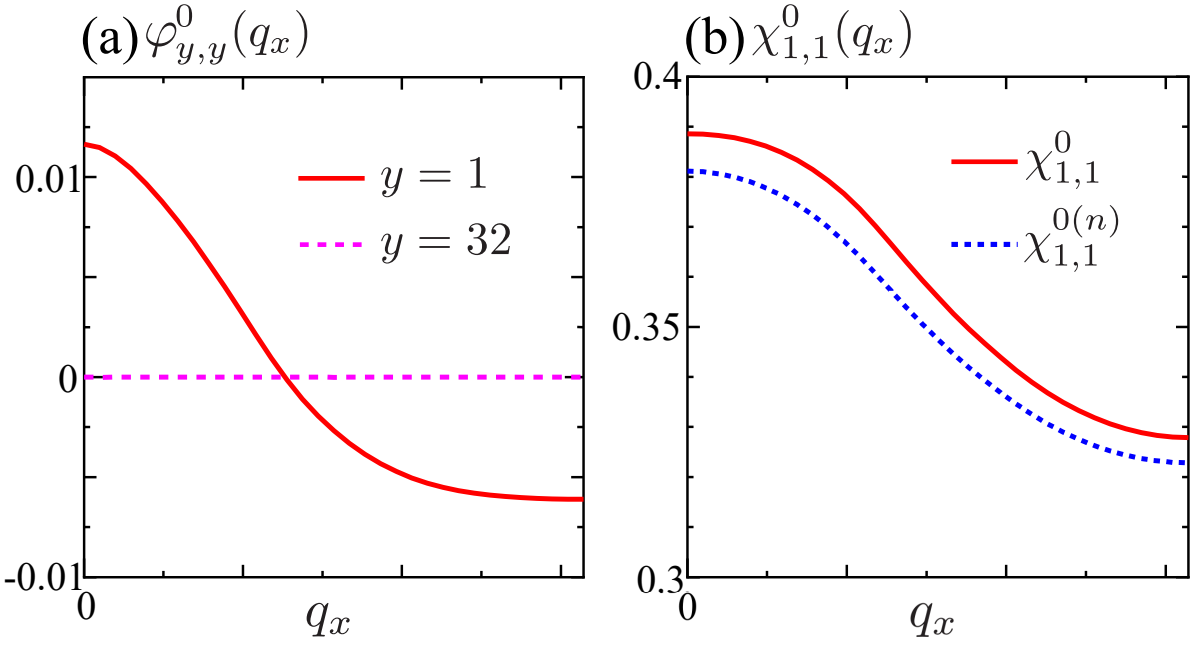

Figure 19: q_x-dependence of irreducible susceptibilities for $\Delta^d_0 = 0.09$ at $T = 0.0365$. (a) Comparison between $\varphi^0_{y,y}(q_x)$ at the edge ($y = 1$) and in the bulk ($y = 32$). (b) Comparison between $\chi^0_{1,1}(q_x)$ and $\chi^{0(n)}_{1,1}(q_x)$.

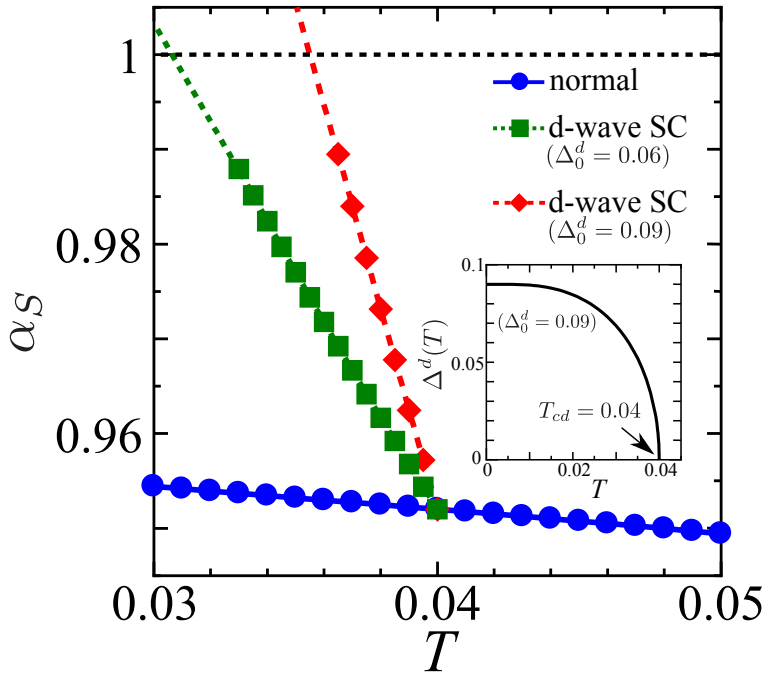

Figure 20: T-dependence of α_S in the RPA. The inset shows the T-dependence of the size of the d-wave gap. We assume that the BCS-like T-dependence given by (19). We set the transition temperature of the d-wave SC as $T_{cd} = 0.04$.

Figure 20 shows the T-dependence of α_S in the RPA. The inset is the T-dependence of the d-wave gap given in Eq.(19). As T decreases, α_S in the SC state increases sharply compared to that in the normal state, due to the development of the ABS.

The increase for $\Delta_0^d = 0.09$ is steeper than that for $\Delta_0^d = 0.06$ because the height of the ABS peak is proportional to Δ_0^d. α_S reaches unity at $T \approx 0.036$ for $\Delta_0^d = 0.09$, and the edge FM order is realized. To summarize, we found the emergence of FM order at $(1, 1)$ edge of $d_{x^2-y^2}$-wave superconductors.

4.4 FLEX analysis

4.4.1 GV^I-FLEX

In this section, we investigate the spin susceptibility using modified FLEX (GV^I-FLEX) approximation proposed in Ref. [54], since the negative feedback effect on $\hat{\chi}$ near the impurity is prominently overestimated in conventional FLEX. The negative feedback is suppressed near the impurity by vertex corrections, which is not taken into account by the FLEX approximation [54]. In the modified FLEX, the cancellation between negative feedback and vertex corrections is assumed, and the experimental result is reproduced even for the single impurity problem [54].

To apply the modified FLEX to the present model, we first calculate the self-energy in the periodic system without the edge, $\Sigma^0(k_x, k_y, i\varepsilon_n)$, using the conventional FLEX ap-

proximation. Then, by performing the Fourier transformation for y-direction, we obtain $\Sigma^0(k_x, y, y', i\varepsilon_n) = \Sigma^0(k_x, y - y', i\varepsilon_n)$. Next, we calculate the Green functions in the $(1,1)$ edge model with $\Sigma^0(k_x, y, y', i\varepsilon_n)$

$$\begin{pmatrix} \hat{G}^I(k_x, \epsilon_n) & \hat{F}^I(k_x, \epsilon_n) \\ \hat{F^I}^\dagger(k_x, \epsilon_n) & -\hat{G}^I(k_x, -\epsilon_n) \end{pmatrix} = \begin{pmatrix} \epsilon_n \hat{1} - \hat{H}^0(k_x) - \hat{\Sigma}^0(k_x, i\varepsilon_n) & -\hat{\Delta}^d(k_x) \\ -\hat{\Delta}^d(k_x) & \epsilon_n \hat{1} + \hat{H}^0(k_x) + \hat{\Sigma}^0(k_x, -i\varepsilon_n) \end{pmatrix}^{-1}, \tag{45}$$

where $\hat{H}^0(k_x)$ is the tight-binding model with the $(1,1)$ edge. In the GV^I-FLEX, the spin susceptibility is calculated by $\hat{G}^I$, $\hat{F}^I$, and $\hat{F^I}^\dagger$ instead of $\hat{G}$, $\hat{F}$, and $\hat{F}^\dagger$ in Eqs.(23)–(26).

In this approximation, the renormalized bulk SC gap function is evaluated by $\Delta_0^{d*} = \Delta_0^d / Z_{\rm bulk}$, where $Z_{\rm bulk}$ is the on-site mass-enhancement factor in the bulk.

4.4.2 Numerical result of $\hat{\chi}$ and α_S in real space

In the numerical study of GV^I-FLEX, we set the number of k_x-meshes as $N_x = 64$, that of sites along the y-direction as $N_y = 64$, and that of Matsubara frequencies as $N_\omega = 1024$. We set the electron filling, $n = 0.95$; the transition temperature for the d-wave is $T_{cd} = 0.04$. The Coulomb interaction is $U = 2.65$.

Figure 21 shows the q_x-dependence of $\chi_{y,y}(k_x)$ in the GV^I-FLEX for $\Delta_0^d = 0.12$ at $T = 0.036$. With this parameter, we obtain $Z_{\rm bulk} = 1.37$, $\Delta_0^{d*} \approx 0.087$ and $2{\Delta_{\rm max}}^*/T_{cd} \approx 7.69$. At the $(1,1)$ edge ($y = 1$), $\chi_{1,1}(q_x)$ has a large peak at $q_x = 0$. The Stoner factor increases to $\alpha_S = 0.989$ by introducing the $(1,1)$ edge, whereas $\alpha_S = 0.699$ in the periodic system with FLEX self-energy. Therefore, the enhancement in the FM fluctuations at the edge is obtained by both the RPA and GV^I-FLEX.

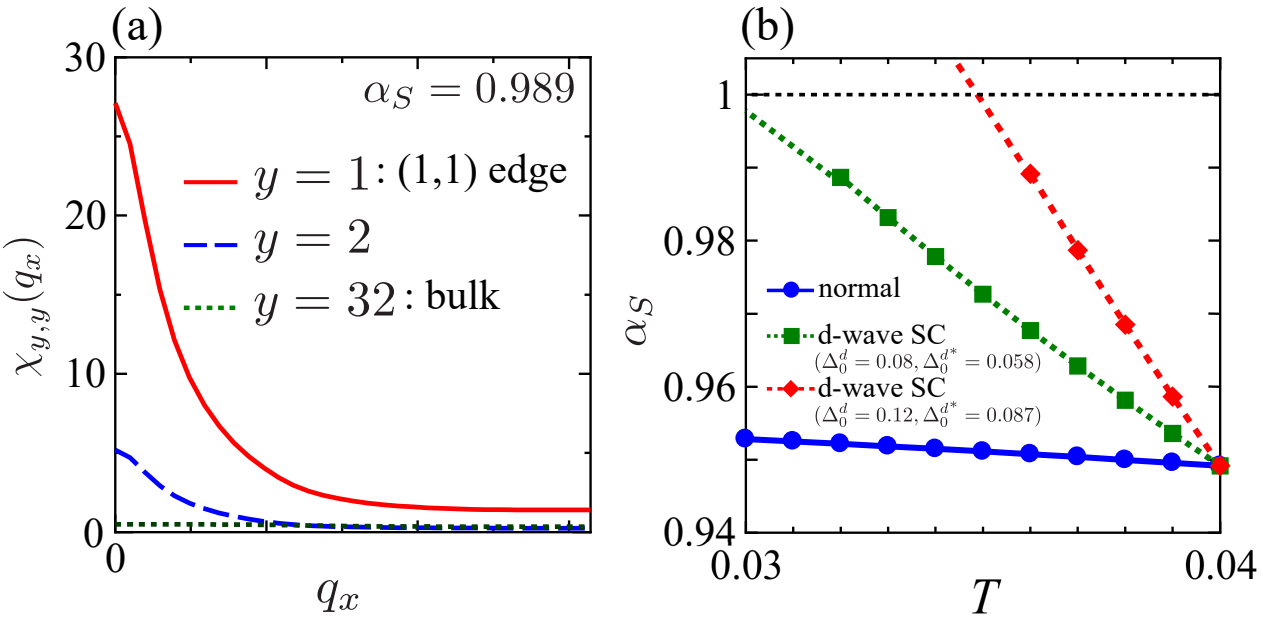

Figure 21: (a)q_x-dependence of $\chi_{y,y}(q_x)$ obtained by the GV^I-FLEX for $\Delta_0^d = 0.12$ at $T = 0.036$. $y = 32$ corresponds to the bulk. With this parameter, we obtain $Z_{\rm bulk} = 1.37$. The renormalized gap is $\Delta_0^{d*} \approx 0.087$ and $2\Delta_{\rm max}{}^*/T_{cd} \approx 7.69$. (b)$T$-dependence of α_S in the GV^I-FLEX. We set the transition temperature of the d-wave SC as $T_{cd} = 0.04$. We obtained $\Delta_0^{d*} \approx 0.058$ and $2\Delta_{\rm max}{}^*/T_{cd} \approx 5.11$ for $\Delta_0^d = 0.08$.

Figure 21 shows the T-dependence of α_S in $(1,1)$ edge cluster model given by the GV^I-FLEX. In the normal state, α_S increases gently as T decreases. On the other hand, in the presence of bulk d-wave SC gap, α_S shows a drastic increase as T decreases. For $\Delta_0^d = 0.08$, the mass-enhancement factor is $Z_{\rm bulk} = 1.38$ at $T = 0.032$. Thus, we obtain $\Delta_0^{d*} \approx 0.058$ and $2\Delta_{\rm max}{}^*/T_{cd} \approx 5.11$. For $\Delta_0^d = 0.12$, α_S reaches 0.99 at $T = 0.036$. For a fixed ratio $2\Delta_{\rm max}{}^*/T_{cd}$, the obtained T-dependence of α_S is comparable in both the RPA and GV^I-FLEX.

4.5 Effect of the finite d-wave coherence length on the edge-induced spin fluctuations

In the real cuprate superconductors, the d-wave gap is suppressed near the edge for a finite range, $1 \le y \le \xi_d$, where ξ_d is the coherence length of the d-wave SC. In this section, we examine the effect of the suppression of the d-wave gap on the edge-induced FM fluctuations. The suppression of the d-wave gap is treated as follow:

$$\Delta^d_{y,y'}(k_x, T)\left\{1 - \exp\left(\frac{y + y' - 2}{2\xi_d}\right)\right\}. \tag{46}$$

Note that, the anomalous self-energy for the d-wave SC gap is calculated self-consistently in the SC FLEX approximation below T_{cd} [4]. If the SC FLEX is applied to the edge cluster

model, the d-wave gap for $y \lesssim \xi_d$ should be naturally suppressed. Instead, we set ξ_d as a parameter to simplify the analysis. From the experimental results [134–137], ξ_d is estimated as 3 sites for $T \ll T_{cd}$. For $T \lesssim T_{cd}$, $\xi_d \gg 3$ due to the relation $\xi_d \propto (1-T/T_{cd})^{-1/2}$ in the GL theory. Therefore, we set $\xi_d = 3$ and 10 in this analysis. Figure 22(a) shows the y-dependence of given $|\Delta^d_{x=0,y+1;x=0,y}|$. The inset represents the corresponding nearest neighbor bonds in the real space. Figure 22(b) shows the LDOS at the edge. Although the height of the peak of the ABS is reduced, the peak structure remains for finite ξ_d ($\lesssim 10$).

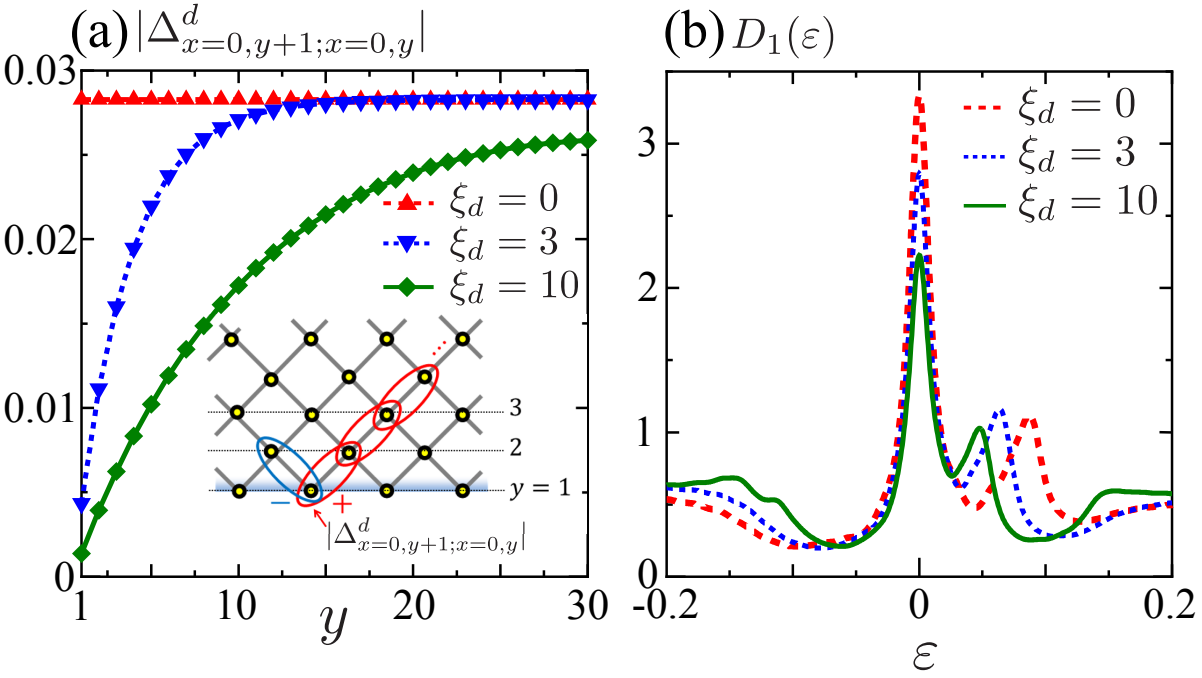

Figure 22: (a) Site-dependence of the d-wave gap suppressed near the edge over ξ_d. We set $\Delta^d_0 = 0.08$, and plot it at $T = 0.032$. $\xi_d = 0$ corresponds to the site-independent d-wave gap. The inset shows the nearest neighbor bonds corresponding to $|\Delta^d_{x=0,y+1;x=0,y}|$. (b) LDOS at the $(1,1)$ edge for the finite ξ_d.

Next, we discuss the effect of the coherence length of d-wave gap on the enhancement of the FM fluctuations. In Figure 23 (a), α_S for $\Delta^d_0 = 0.06$ is represented. When the suppression of d-wave gap is taken into account ($\xi_d = 3, 10$), the increase in α_S becomes moderate, because the ABS is suppressed by ξ_d as shown in Fig. 22. Especially for $\xi_d = 10$, $\alpha_S \approx 0.97$ even at $T = 0.03$. On the other hand, for $\Delta^d_0 = 0.06$ shown in Fig. 23 (b), α_S reaches 0.986 at $T = 0.03$ even for $\xi_d = 10$. Therefore, we conclude that the drastic enhancement in the FM fluctuations is realized under the conditions $2\Delta_{\max}/T_{cd} \gtrsim 6$ and $\xi_d \ll 10$, both of which are satisfied in real cuprate superconductors.

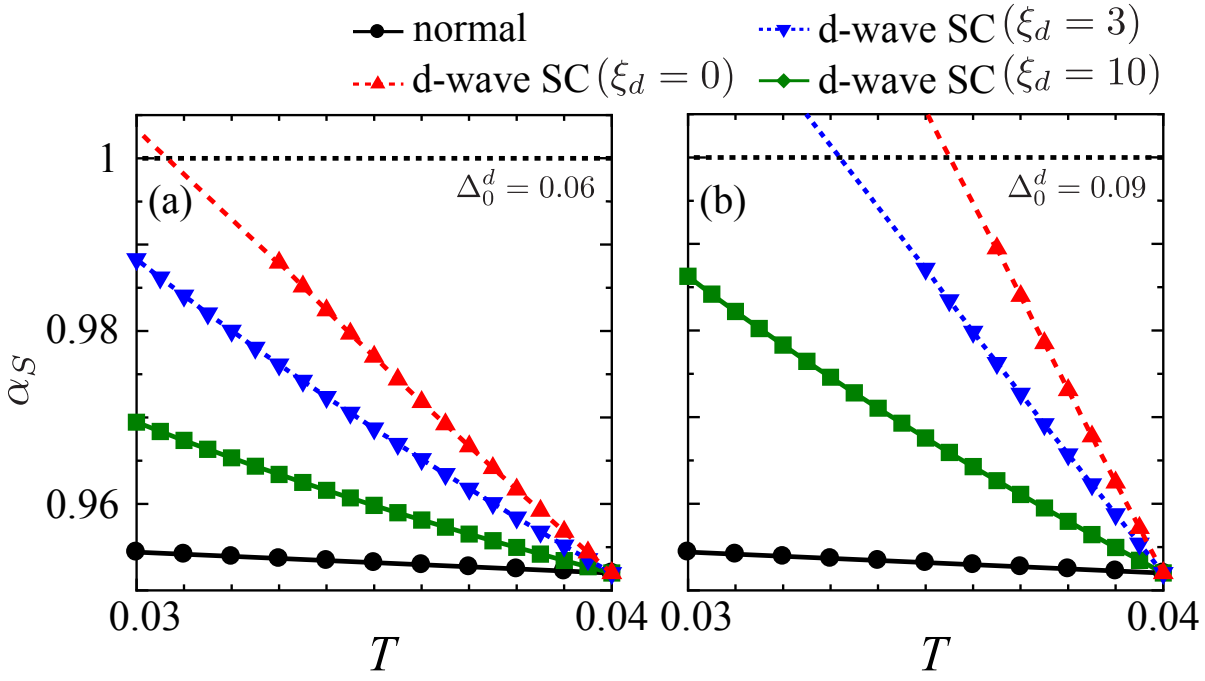

Figure 23: T-dependence of α_S by the RPA for (a) $\Delta_0^d = 0.06$ or (b) 0.09 with finite ξ_d. The red dashed line represents α_S for the site-independent d-wave gap. The black solid line represents α_S in the normal state.

4.6 Summary

In this section, we discussed the effect of the ABS on the electron correlation near the $(1,1)$ edge. We found that the FM fluctuations are drastically enhanced by the ABS in the presence of the bulk d-wave SC gap. We construct the two-dimensional square lattice Hubbard model with the open edge in the presence of the bulk d-wave SC gap. Then we perform the numerical calculation of the site-dependent RPA. By the detailed analysis, we clarified that the ABS enhances the FM fluctuations through the increment of irreducible susceptibility $\hat{\varphi}^0$. Furthermore, the Stoner factor α_S exhibits drastic increase just below the bulk d-wave T_c, and edge-induced FM order or strong fluctuations is realized. We obtained this ABS-induced magnetic critical phenomena also in the GV^I-FLEX. The present analysis is performed under the conditions $2\Delta_{\max}/T_{cd} \gtrsim 6$ and $\xi_d \ll 10$, which are satisfied in cuprate superconductors. Therefore, we conclude that the ABS-induced FM order or strong FM fluctuations emerge in real cuprate superconductors. If the edge FM order is realized, the ABS peak splits due to the time-reversal-symmetry breaking. Figure 24 shows the LDOS for up and down spins at the edge with the magnetization ($M_0 = 0.10$). The magnetization is given by the Zeeman term $H_M = M_0/2 \sum_{k_x,\sigma} \sigma c^\dagger_{k_x 1\sigma} c_{k_x 1\sigma}$. This splitting may be observed by STM/STS experiment. In addition, an edge-induced triplet SC is expected to be realized theoretically, and we examine this scenario in the next section.

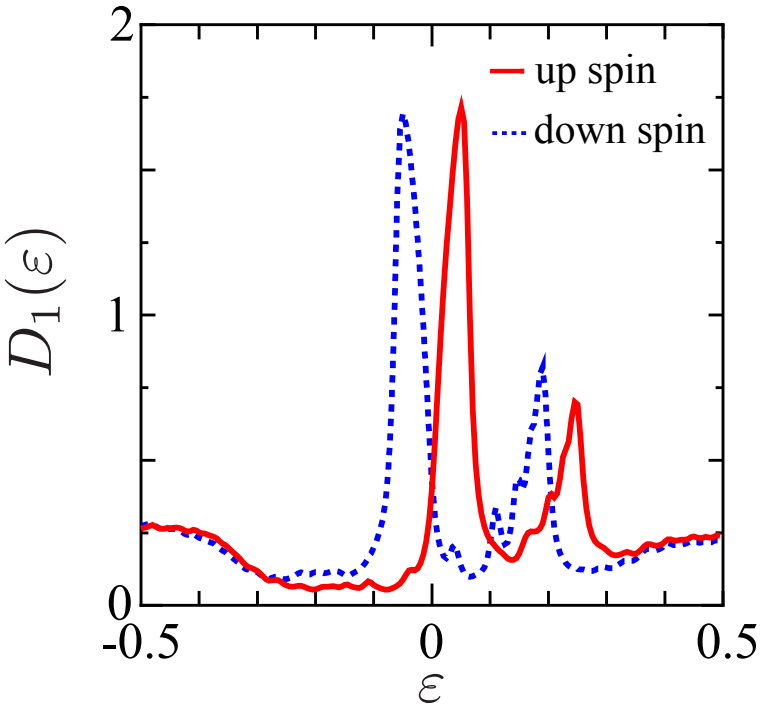

Figure 24: LDOS at the edge of d-wave superconductor ($\Delta^d = 0.20$) when the magnetization ($M_0 = 0.10$) emerges. The red solid line and blue dotted line represent the LDOS for up and down spins, respectively. For convenience, we set $\delta = 0.01$.

5 Edge-induced $d \pm ip$-wave superconducting state mediated by Andreev-bound-state-driven ferromagnetic fluctuations in d-wave superconductors

5.1 Introduction

In the superconducting (SC) states, the effects of real-space structures on the electron correlation had not been revealed until recently. Recently, interesting impurity-induced critical phenomena have been analyzed theoretically [140, 141]. In addition, we discussed surface-induced critical phenomena in the d-wave superconductors in section 4, and we found that the key ingredient is the surface Andreev bound states (ABS) [64–69], which is observed in the STM experiment as the zero-bias conductance peak [71–74]. In the previous section we revealed that the strong FM fluctuations around the $(1, 1)$ edge is triggered by the huge edge DOS due to the ABS by performing the site-dependent random-phase approximation (RPA) and modified fluctuation-exchange (FLEX) approximation. In this case, the strong FM fluctuations may induce exotic phenomena such as the triplet superconductivity [82–86].

At surface or interface, emergence of exotic SC state that cannot be realized in the bulk is expected and has been studied very actively. Near the $(1, 1)$ edge of the $d_{x^2-y^2}$-wave superconductor, the s-wave superconductivity can emerge by using the ABS, and an $d \pm is$-wave SC state is realized [76–78, 142–145]. In this case, the zero-bias conductance peak splits and the edge current flows along the edge due to the time-reversal symmetry breaking. At the domain wall, the emergence of time-reversal breaking superconductivity is also pointed out with regards to the polycrystalline $YBa_2Cu_3O_{7-x}$ (YBCO) [79, 146, 147] and twined iron-based superconductor FeSe in the nematic phase [80]. However, the site-dependence of pairing interaction has not been considered, although the edge-induced strong FM fluctuations are large only near the edge and have strong site-dependence. Recently, the emergence of the fractional vortices and supercurrent near the $(1, 1)$ edge is proposed [148, 149]. In this case, the ABS is shifted to the finite energy, and the time-reversal symmetry is broken.

In this section, we explain the emergence of the triplet superconductivity near the $(1, 1)$ edge of the d-wave superconductors. The origin of the triplet gap is the strong FM fluctuations discussed in section 4. We first explain the linearized gap equation for the even-frequency triplet superconductivity and apply it to the two-dimensional cluster Hubbard model with the $(1, 1)$ edge in the bulk d-wave SC state. We calculate the site-dependent pairing interaction based on the RPA or GV^I-FLEX. By analyzing the linearized gap equation, we found that the relative phase difference between the bulk d-wave gap and the edge triplet gap is $\pi/2$ in the $\boldsymbol{k}$-space. Therefore, we predict the emergence of the exotic edge-induced $d \pm ip$-wave SC state at $T = T_{cp}$, which is slightly low temperature compared to the bulk d-wave transition temperature T_{cd}. This $(1, 1)$ edge system may be used for a platform of realizing exotic SC states.

5.2 Theoretical method of triplet gap equation

To study the edge-induced triplet superconductivity, we introduce a two-dimensional square lattice Hubbard model with the $(1,1)$ edge in the bulk d-wave SC state:

$$\mathcal{H} = \sum_{i,j,\sigma} t_{i,j} c^{\dagger}_{i\sigma} c_{j\sigma} + U \sum_{i} n_{i\uparrow} n_{i\downarrow} + \sum_{i,j} \left(\Delta^{\uparrow\downarrow}_{i,j} c^{\dagger}_{i\uparrow} c^{\dagger}_{j\downarrow} + h.c. \right), \tag{47}$$

where $t_{i,j}$ is the hopping integral between sites i and j. We set the nearest, next nearest, and third-nearest hopping integrals as $(t, t', t'') = (-1, 1/6, -1/5)$, which correspond to the YBCO TB model. $c^{\dagger}_{i\sigma}$ and $c_{i\sigma}$ are creation and annihilation operators of an electron with spin σ, respectively. U is the on-site Coulomb interaction, and $\Delta^{\uparrow\downarrow}_{i,j} = -\Delta^{\uparrow\downarrow}_{i,j} \equiv \Delta_{i,j}$ is the bulk d-wave SC gap. $y = 1$ corresponds to the $(1,1)$ edge layer. In this model, the translational symmetry along y direction is violated, whereas the model is periodic along the x direction. Thus, following analysis have to be analyzed in (k_x, y, y')-representation obtained by the Fourier transformation only on the x direction. Next, we assume that $\Delta_{i,j}$ is real and nonzero only between the nearest neighbor sites, and set it as $\Delta_{i,j} = \Delta/2(\delta_{x,x'+1}\delta_{y,y'+1} + \delta_{x,x'-1}\delta_{y,y'-1} - \delta_{x,x'}\delta_{y,y'+1} - \delta_{x,x'}\delta_{y,y'-1})$. By performing the Fourier transformation on x direction, we obtain its (k_x, y, y')-representation as

$$\Delta_{y,y'}(k_x, T) = \Delta(T) \left\{ \frac{e^{-ik_x} - 1}{2} \delta_{y,y'+1} + \frac{e^{ik_x} - 1}{2} \delta_{y,y'-1} \right\}, \tag{48}$$

$$\Delta(T) = \Delta_0 \tanh \left(1.74 \sqrt{\frac{T_{cd}}{T} - 1} \right), \tag{49}$$

where $\Delta(T)$ is the temperature-dependent d-wave gap and $\Delta_0 \equiv \Delta(T = 0)$. Note that the $\boldsymbol{k}$-dependence of d-wave gap in the bulk is represented by $\Delta(\boldsymbol{k}, T) = \Delta(T)(\cos k_x - \cos k_y)$.$T_{cd}$ is the transition temperature of the d-wave superconductivity.

Next, we confirm the relations of the bulk d-wave gap because it is important for the analysis of the relative phase between bulk d-wave gap and edge-induced triplet gap. Due to the anticommutation relation of the fermion, the SC gap satisfies

$$\Delta_{y,y'}(k_x) \equiv \Delta^{\uparrow\downarrow}_{y,y'}(k_x) = -\Delta^{\downarrow\uparrow}_{y',y}(-k_x). \tag{50}$$

The singlet SC gap is defined as

$$\Delta^{\uparrow\downarrow}_{y,y'}(k_x) = -\Delta^{\downarrow\uparrow}_{y,y'}(k_x). \tag{51}$$

By using (50) and (51), the singlet gap satisfies

$$\Delta^{\uparrow\downarrow}_{y,y'}(k_x) = \Delta^{\uparrow\downarrow}_{y',y}(-k_x). \tag{52}$$

Because we set $\Delta_{i,j}$ without the loss of generality, the present real d-wave gap given by (48) satisfies

$$\Delta^{\uparrow\downarrow}_{y,y'}{}^{*}(-k_x) = \Delta^{\uparrow\downarrow}_{y,y'}(k_x). \tag{53}$$

Hereafter, we introduce the $N_y \times N_y$ matrix representations of the d-wave gap function $\hat{\Delta}(k_x)$, which is defined as $\{\hat{\Delta}(k_x)\}_{y,y'}=\Delta_{y,y'}(k_x)$.

Then, $N_y \times N_y$ Green functions in the d-wave SC state $\hat{G}$, $\hat{F}$, and $\hat{F}^\dagger$ are defined as follows:

$$\begin{pmatrix} \hat{G}(k_x, i\epsilon_n) & \hat{F}(k_x, i\epsilon_n) \\ \hat{F}^\dagger(k_x, i\epsilon_n) & -\hat{G}(k_x, -i\epsilon_n) \end{pmatrix} = \begin{pmatrix} i\epsilon_n \hat{1} - \hat{H}^0(k_x) & -\hat{\Delta}(k_x) \\ -\hat{\Delta}(k_x) & i\epsilon_n \hat{1} + \hat{H}^0(k_x) \end{pmatrix}^{-1}, \tag{54}$$

where $\epsilon_n = (2n+1)\pi T$ is the fermion Matsubara frequency. $\hat{F}$ and $\hat{F}^\dagger$ are anomalous Green functions, which have non-zero value only in the bulk d-wave SC state. Due to the relation about the d-wave gap (51), the anomalous Green function $\hat{F}$ satisfies the relation

$$\hat{F}^{\uparrow\downarrow} = -\hat{F}^{\downarrow\uparrow} \equiv \hat{F}. \tag{55}$$

In this model, the edge-induced strong FM fluctuations are obtained by the RPA or GV^I-FLEX approximation as discussed.

Next, we explain the formulation of the edge-induced triplet superconductivity in the presence of the bulk d-wave SC gap. Here, we represent the triplet SC gap in (k_x, y, y')-representation as $\phi^{\uparrow\downarrow}_{y,y'}(k_x)$. In this study, we ignore the spin orbit interaction. The d-vector can be set as $\hat{\boldsymbol{d}}(k_x) = (0, 0, \hat{\phi}(k_x))$ without losing generality. In this case, it is enough to consider only $\phi^{\uparrow\downarrow}_{y,y'}(k_x)$ and $\phi^{\downarrow\uparrow}_{y,y'}(k_x)$. Due to the anticommutation relation of the fermion, the SC gap satisfies

$$\phi_{y,y'}(k_x) \equiv \phi^{\uparrow\downarrow}_{y,y'}(k_x) = -\phi^{\downarrow\uparrow}_{y',y}(-k_x). \tag{56}$$

The definition of the triplet gap is

$$\phi^{\uparrow\downarrow}_{y,y'}(k_x) = \phi^{\downarrow\uparrow}_{y,y'}(k_x). \tag{57}$$

From, (56) and (57), the triplet gap follows

$$\phi^{\uparrow\downarrow}_{y,y'}(k_x) = -\phi^{\uparrow\downarrow}_{y',y}(-k_x). \tag{58}$$

Here, we introduce $N_y \times N_y$ matrix representation $\hat{\phi}(k_x)$, which is defined as $\{\hat{\phi}(k_x)\}_{y,y'}=\phi_{y,y'}(k_x)$. To determine the edge-induced SC state, we need the phase difference between the bulk d-wave gap and the edge triplet gap. Although we can use the Bogoliubov-de Gennes (BdG) equation, heavy self-consistent calculation at various temperatures is required. To perform the numerical analysis efficiently, we derive the linearized gap equation for the edge triplet superconductivity, by extracting the first-order terms of $\hat{\phi}$ and $\hat{\phi}^\dagger$ in the BdG equation. λ denotes the eigenvalue of the linearized equation. When $\lambda \geq 1$, the triplet superconductivity emerges and coexists with the bulk d-wave superconductivity. In this method, we can judge the emergence of triplet superconductivity by the temperature-dependence of the eigenvalue, which is obtained by just performing the diagonalization, The detail derivation of linearized equation is explained in section 2. Note that we use the relation (55) and (57)

in the derivation of the linearized gap equation, and it is given as

$$\begin{aligned}\lambda\phi_{y,y'}(k_x) = &= -T\sum_{k'_x,Y,Y',n} V_{y,y'}(k_x-k'_x, i\epsilon_n - i\epsilon_0) \\ &\times\Big\{G_{y,Y}(k'_x,i\epsilon_n)\phi_{Y,Y'}(k'_x)G_{y',Y'}(-k'_x,-i\epsilon_n) - F_{y,Y}(k'_x,i\epsilon_n)\phi^\dagger_{Y,Y'}(k'_x)F_{Y',y'}(k'_x,i\epsilon_n)\Big\},\end{aligned} \tag{59a}$$

$$\begin{aligned}\lambda\phi^\dagger_{y,y'}(k_x) &= -T\sum_{k'_x,Y,Y',n} V_{y,y'}(k'_x-k_x, i\epsilon_n - i\epsilon_0) \\ &\times\Big\{G_{Y,y}(-k'_x,-i\epsilon_n)\phi^\dagger_{Y,Y'}(k'_x)G_{Y',y'}(k'_x,i\epsilon_n) - F^\dagger_{y,Y}(k'_x,i\epsilon_n)\phi_{Y,Y'}(k'_x)F^\dagger_{Y',y'}(k'_x,i\epsilon_n)\Big\},\end{aligned} \tag{59b}$$

$$\hat{V}(q_x,i\omega_l) = U^2\left(-\frac{1}{2}\hat{\chi}^s(q_x) - \frac{1}{2}\hat{\chi}^c(q_x)\right)C(\omega_l,\omega_d), \tag{60}$$

where $\hat{V}(q_x,\omega_l)$ is the site-dependent pairing interaction for triplet superconductivity. $\hat{\chi}^{s(c)}(q_x)$ is the static spin (charge) susceptibility in the d-wave SC state obtained by the RPA or GV^I-FLEX approximation. Here, $\omega_l = 2l\pi T$ is the boson Matsubara frequency. To simplify the analysis, we introduced the cut off function $C(\omega_l,\omega_d) = \omega_d^2/\left(|\omega_l|^2+\omega_d^2\right)$,where ω_d is the cutoff energy, and we set $\omega_d = 0.5$. We then solve the gap equation (59) under the restriction (58). In this section, the frequency dependence of the gap function is not considered, because we assume the even-frequency superconductivity. Note that the first and second terms of the gap equation have different sign due to the relation (55). This fact greatly affects the phase difference between the bulk gap function and the edge one. As we explained in section 2, This equation can determine the relative phase because the FF terms mix ϕ and ϕ^+.

5.3 Numerical result of triplet gap equation

In this section, we explain the result of the linearized triplet gap equation (59). k_x-mesh is $N_x = 64$, site number along y-direction is $N_y = 64$, the number of Matsubara frequencies is 1024. The transition temperature of the bulk d-wave superconductivity is $T_{cd} = 0.04$. The Coulomb interaction is $U = 2.25$ in the RPA, and $U = 2.65$ in the GV^I-FLEX. Here, the unit of energy is $|t|$, which corresponds to $\sim$ 0.4eV in cuprate superconductors. In addition, we define $\Delta_{\max}$ as the maximum value of the d-wave gap on the Fermi surface. In the present model, $\Delta_{\max} = 1.76\Delta_0$ for $n = 0.95$. Experimentally, $4 < 2\Delta_{\max}/T_{cd} < 10$ in YBCO [138, 139]. Therefore, in the RPA, we set $\Delta_0 = 0.06$ or 0.09, which corresponds to $\Delta_{\max} = 5.28$ or 7.92 for $T_{cd} = 0.04$.

5.3.1 $d \pm ip$-wave SC state

First, we analyze the linearized triplet gap equation for the RPA based pairing interaction. In figure 25 (a), k_x-dependence of the obtained triplet gap in the same layer y is represented. This is the p_x-wave gap with a node at $k_x = 0$. We can consider that this triplet SC is induced by the large LDOS and triplet pairing interactions caused by the ABS.

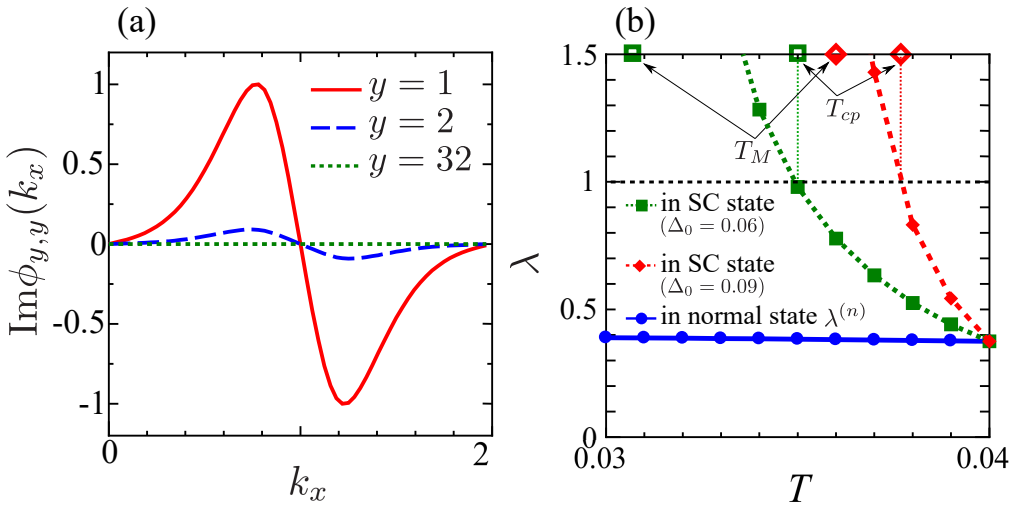

Figure 25: (a) k_x-dependence of obtained p_x-wave SC gap $\phi_{y,y}(k_x)$ for $\Delta_0 = 0.09$ at $T = 0.0375$. The pairing interaction is calculated by the RPA. $y = 1$ and $y = 32$ correspond to the edge and bulk, respectively. We normalize the gap as $\max_{k_x,y}|\phi_{y,y}(k_x)| = 1$. (b) T-dependence of λ for the pairing interaction by the RPA. The red and green line represent λ for $\Delta_0 = 0.06$ and 0.09, respectively. The blue line shows $\lambda^{(n)}$ in the normal state ($\Delta_0 = 0$). Below T_{cp}, the p-wave superconductivity emerges. At $T = T_M$, α_S reaches unity in the RPA.

Next, we discuss the phase difference between the d- and p-wave gap. The triplet SC gap in the real space $\phi_{x,y,y'}$ is given by the Fourier transformation on the x-direction of $\phi_{y,y'}(k_x)$. By using (58), we obtain

$$\phi_{x,y,y'} = -\left\{ \sum_{k_x} \phi^{\dagger}_{y,y'}(k_x) e^{ik_x x} \right\}^* . \tag{61}$$

This relation holds for the general triplet SC gap. In addition, the obtained p-wave gap satisfies

$$\phi_{y,y'}(k_x) = -\phi^{\dagger}_{y,y'}(k_x), \tag{62}$$

in the present numerical study. Thus, we find that the obtained p-wave gap is $\phi_{x,y,y'} = \phi^*_{x,y,y'}$ in real space representation, On the other hand, by the Fourier transformation, the phase difference in the $\boldsymbol{k}$-space is $\pm\pi/2$ and the obtained coexistence SC state corresponds to the $d \pm ip$-wave SC state. Therefore, by selecting the relative phase as $\pm\pi/2$ in the $\boldsymbol{k}$-space,

the edge-induced triplet p-wave SC can coexist with the bulk d-wave SC gap rather than competing with each other. To understand the origin of this phase difference $\pm\pi/2$, we examine the contribution from the second term of (59). Since the triplet pairing interaction $V_{y,y'}(k_x - k'_x, \epsilon_n - \epsilon_0)$ has large value only at the edge ($y = 1$) and $\Delta_{i,j}$ is real function, By setting $Y = Y' = 1$, the contribution to $\phi_{1,1}(k_x)$ from second term of (59a) is approximately evaluated as

$$\text{second term of (59a)} \approx -T \sum_{k'_x,n} |V_{1,1}(k_x - k'_x, \epsilon_n - \epsilon_0)||F_{1,1}(k'_x, \epsilon_n)|^2 \phi^*_{1,1}(k'_x). \tag{63}$$

Here, $V_{y,y'}(k_x - k'_x, \epsilon_n - \epsilon_0)$ has a large peak at $k_x = k'_x$. Therefore, the triplet superconductivity is stabilized if $\phi^*_{1,1}(k_x) = \phi^\dagger_{1,1}(k_x) = -\phi_{1,1}(k_x)$ is satisfied, and it is actually confirmed by numerical calculation.

In the $d \pm ip$-wave SC state, the time-reversal (TR) symmetry is broken. To verify it, we apply the time-reversal operator $\Theta = -i\sigma^y K$ to the present gap functions.

$$\Delta^{\uparrow\downarrow}_{y,y'}(k_x) + \phi^{\uparrow\downarrow}_{y,y'}(k_x) \underset{\text{TR}}{\longrightarrow} -{\Delta^{\downarrow\uparrow}_{y,y'}}^*(-k_x) - {\phi^{\downarrow\uparrow}_{y,y'}}^*(-k_x). \tag{64}$$

By using the conditions (51), (53), (57), and (62), we confirm that the $d + ip$-wave gap is transformed to the $d - ip$-wave gap. In Appendix D, we calculate the LDOS in the $d \pm ip$-wave SC state. The LDOS for up and down spin electrons are separated because the time-reversal symmetry is broken in the $d \pm ip$-wave SC state. The LDOS for up and down spin electrons are separated because the time-reversal symmetry is broken in the $d \pm ip$-wave SC state.

5.3.2 Temperature-dependence of λ

Next, we examine the T-dependence of the eigenvalue of the edge p-wave superconductivity. Here, λ and $\lambda^{(n)}$ denotes the eigenvalue in the d-wave superconductivity and normal state, respectively. Figure 25 (b) shows the T-dependence of the eigenvalue based on the RPA. $\lambda^{(n)}$ hardly increases and does not reach unity. On the other hand, λ drastically increases as T decreases and exceeds unity below $T_{cp} \lesssim T_{cd}$. At these temperatures, the $d \pm ip$-wave SC state is realized. Note that the edge FM order is realized at $T_M \lesssim T_{cp}$. For $\Delta_0 = 0.09$ ($2\Delta_{\max}/T_{cd} = 7.92$), the increase in λ is steeper than that for $\Delta_0 = 0.06$ ($2\Delta_{\max}/T_{cd} = 5.28$) due to the stronger development of the FM fluctuations.

To examine the effect of the FM fluctuations on the increase in λ, we introduce two types of gap equations, (i) and (ii), from which the effect of the d-wave gap is partially subtracted. In (i), we use the pairing interaction in the normal state $\hat{V}_{\text{normal}}$ instead of $\hat{V}$ in the d-wave SC state, and λ' denotes the eigenvalue. In (ii), we replace the Green functions $\hat{G}$, $\hat{F}$ and $\hat{F}^\dagger$ with those in the normal state, $\hat{G}^0$ and $\hat{F} = \hat{F}^\dagger = 0$. In this case, the eigenvalue is represented by λ''. Figure 26 shows the T-dependence of λ' and λ''. λ' is strongly suppressed from λ, and it does not reach unity. On the other hand, λ'' is almost equal to λ and exceeds unity at $T \lesssim T_{cp}$. Therefore, we conclude that the ABS-driven FM fluctuations cause the drastic increase in λ under T_{cd} Therefore, we conclude that the ABS-driven FM fluctuations cause the drastic increase in λ under T_{cd}

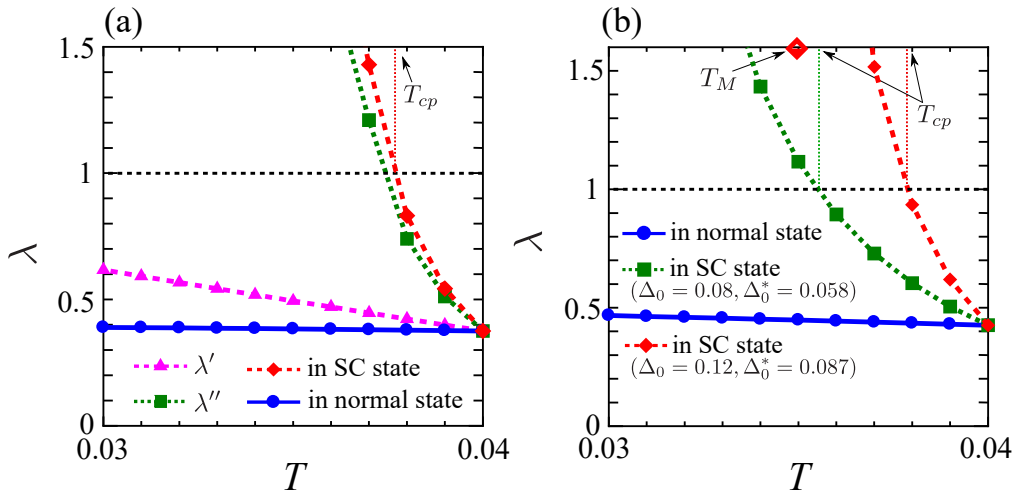

Figure 26: (a)T-dependence of λ' and λ''. We set $\Delta_0 = 0.09$ The red dotted line and blue solid line represent λ and $\lambda^{(n)}$ in the d-wave SC state and normal state, respectively. (b)T-dependence of λ for the pairing interaction by the GV^I-FLEX. ${\Delta_0}^*$ is renormalized gap by the self-energy. We obtain ${\Delta_0}^* = 0.058$ for $\Delta_0 = 0.08$ and ${\Delta_0}^* = 0.087$ for $\Delta_0 = 0.12$.

5.3.3 Result of the GV^I-FLEX approximation

In this section, we analyze the linearized triplet gap equation for the pairing interaction based on the GV^I-FLEX approximation in the $(1,1)$ edge cluster Hubbard model.In the conventional FLEX, the suppression of the spin susceptibility due to the negative feedback effect is overestimated near an impurity because the vertex corrections for the spin susceptibility are not considered [54]. In the GV^I-FLEX, the cancellation between negative feedback and vertex corrections is assumed, and then reliable results are obtained for the single impurity problem [54].

${\Delta_0}^*$ is the renormalized gap by the normal self-energy. We obtain ${\Delta_0}^* \approx 0.087$ and $2{\Delta_{\max}}^*/T_{cd} \approx 7.69$ for $\Delta_0 = 0.12$, and ${\Delta_0}^* \approx 0.058$ and $2{\Delta_{\max}}^*/T_{cd} \approx 5.11$ for $\Delta_0 = 0.08$. To simplify the analysis, the normal self-energy is not included in the Green functions in the gap equation.

Figure 26 shows the T-dependence of λ based on the GV^I-FLEX. λ increases as T decreases also in the GV^I-FLEX. In the case of $\Delta_0 = 0.08$, λ exceeds unity at $T \approx 0.02$. For $\Delta_0 = 0.12$, the increase in λ is sharper than that for $\Delta_0 = 0.08$ because of the stronger development of the FM fluctuations. Due to the negative feedback effect of self-energy, λ increases more moderately than that in the RPA. However, the emergence of a $d\pm ip$-wave superconductivity is obtained even if the self-energy effect is considered. Note that the T-dependence of λ based on the RPA and GV^I-FLEX is comparable when $(2\Delta_{\max}/T_{cd})_{\rm RPA} \approx (2{\Delta_{\max}}^*/T_{cd})_{\rm FLEX}$.

5.3.4 Effect of finite d-wave coherence length on edge-induced triplet superconductivity

In this subsection, we examine the effect of coherence length ξ_d of the bulk d-wave superconductivity on the emergence of the edge-induced p-wave superconductivity. We set the y-dependence of the d-wave gap as follows:

$$\Delta_{y,y'}(k_x, T)\left(1 - \exp\left(\frac{y + y' - 2}{2\xi_d}\right)\right). \tag{65}$$

For convenience, we set ξ_d as a parameter to simplify the analysis. For $T \lesssim T_{cd}$, $\xi_d \gg 3$ because of the relation $\xi_d \propto (1 - T/T_{cd})^{-1/2}$ in the GL theory. Thus, we set $\xi_d = 3$ and 10 in the present analysis.

Figure 27 (a) shows the site-dependence of the d-wave gap expressed by (65). Fig. 27 (b) shows the obtained LDOS. At the $(1, 1)$ edge, the LDOS has a large peak at $\varepsilon = 0$ due to the ABS. The peak structure due to the ABS still exists for finite ξ_d although the height of the peak becomes lower.

The inset shows the LDOS in the bulk, and it shows V-shaped ε-dependence because the d-wave gap has line nodes. In section 4, we confirmed that α_S increases as T decreases for finite ξ_d.

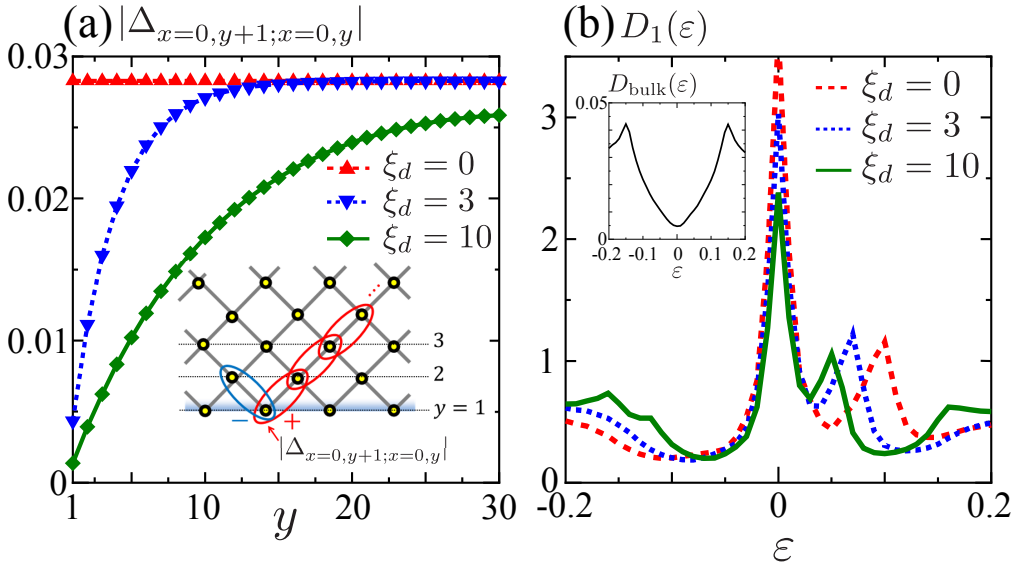

Figure 27: (a) Site-dependence of d-wave gap suppressed near the edge over ξ_d. The inset shows the nearest neighbor bonds corresponding to $|\Delta_{x=0,y+1;x=0,y}|$. We set $\Delta_0 = 0.08$ and calculated at $T = 0.032$. (b) ε-dependence of LDOS at the $(1, 1)$ edge for the d-wave gap with finite ξ_d. The inset shows the LDOS in the bulk ($y = 400$).

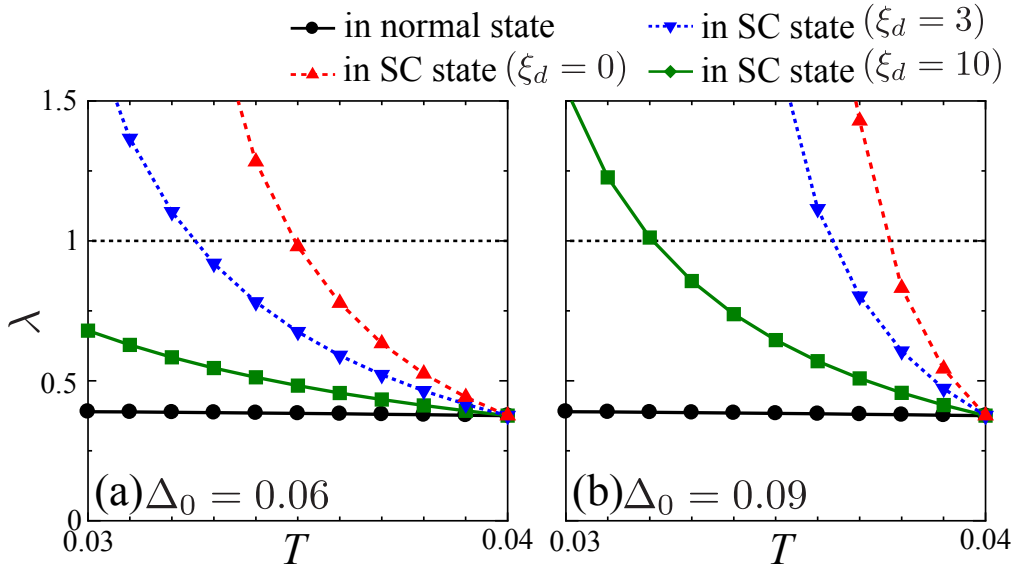

Figure 28: T-dependence of λ for (a) $\Delta_0 = 0.06$ or (b) $\Delta_0 = 0.09$ with finite ξ_d. The pairing interaction is calculated by the RPA for finite ξ_d.

Then, we explain the result of the gap equation based on the RPA for finite ξ_d. Figure 28 shows the T-dependence of λ. For $\Delta_0 = 0.09$, λ increases as the temperature decreases and exceeds unity even for finite ξ_d. On the other hand, the increase in λ is mild for $\Delta_0 = 0.06$ and $\xi_d = 10$, and $\lambda \approx 0.68$ even at $T = 0.03$. Therefore, we confirm that the strong increase in λ is still realized under the conditions $2\Delta_{\rm max}/T_{cd} \gtrsim 6$ and $\xi_d \ll 10$. These conditions are satisfied in real cuprate superconductors.

5.4 Cancellation of edge supercurrent in $d \pm ip$-wave SC state

In the $d \pm p$ SC state, we expect the emergence of the edge supercurrent because the time-reversal symmetry is broken. Thus, we calculate the edge supercurrent in the $d \pm ip$-wave SC state in this subsection. The current operator for σ-spin electron along x-direction is given as [150]

$$J^x_{y,y'}(k_x) = \frac{\partial}{\partial k_x} H^0_{y,y'}(k_x). \tag{66}$$

Note that the SC gaps are not included in $J^x_{y,y'}(k_x)$. We calculate the spontaneous super current between layer y and layer y' as follows:

$$\langle J^x_{y,y'} \rangle = -\frac{e}{2} \sum_{k_x} \left\{ J^x_{y,y'}(k_x) n^{\sigma\sigma}_{y,y'}(k_x) + (y \leftrightarrow y') \right\}, \tag{67}$$

where $n^{\sigma\sigma}_{y,y}(k_x)$ is given as

$$n^{\sigma\alpha}_{y,y'}(k_x) = \langle c^\dagger_{k_x,y,\sigma} c_{k_x,y',\alpha} \rangle = \sum_b U_{(y\sigma),b}(k_x) U^*_{(y'\alpha),b}(k_x) \left\{ T \sum_n {\rm Re} G_b(k_x, \epsilon_n) + \frac{1}{2} \right\}. \tag{68}$$

$\hat{U}$ is the unitary matrix used in the diagonalization of BdG hamiltonian. Here, the edge current though the layer y is defined as

$$\langle J_y^x \rangle = \sum_{y'} \langle J_{y,y'}^x \rangle. \tag{69}$$

Then, the total super current is obtained by $\langle J^x \rangle = \sum_y \langle J_y^x \rangle$.

Figure 29 shows the obtained y-dependence of the edge current in the d+ip- and d+is-wave SC state. For simplicity, we assume the the edge s-wave gap as $i\Delta^s \delta_{y,y'=1}$ and $\Delta^s = 0.09$. In spite of the time-reversal symmetry breaking, no edge current does flows. On the other hand, the non-zero edge current emerges in the $d+is$-wave SC state as pointed out in Refs. [77].

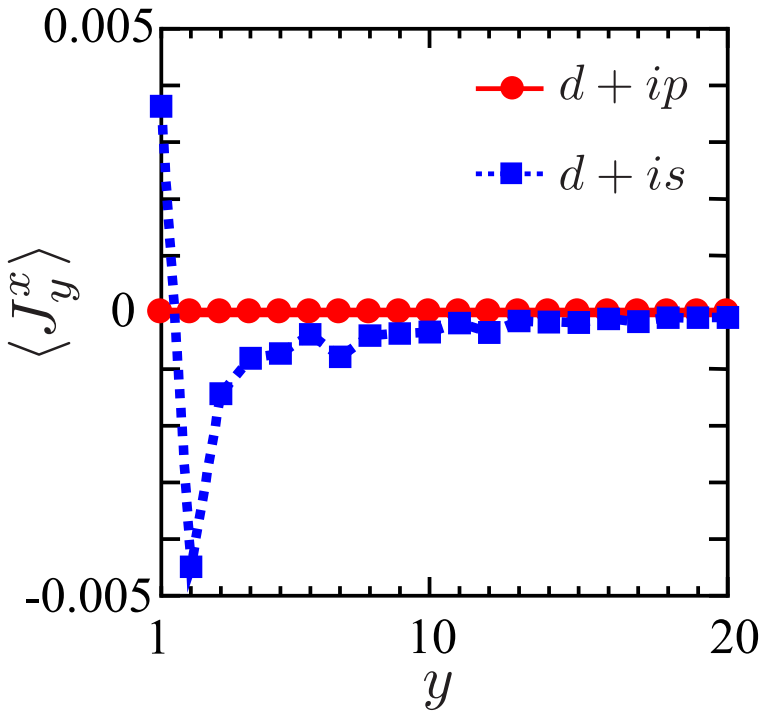

Figure 29: y-dependence of edge supercurrent $\langle J_y^x \rangle$ in the $d+ip$- and $d+is$-wave SC state. We set $\Delta_0 = 0.09$ and $\max_{i,j}|\phi_{i,j}| = 0.09$. We set the size of edge s-wave gap as $\Delta^s = 0.09$.

To explain why the spontaneous edge current cancels in the $d+ip$-wave SC state, we analyze the Green function $G_{y,y'}^{\uparrow\uparrow}(k_x, i\varepsilon_n)$, which corresponds to the transfer process of up spin electron from site y' to y. Here, its second-order term in proportion to $\Delta\phi^\dagger$ is evaluated as

$$\delta G_{y,y'}^{\uparrow\uparrow}(k_x, i\varepsilon_n) = -G_{y,y_1}^0(k_x, i\varepsilon_n)\Delta_{y_1,y_2}^{\uparrow\downarrow}(k_x)G_{y_3,y_2}^0(-k_x, -i\varepsilon_n)\phi_{y_3,y_4}^{\uparrow\downarrow\ \dagger}(k_x)G_{y_4,y'}^0(k_x, i\varepsilon_n), \tag{70}$$

where $G_{y,y'}^0(k_x, i\varepsilon_n)$ is the Green function in the normal state. Then, we consider the second

order term contributing to $G^{\uparrow\uparrow}_{y',y}(-k_x, i\varepsilon_n)$, which is the inverse transfer process of (70).

$$\delta G^{\uparrow\uparrow}_{y',y}(-k_x, i\varepsilon_n) = -G^0_{y',y_4}(-k_x, i\varepsilon_n)\phi^{\uparrow\downarrow}_{y_4,y_3}(-k_x)G^0_{y_2,y_3}(k_x, -i\varepsilon_n){\Delta^{\uparrow\downarrow}_{y_2,y_1}}^{\dagger}(-k_x)G^0_{y_1,y}(-k_x, i\varepsilon_n). \tag{71}$$

Note that $\hat{G}^0$ satisfies $G^0_{y,y'}(k_x, i\varepsilon_n) = G^0_{y',y}(-k_x, i\varepsilon_n)$. In addition, by using (52), (53), (58), and (62), $\delta G^{\uparrow\uparrow}_{y,y'}(k_x, i\varepsilon_n) = \delta G^{\uparrow\uparrow}_{y',y}(-k_x, i\varepsilon_n)$ is obtained. It means $n^{\sigma\sigma}_{y,y'}(k_x) = n^{\sigma\sigma}_{y',y}(-k_x)$, and therefore the current does not flow.

5.5 Summary

In this section, we discussed the emergence of the the $d \pm ip$-wave SC state at the $(1,1)$ edge of the d-wave superconductors. We analyzed the linearized triplet SC gap equation numerically in the $(1,1)$ edge cluster Hubbard model in the presence of the bulk d-wave SC gap. To consider FM fluctuation-induced triplet SC, the site-dependent pairing interaction is calculated based on the RPA or GV^I-FLEX. By solving the linearized gap equation, we obtain the edge-localized p-wave gap. In addition, the phase difference between the bulk d-wave gap and the edge p-wave gap is determined as $\pi/2$ in the $\boldsymbol{k}$-space, and it corresponds to the time-reversal symmetry breaking $d \pm ip$-wave SC state. Next, we discussed the T-dependence of the eigenvalue λ for the edge-induced triplet SC state. In the bulk d-wave SC state ($T < T_{cd}$), λ for the triplet state increases drastically as T decreases, and reaches unity at $T = T_{cp}$. The edge current does not flow nevertheless the time-reversal symmetry is broken in the $d \pm ip$-wave SC state.

The realization of the $d \pm ip$-wave SC state is also expected when the direction of the open edge is near the $(1,1)$ edge. The present edge p-wave SC is generated by the ABS-induced strong FM fluctuations, and the ABS is formed for other edges as pointed out in Refs. [65,78,143]. Therefore, or the small deviation from the (1,1) edge, we consider that the FM fluctuations develop and the $d \pm ip$-wave SC state is induced.

In the derivation of the linearized edge gap equation (59), we linearize the equation only for the first-order terms of triplet gap ϕ, and the effect of the bulk SC gap is still fully included. This method is useful in analyzing edge-induced superconductivity in the presence of bulk superconductors. Due to the interference between the bulk and edge gap functions, interesting $d \pm ip$-wave state becomes naturally stable.

In the present study, we can regard the edge layer as a 1-dimensional p-wave superconductor due to the absence of the d-wave gap in the edge layer. In Ref. [151], the Majorana fermion emerges at the endpoint of the 1-dimensional p-wave superconductor. Therefore, we expect that the Majorana fermion appears at the endpoint of the $(1,1)$ edge. Thus, the present edge-induced novel superconductivity may be a useful platform for SC devices Finally, we note that the emergence of the p-wave SC and Majorana edge state had been discussed at the interface between the bulk s-wave superconductor and magnetic material [152,153].

6 Generation of edge-induced odd-frequency superconductivity with spontaneous spin current due to zero-energy Andreev-bound-state

6.1 Introduction

In the previous section, we discussed the edge-induced p wave SC state on the d wave superconductors. Another possible scenario is the edge-induced "odd-frequency SC state". However, regardless of the difficulties in its realization, the odd-frequency SC state has attracted a lot of attention in the field of superconductivity because the possibility of the pairing symmetry is doubled by allowing the odd-parity with respect to frequency [87–92]. Therefore, we propose an accessible method to induce the odd-frequency gap function in this study.

In this section, we study the edge-induced odd-frequency spin-triplet SC mediated by the strong FM fluctuations originated from the ABS. To analyze edge-induced odd-frequency superconductivity, we consider the open $(1,1)$ edge cluster Hubbard model used in the previous sections. In addition, we include the frequency-dependence of the triplet gap in the analysis of the linearized gap equation. By this extension, we can treat the both even and odd-frequency SC gap in the same equation. We obtain the edge-localized odd-frequency s-wave gap as the largest eigenvalue solution. The coexistent state between bulk d-wave and edge odd-frequency s conserve the time-reversal symmetry (TRS). Interestingly, we obtain non-zero spontaneous spin current flowing along the edge. This is a useful probe to detect the emergence of the odd-frequency SC gap. Furthermore, by calculating the edge current, the Hermite relation of the odd-frequency gap is justified. Finally, we analyze the triplet gap equation without linearization, and the finite odd-frequency gap is obtained for $\lambda \lesssim 1$. This unconventional behavior is understood from the viewpoint of free energy.

6.2 Model and Theoretical Method

The Hamiltonian is expressed as:

$$\mathcal{H} = H_0 + U \sum_i n_{i\uparrow} n_{i\downarrow} + \sum_{i,j} \Delta^d_{i,j} \left(c^\dagger_{i\uparrow} c^\dagger_{j\downarrow} + \text{h.c} \right), \tag{72}$$

where U denotes the on-site Coulomb interaction. $H_0 = \sum_{i,j,\sigma} t_{i,j} c^\dagger_{i\sigma} c_{j\sigma}$ represents the kinetic term, where $t_{i,j}$ denotes the hopping integral between sites i and j. In this study, we set $(t_1, t_2, t_3) = (-1, 1/6, -1/5)$, where t_n is the n-th nearest neighbor hopping integral and it corresponds to $YBa_2Cu_3O_{7-x}$ (YBCO) model [14, 131–133]. The energy unit is $|t_1| = 1$. The Fermi surface (FS) in the periodic system is illustrated in Fig. 8 (b) in section 2. $\Delta^d_{i,j}$ is the bulk d_{xy} wave (=$d_{X^2-Y^2}$ wave) gap function given as $\Delta^d_{i,j} = (\Delta^d/4)(\delta_{\boldsymbol{r}_i - \boldsymbol{r}_j, \pm\hat{\boldsymbol{X}}} - \delta_{\boldsymbol{r}_i - \boldsymbol{r}_j, \pm\hat{\boldsymbol{Y}}})$. Similar bulk d wave gap function is microscopically obtained based on spin-fluctuation theories. Considering this fact, we introduce Δ^d as the model parameter to simplify the discussion. To reproduce the suppression of the d wave gap near the edge, we

multiplied the d wave gap function by decay factor $(1-\exp[(y_i+y_j-2)/2\xi_d])$ [133]. Then, we set the coherence length $\xi_d = 10$. In this system, LDOS has a sharp SABS-induced peak, and it drives the system towards a strong correlation state as discussed in section 4

In the following numerical study, we set the filling as $n = 0.95$. The numerical results are essentially unchanged for $n = 0.8$–1.2.

Next, we introduce the $2N_y \times 2N_y$ Green functions in the bulk+edge SC state as follows:

$$\begin{aligned}\hat{\mathcal{G}}_{\rm Nam} &\equiv \begin{pmatrix} \hat{\mathcal{G}}^{\uparrow\uparrow}(k_x, i\epsilon_n) & \hat{\mathcal{F}}^{\uparrow\downarrow}(k_x, i\epsilon_n) \\ \hat{\mathcal{F}}^{+\uparrow\downarrow}(k_x, i\epsilon_n) & -{}^t\hat{\mathcal{G}}^{\downarrow\downarrow}(-k_x, -i\epsilon_n) \end{pmatrix} \\ &= \begin{pmatrix} i\epsilon_n - \hat{H}^0(k_x) & -\hat{\Delta}^d(k_x) - \hat{\phi}(k_x, i\epsilon_n) \\ -\hat{\Delta}^d(k_x) - \hat{\phi}^+(k_x, i\epsilon_n) & i\epsilon_n + {}^t\hat{H}^0(-k_x) \end{pmatrix}^{-1}. \end{aligned} \tag{73}$$

The linearized triplet gap equation for $\hat{\phi}(k_x, i\epsilon_n)$ ($\propto \langle c_{k_x\uparrow} c_{-k_x\downarrow}\rangle$) and $\hat{\phi}^+(k_x, i\epsilon_n)$ ($\propto \langle c^\dagger_{-k_x\downarrow} c^\dagger_{k_x\uparrow}\rangle$) is represented in Fig. 13 in section 2, and its analytic expression is

$$\begin{aligned}\lambda^{\rm edge}\phi_{y,y'}(k_x, i\epsilon_n) = -T \sum_{k'_x, Y, Y', m} & V_{y,y'}(k_x - k'_x, i\epsilon_n - i\epsilon_m) \\ & \times \{G_{y,Y}(k'_x, i\epsilon_m)\phi_{Y,Y'}(k'_x, i\epsilon_m)G_{y',Y'}(-k'_x, -i\epsilon_m) \\ & \times -F_{y,Y}(k'_x, i\epsilon_m)\phi^+_{Y,Y'}(k'_x, i\epsilon_m)F_{Y',y'}(k'_x, i\epsilon_m)\}, \end{aligned} \tag{74}$$

$$\begin{aligned}\lambda^{\rm edge}\phi^+_{y,y'}(k_x, i\epsilon_n) = -T \sum_{k'_x, Y, Y', m} & V_{y,y'}(k_x - k'_x, i\epsilon_n - i\epsilon_m) \\ & \times \{G_{Y,y}(-k'_x, -i\epsilon_m)\phi^+_{Y,Y'}(k_x, i\epsilon'_m)G_{Y',y'}(k'_x, i\epsilon_m) \\ & -F^+_{y,Y}(k'_x, i\epsilon_m)\phi_{Y,Y'}(k'_x, i\epsilon_m)F^+_{Y',y'}(k'_x, i\epsilon_m)\}. \end{aligned} \tag{75}$$

The pairing interaction for the triplet SC is given by

$$\hat{V}(q_x, i\omega_l) = U^2\left(-\frac{1}{2}\hat{\chi}^s(q_x, i\omega_l) - \frac{1}{2}\hat{\chi}^c(q_x, i\omega_l)\right). \tag{76}$$

In this study, we consider only the triplet gap because FM fluctuations suppress spin-singlet gaps. For convenience, we assume that $\boldsymbol{d} \parallel \boldsymbol{z}$ ($S_z^{\rm triplet} = 0$) in the triplet gap without the loss of generality because we ignore the spin-orbit interaction in the present analysis. In section 5, we discussed the emergence of even-frequency p wave triplet gap $\hat{\phi}(k_x, i\epsilon_n) = \hat{\phi}(k_x, -i\epsilon_n)$, where $\epsilon_n = (2n+1)\pi T$. However, this is not a unique possibility because the odd-frequency pairing state $\hat{\phi}(k_x, i\epsilon_n) = -\hat{\phi}(k_x, -i\epsilon_n)$ is not prohibited in principle.

6.3 Numerical Results

In the triplet state, the even/odd-frequency gap exhibits an odd/even-parity in space due to fermion anticommutation relations. Considering both possibilities equally, we analyze

the linearized gap equation by considering the $i\epsilon_n$-dependence of $\hat{\phi}(k_x, i\epsilon_n)$ comprehensively. Here, we assume the Hermite odd-frequency gap function [93, 94]:

$$\phi^{+}_{y,y'}(k_x, i\epsilon_n) = [\phi_{y',y}(k_x, -i\epsilon_n)]^* \tag{77}$$

The reliability of this relationship will be clarified later. We assumed the BCS-type bulk gap function $\Delta^d(T) = \Delta^d_0 \tanh(1.74\sqrt{T_{cd}/T - 1})$ with the transition temperature $T_{cd} = 0.06$, which corresponds to $\sim$ 100K in cuprates for $z|t_1| \sim 1500$K with $z = m/m^* \sim 0.3$. Experimentally, $4 < 2\Delta^d_0/T_{cd} < 10$ in YBCO [138, 139]. Thus, we set $\Delta^d_0 = 0.12$ or 0.16, which corresponds to $2\Delta^d_0/T_{cd} = 4.0$–5.3. We set $U = 2.32$, where the spin Stoner factor α_S is 0.975 at $T = T_{cd}$.

6.3.1 $s^{\rm odd}$-wave SC state

Figures 30 (a) and (b) exhibit the k_x- and $i\epsilon_n$-dependences of the odd-frequency s wave ($s^{\rm odd}$ wave) gap for $\Delta^d_0 = 0.16$ at $T = 0.05$, respectively. Note that, the odd-frequency $s^{\rm odd}$ wave state is the largest eigenvalue state in the solutions of the linearized gap equation. At the edge, pure $s^{\rm odd}$ state is realized because the direction of the d wave gap node is along the $(1, 1)$ edge.

T-dependence of the spin Stoner factor α_S and the eigenvalue $\lambda^{\rm edge}$ are plotted in Figures 30 (c) and (d), respectively. When $\lambda^{\rm edge} \sim 1$ is satisfied, the edge-gap function appears because SC susceptibility is proportional to $1/|1 - \lambda^{\rm edge}|$,

In the normal state ($\Delta^d_0 = 0$), $\lambda^{\rm edge}$ decreases as T decreases because the pairing interaction for the odd-frequency SC gap is proportional to $T\chi^s(\boldsymbol{q}_x, 0) \propto T/(1 - \alpha_S)$ [96, 100–104]. Thus, there is a difficulty for the emergence of the spin-fluctuation mediated odd-frequency SC in the bulk. In contrast, at the edge of d wave superconductor, LDOS has a large peak at the Fermi level due to the SABS, and spin fluctuations drastically develop. [132, 154]. Therefore, $\lambda^{\rm edge}$ rapidly approaches unity owing to the SABS-induced magnetic criticality [133]. Thus, the SABS-driven odd-frequency SCis naturally realized at the edge of d wave superconductors.

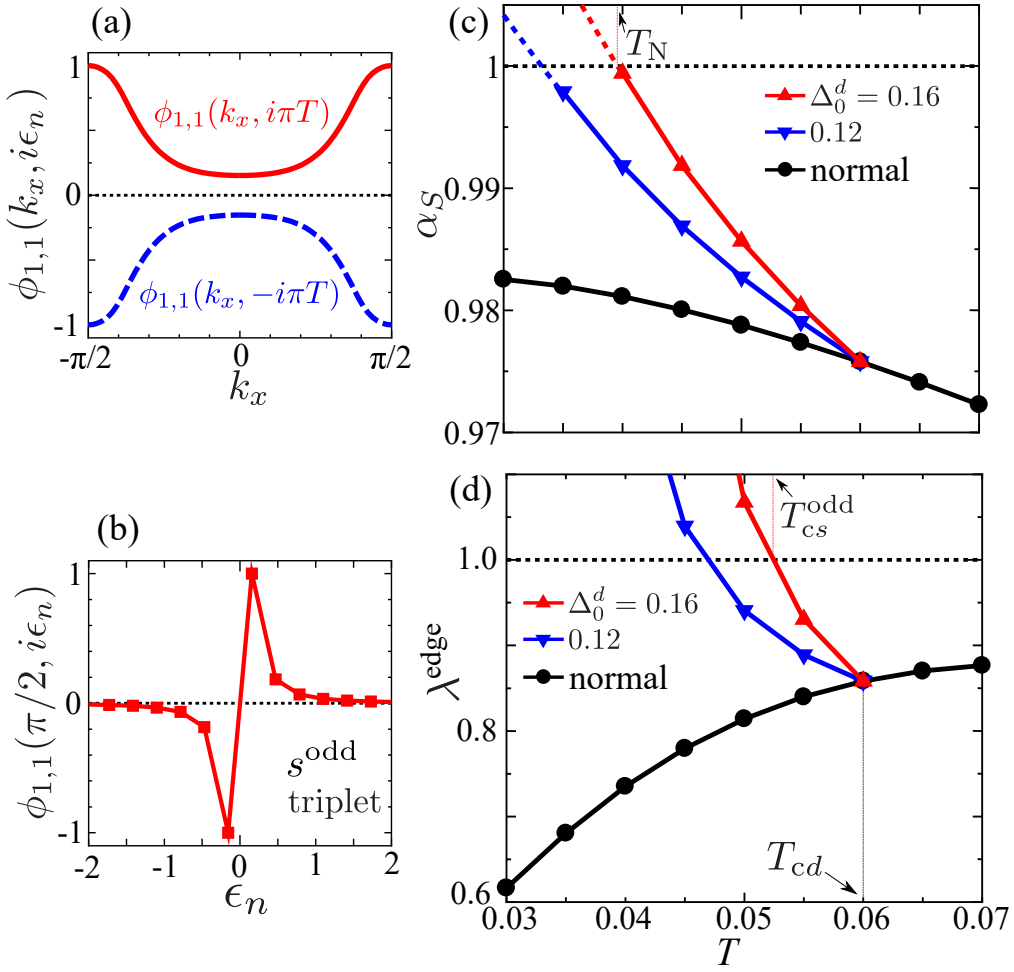

Figure 30: (a)(b) Obtained $s^{\rm odd}$ wave triplet gap at the edge: (a) $\phi_{1,1}(k_x, \pm i\pi T)$ in the 1st BZ ($-\pi/2 < k_x \leq \pi/2$) and (b) $\phi_{1,1}(k_x = \pi/2, i\epsilon_n)$ in $\Delta_0^d = 0.16$ case at $T = 0.05$. (c)(d) Obtained T-dependences of (c) the Stoner factor α_S and (d) the eigenvalue $\lambda^{\rm edge}$ for the $s^{\rm odd}$ wave state. Here, the bulk d wave SC gap appears at $T_{cd} = 0.06$. In addition, $2\Delta_0^d/T_{cd} = 4.0$–5.3 for $\Delta_0^d = 0.12$–0.16. The edge $s^{\rm odd}$ wave gap is obtained for $\alpha_S \gtrsim 0.95$ at $T = T_{cd}$.

6.3.2 $s^{\rm odd}$ wave SC state dominates $p^{\rm even}$ wave SC state

Here, we discuss the reason behind the edge $s^{\rm odd}$ wave state dominating the edge even-frequency $p^{\rm even}$ wave state in this study. In this subsection, we consider the reason why edge $s^{\rm odd}$ wave state dominates the edge even-frequency $p^{\rm even}$ wave state.In the k_x-space argument, nodeless $s^{\rm odd}$ wave state can gain the larger condensation energy than nodal p-wave gap. On the other hand, in the ϵ_n-space argument, closeness to the magnetic criticality ($\alpha_S \lesssim 1$) is essential.The edge pairing interaction $V_{1,1}(q_x, i\omega_l) \propto \chi^s_{1,1}(q_x, i\omega_l)$ at $q_x \sim 0$ is well fitted by the function $\Omega(\omega_l; \omega_d) = \omega_d/(|\omega_l| + \omega_d)$. The obtained ω_d based on the real-space RPA is shown in Fig. 31 (a). ω_d ($\propto 1 - \alpha_S$) approaches 0 at the magnetic critical point, and the

eigenvalues of even- and odd-frequency solutions become comparable [96,100–104]. To verify this discussion, we examine the eigenvalue $\lambda^{\rm edge}$ of both $s^{\rm odd}$ wave and $p^{\rm even}$ wave states, by introducing a separable pairing interaction $V_{y,y'}(q_x, i\omega_l) \propto \chi^s_{y,y'}(q_x, 0) \cdot \Omega(\omega_l; \omega_d)$. Fig. 31 shows the obtained results for (b) $\omega_d = 0.04$ and (c) $\omega_d = 0.1$. It is verified that the $s^{\rm odd}$ wave dominates the $p^{\rm even}$ wave near the quantum criticality $\omega_d = 0.04$, which corresponds to the RPA study demonstrated in Fig. 30. The obtained $s^{\rm odd}$ wave state should be robust against impurity scattering according to the Anderson theorem.

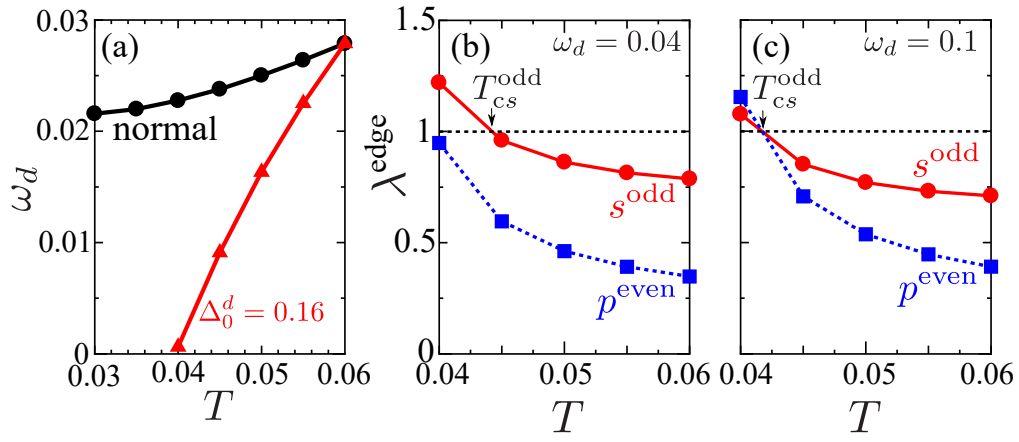

Figure 31: (a) Obtained energy-scale of the dynamical spin susceptibility ω_d ($\propto 1 - \alpha_S$) as a function of T. (b)(c) Eigenvalues $\lambda^{\rm edge}$ obtained by the pairing interaction $\hat{\chi}^s(q_x, 0)\Omega(\omega_l; \omega_d)$ for (b) $\omega_d = 0.04$ and (c) 0.1. As it approaching to the magnetic criticality $\omega_d \to 0$, $T_{cs}^{\rm odd}$ increases whereas $T_{cp}^{\rm even}$ decreases. In (b), $T_{cs}^{\rm odd}$ is higher than $T_{cp}^{\rm even}$.

In the present analysis, we set the bulk d-wave gap Δ^d as real, and the obtained edge $s^{\rm odd}$ wave gap is also real in the ϵ_n-representation. That is, $\phi_{1,1}(k_x, i\epsilon_n) \propto \epsilon_n$ is real for small ϵ_n. Then, by the analytic continuation, $\phi' = [\phi^{\rm R}_{1,1}(k_x, \epsilon) + \phi^{\rm A}_{1,1}(k_x, \epsilon)]/2 \propto i\epsilon$ becomes purely imaginary. In addition, the triplet gap function is odd with respect to the time-reversal. Therefore, the obtained state is the TRS "$d + s^{\rm odd}$ wave state". Because $\phi'' = [\phi^{\rm R}_{1,1}(k_x, 0) - \phi^{\rm A}_{1,1}(k_x, 0)]/2$ also approaches to zero near the magnetic criticality [96], the edge $s^{\rm odd}$ wave gap will not affect the LDOS at zero-energy. This result is consistent with the ubiquitous presence of zero-bias conductance peak observed by the tunneling spectroscopy of cuprates [73, 75, 155, 156]

6.3.3 Edge Super Current

Next, we explain the emergence of spontaneous edge current in the $d + s^{\rm odd}$ wave state. The charge current along the x-axis from layer y to any layer is given by:

$$J^{\rm C}_x(y) = \sum_{k_x, y', \sigma, \rho} \left\{ (-e\delta_{\sigma,\rho}) v_x(k_x, y, y') \mathcal{G}^{\sigma,\rho}_{y',y}(k_x, i\epsilon_n) e^{-i\epsilon_n 0} + (y \leftrightarrow y') \right\}, \tag{78}$$

where $v_x(k_x, y, y') \equiv \partial H^0_{y,y'}(k_x)/\partial k_x$ [150], and $\mathcal{G}^{\sigma,\rho}_{y',y}$ presents the Green function for the $d + s^{\rm odd}$ state. For simplicity, we set $\phi_{y,y'}(i\epsilon_n) = \phi^{\rm o} f^{\rm o}(\epsilon_n)\delta_{y,1}\delta_{y',1}$ with $\phi^{\rm o} = \Delta^d_0 = 0.16$, where $f^{\rm o}(\epsilon_n)$ is the obtained frequency-dependence shown in Fig. 30 (b).

We note that the total edge current is $J^{\rm C}_x = \sum_y J^{\rm C}_x(y)$. In addition, we consider the spin current along the x-axis $J^{{\rm S}\mu}_x(y)$, where μ is the direction of spin polarization. We can evaluate the spin current by using $(\hbar\hat{\sigma}^\mu_{\sigma,\rho})$ instead of $(-e\delta_{\sigma,\rho})$in Eq. (80), where $\hat{\sigma}^\mu$ is the Pauli matrix. $J^{{\rm S}_x}_x(y)$ and $J^{{\rm S}_y}_x(y)$ are zero because of the conservation of $s_z$in the present SC state, We stress that $J^{{\rm S}\mu}_x(y)$ does not change under the operation of time-reversal.

Figure 32 (a) exhibits the obtained edge currents in the $d + s^{\rm odd}$ wave state by setting $e = \hbar = 1$. The charge-current $J^{\rm C}_x(y)$ does not flow identically. This result is consistent with the experimental result of μ-SR [157]; however, the non-zero spin current $J^{{\rm S}z}_x(y)$ flows spontaneously. The polarization of the obtained spin current is parallel to the $\boldsymbol{d}$-vector. Note that the total gap function changes the sign by the mirror operation $\mathcal{M}_x$ because the d_{xy} and $s^{\rm odd}$ gap have odd and even parity,respectively. In addition, the total gap function is odd for the exchange of spin index due to the coexistence between singlet and triplet SC. Consequently, conduction electrons acquire spin-dependent velocity, and therefore $J^{{\rm S}z}_x(y) \neq 0$. The obtained total spin current $J^{{\rm S}z}_x \equiv \sum_y J^{{\rm S}z}_x(y)$ is proportional to $\phi^{\rm o}$, as shown in Fig. 32 (b). We expect the emergence of a sizable amount of spin current enough to observe because $J^{{\rm S}z}_x$ is linear in $|\phi^{\rm o}|$.

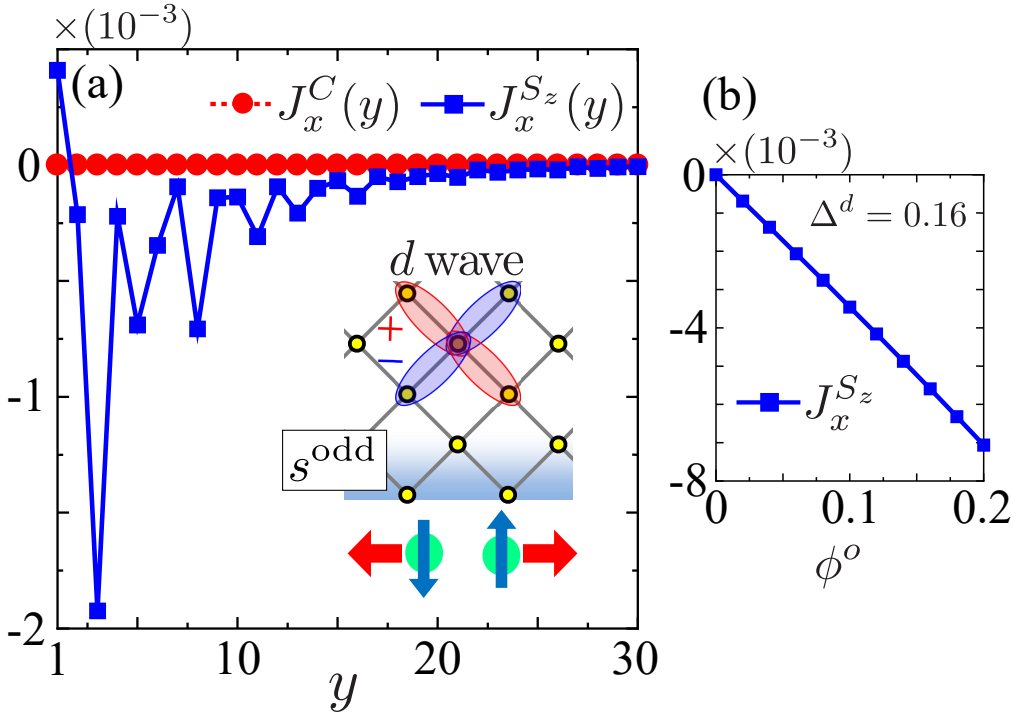

Figure 32: (a) Obtained edge currents in the $d + s^{\rm odd}$ state derived from the edge gap equation.Here, $d = d_{xy}$. The edge currents in the $p + is^{\rm odd}$, $d + is^{\rm even}$, and $p + s^{\rm even}$ states are illustrated in Appendix Dand listed in Table 3. Here, we set $\Delta^d = 0.16$ while the $s^{\rm odd}$ wave gap function is set as $\phi_{y,y'}(i\epsilon_n) = \phi^{\rm o} f^{\rm o}(\epsilon_n)\delta_{y,1}\delta_{y',1}$ with $\phi^{\rm o} = 0.16$, where $f^{\rm o}(\epsilon_n)$ is given in Fig. 30 (b). (b) Obtained total edge current J_x^{Sz} for $\Delta^d = 0.16$ as a function of $\phi^{\rm o}$.

Moreover, we also consider the emergence of the edge currents for the other coexistent SC state such as $d+is^{\rm even}$, $p+is^{\rm odd}$, and $p+s^{\rm even}$ wave states. In the TRS breaking $p+is^{\rm odd}$ wave state ($p = p_x$), non-zero charge current flows as shown in Fig. 33 (a), whereas spin current is absent. On the other hand, the $p+is^{\rm odd}$ wave state is odd for $\mathcal{M}_x$, while the parity of the spin part is even. Consequently, $J_x^{\rm C} \neq 0$ is obtained. The present study is a nontrivial extension of the theory of the $d + is^{\rm even}$ wave state Refs. [77].

We notice that, the bulk p_x wave SC gap does not induce the SABS, which can drive the edge $s^{\rm odd}$ wave SC gap. However, the SABS is formed at the edge of the bulk p_X wave SC state, which is not completely even for the mirror operation $\mathcal{M}_x$. Therefore, the p_X wave SC state is favorable to realize the odd-frequency SC state that accompanies finite edge current. The p_X wave can be realized by applying the uniaxial strain in the chiral or the helical p wave state.

Next, we discuss the edge-induced currents due to the edge even-frequency s wave states. Figures 33 (b) and (c) are the obtained edge currents in the $d + is^{\rm even}$ wave the $p + s^{\rm even}$ wave states, respectively. The non- zero charge current in Fig. 33 (b) is consistent with the Matsumoto-Shiba theory [77]. The relation between parities and edge currents in the edge odd- and even-frequency SC states are summarized in table 3.

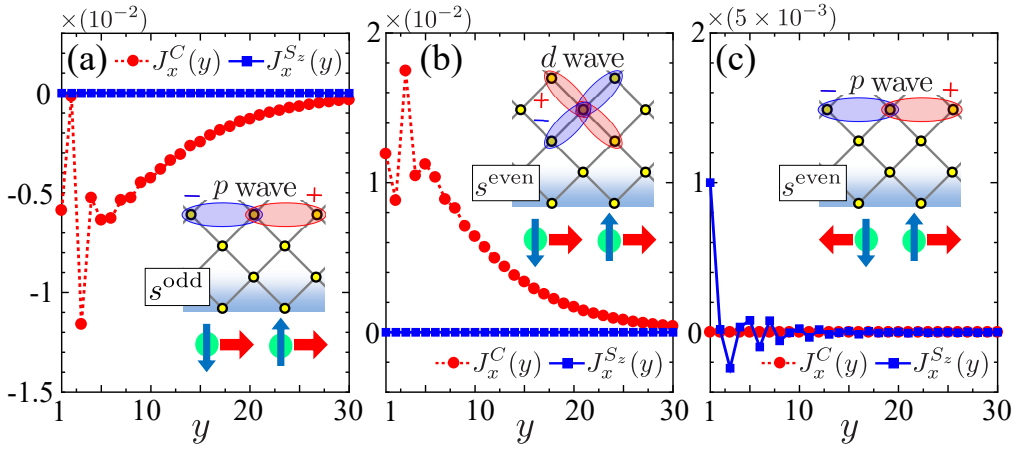

Figure 33: Obtained edge currents in (a) the $p + is^{\rm odd}$ wave state, (b) the $d + is^{\rm even}$ wave state, and (c) the $p + s^{\rm even}$ wave state. Here, $p = p_x$ and $d = d_{xy}$, and $\Delta^{p,d} = 0.16$. We set the $s^{\rm odd}$ wave gap function as $\phi_{y,y'}(i\epsilon_n) = \phi^{\rm o} f^{\rm o}(\epsilon_n)\delta_{y,1}\delta_{y',1}$ with $\phi^{\rm o} = 0.16$, where $f^{\rm o}(\epsilon_n)$ is given in Fig. 2 (b). We also set the $s^{\rm even}$ wave gap $\phi_{y,y'}(i\epsilon_n) = \phi^{\rm e}\delta_{y,1}\delta_{y',1}$ with $\phi^{\rm e} = 0.16$.

Table 3: Parities and edge currents in $d + s^{\rm odd}$ $p + is^{\rm odd}$, $d + is^{\rm even}$, and $p + s^{\rm even}$ wave states for $d = d_{xy}$ and $p = p_x$. These states satisfy $\mathcal{M}_x = -1$. All currents disappear if phase of the edge gap is shifted by $\pi/2$. No currents flow for $d = d_{x^2-y^2}$ and $p = p_y$ because $\mathcal{M}_x = +1$.

SC state	time-reversal	spin exchange	$J_x^{\rm C}$	$J_x^{\rm Sz}$
$d + s^{\rm odd}$	+	−	0	non-zero
$p + is^{\rm odd}$	−	+	non-zero	0
$d + is^{\rm even}$	−	+	non-zero	0
$p + s^{\rm even}$	+	−	0	non-zero

6.4 Relationship between ϕ and ϕ^+

Next, we discuss an important problem on the relationship between ϕ and ϕ^+ in the odd-frequency gap function. In this study, we use the relationship in Eq. (77) which is consistent with the Lehmann representation of Green functions. The para-Meissner effect is caused by this relationship and therefore odd-frequency SC state is unstable as a bulk SC state. Nonetheless, the edge-localized odd-frequency gap function is expected to be realized. On the other hand, a non-Hermite relationship $\bar{\phi}^+_{y,y'}(k_x, i\epsilon_n) = [\phi_{y',y}(k_x, +i\epsilon_n)]^*$ [88,97–99], which exhibits usual Meissner effect gives rise to imaginary spin current in the $d + s^{\rm odd}$ wave state. Therefore, the Hermite condition (77) should be the true equation.

To observe the edge $s^{\rm odd}$ gap function, it is helpful to focus on the anomalous proximity effect in a diffusive normal metal (DN), where the quasiparticle in the DN exhibits a zero-energy peak of LDOS [123]. If the $s^{\rm odd}$ gap function is absent at the interface, the emergence of the odd-frequency singlet p wave is expected. However, it cannot penetrate into the DN.

Once the interface induced $s^{\rm odd}$ triplet SC state is realized, it penetrates into the DN, and the zero-energy peak of LDOS is generated.

6.5 Analysis of gap equation without linearization

To discuss the behavior of ϕ below T_c, we analyze gap equation without linearization, and we obtain finite odd-frequency gap. Figure 35(a) shows the α_S dependence of odd-f gap ϕ at the edge. The non-zero ϕ is obtained in $0.85 < \alpha_S < 0.93$. Figure 35(b) shows the λ dependence of odd-f gap ϕ at the edge. ϕ is finite in the range of $0.35 < \lambda < 1$. At $\lambda = 0.35$, odd-f gap appears by the first order transition, while the odd-f gap vanishes by the second order transition at $\lambda = 1$. It is quite different from even-frequency superconductivity, which is realize $\lambda > 1$.

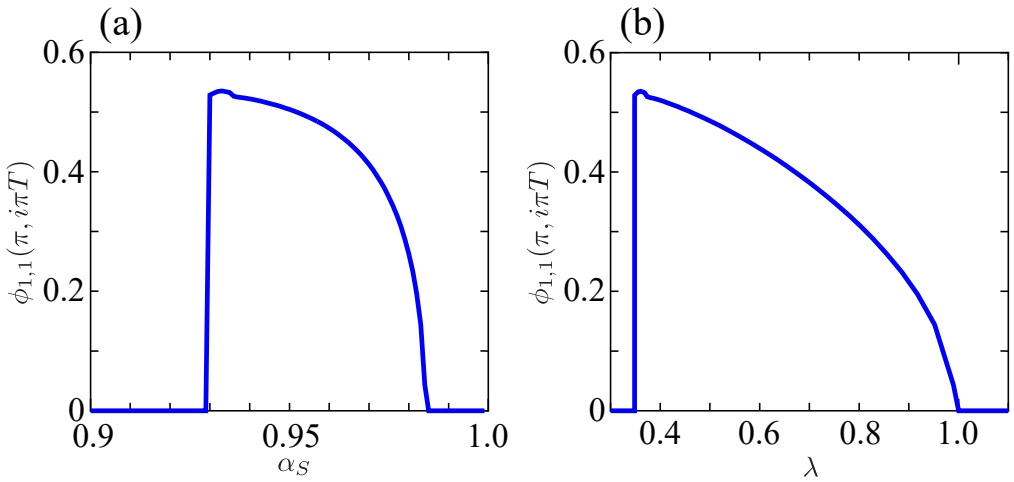

Figure 34: (a) α_S dependence of ϕ (b) λ dependence of ϕ

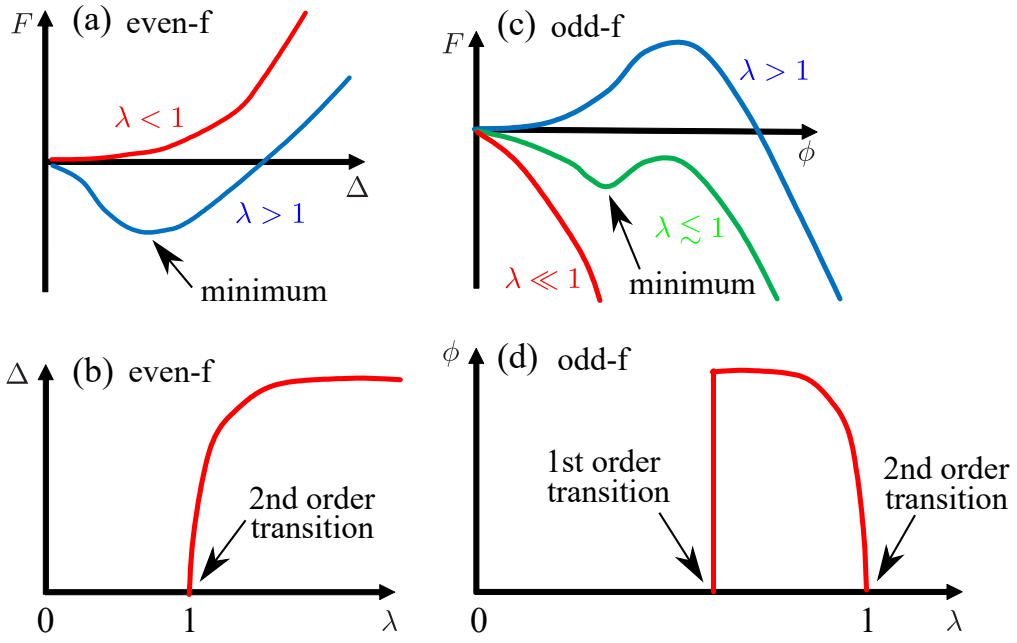

Figure 35: (a) Free energy for even-frequency superconductivity (b) λ dependence of even-frequency gap Δ (c) Free energy for odd-frequency superconductivity (d) λ dependence of odd-frequency gap ϕ

To explain this behavior, we discuss free energy based on GL theory. First, we explain GL theory for even-frequency superconductivity. In this case, free energy is expanded as follows:

$$F = a(1-\lambda)|\Delta|^2 + b|\Delta|^4 + c|\Delta|^6 \cdots \tag{79}$$

a is a positive coefficient for even frequency superconductivity. Figure 35 is the free energy for even-frequency superconductivity. For $\lambda < 1$, $\Delta = 0$ gives the minimum of F and it corresponds to the normal state. For $\lambda > 1$, there is a minimum at non-zero Δ and superconducting state is realized. Therefore, the second order transition is realized at $\lambda = 1$, and the superconducting state is realized in $\lambda > 1$.

In contrast, the free energy for odd-frequency SC is expanded as follows:

$$F = -a(1-\lambda)|\phi|^2 + b|\phi|^4 + c|\phi|^6 \cdots \tag{80}$$

There is a negative sign in the first term for odd frequency superconductivity, because $\phi(i\varepsilon_n)\phi^+(i\varepsilon_n) = -|\phi(i\varepsilon_n)|^2$ is satisfied. For $\lambda > 1$, the normal state is realized because the free energy has a minimum at $\phi = 0$. At $\lambda = 1$, odd-f superconductivity emerges by the second order transition. As λ becomes smaller, the minimum gradually moves to larger ϕ. For small λ, the minimum of the free energy suddenly vanishes and the odd-f superconductivity is broken by first order transition.

In the present system, the magnetic field does not diverge by the para-Meissner effect because the odd-frequency SC is localized at the edge. Therefore, the edge-localized odd-f SC can be realized stably. However, if the size of ϕ becomes too large, free energy increases by the

induced magnetic field and odd-f SC state is expected to be broken. The free energy should be evaluated including the effect of the magnetic field, while this effect is not considered in this discussion. If the magnetic field is taken into account, minimum of the free energy becomes $\phi = 0$ at high temperature or $\lambda \ll 1$. The detailed analysis of the realization condition of the odd-f SC gap is an important future work.

6.6 Evaluation of Free energy by Luttinger-Ward theory

Next, we evaluate the free energy of this system by using the Luttinger-Ward theory. By Luttinger-Ward theory, we can evaluate the free energy of strongly correlated superconductors. The free energy is given by

$$\Omega = \Omega_F + \Phi \tag{81}$$

$$\begin{aligned}\Omega_F &= -T\sum_{k_x,n}\log\left(\frac{\det \hat{G}(k_x,i\varepsilon_n)}{\det \hat{G}^0(k_x,i\varepsilon_n)}\right)\\ &\quad -T\sum_{k_x,n}\mathrm{Tr}\left(\hat{G}(k_x,i\varepsilon_n)\Delta\hat{\Sigma}(k_x,i\varepsilon_n)+\hat{D}(k_x,i\varepsilon_n)\hat{\Sigma}(k_x,i\varepsilon_n)+\hat{D}(k_x,i\varepsilon_n)\hat{\Sigma}(k_x,i\varepsilon_n)\right),\end{aligned} \tag{82}$$

$$\begin{aligned}\Phi &= T\sum_{q_x,n}\mathrm{Tr}\left\{\frac{1}{2}\log\left(1-U\hat{\chi}^0_{sz}(q_x,i\omega_n)\right)\right\}+T\sum_{q_x,n}\mathrm{Tr}\left\{\log\left(1-U\hat{\chi}^0_{s\pm}(q_x,i\omega_n)\right)\right\}\\ &\quad +T\sum_{q_x,n}\mathrm{Tr}\left\{\log\left(1+U\hat{\chi}^0_{c}(q_x,i\omega_n)\right)\right\}\\ &\quad +T\sum_{q_x,n}\frac{1}{4}U^2\left\{(\hat{\chi}^0_{sz}(q_x,i\omega_n))^2+(\hat{\chi}^0_{s\pm}(q_x,i\omega_n))^2\right\}\\ &\quad +T\sum_{q_x,n}U\left\{\frac{1}{2}\hat{\chi}^0_{sz}(q_x,i\omega_n)+\hat{\chi}^0_{s\pm}(q_x,i\omega_n)-\frac{1}{2}\hat{\chi}^0_{c}(q_x,i\omega_n)\right\},\end{aligned} \tag{83}$$

$$\Delta\hat{\Sigma}(k_x,i\varepsilon_n) = \hat{\Sigma}(\phi)-\hat{\Sigma}(\phi_0=0). \tag{84}$$

Ω is total free energy. Φ is Luttinger-Ward functional which represents contributions from spin fluctuations. In the $d+s^{\mathrm{odd}}$ state, $\Delta\hat{\Sigma}$ is normal self-energy due to $\phi \neq 0$ In this study, we only consider $\Delta\hat{\Sigma}$ for normal self-energy to simplify the analysis. $\Delta\hat{\Sigma}$ is calculated by FLEX approximation by using self-energy $\Delta\hat{\Sigma}$ instead of whole $\hat{\Sigma}$.

Figure 36 shows free energy calculated by (81), (82), (83), (84). Φ increases as ϕ increases because, edge odd-f gap suppresses $\chi_{s\pm}$. When $U = 2.32$, there is no minimum. Then, odd-f superconductivity does not realize. On the other hand, for $U = 2.35$, there is a minimum at $\phi \neq 0$. For $U = 2.37$, the minimum moves to smaller ϕ than that of $U = 2.35$. It corresponds

to α_S dependence of ϕ. Therefore, we verified the realization of odd-f superconductivity from the viewpoint of free energy.

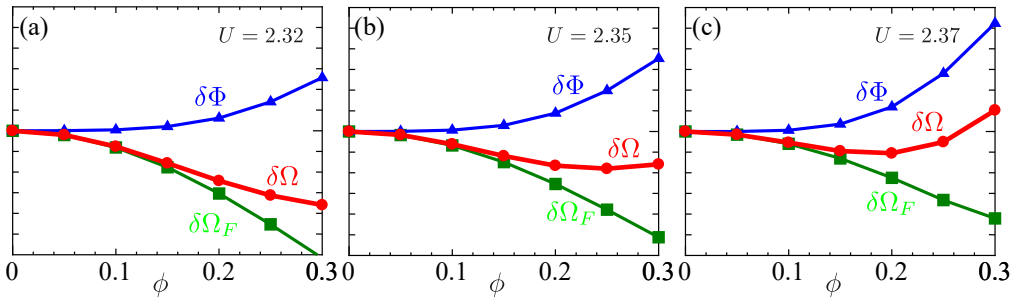

Figure 36: Free energy calculated by Luttinger-Ward theory. (a) $U = 2.32$ (b) $U = 2.32$ (b) $U = 2.32$ as a function of ϕ.

6.7 Summary

In this section, we proposed the emergence of the odd-frequency spin-triplet s wave gap function at the edge of d wave superconductors, which is mediated by the zero-energy SABS-induced ferromagnetic fluctuations. This prediction is obtained from the analysis of the edge SC gap equation based on the cluster Hubbard model with bulk d wave gap.

This odd-frequency s wave gap function is expected to be robust against randomness because it has even parity in k-space. The obtained SC state preserves the TRS and accompanies the spontaneous edge spin current because the coexistence of singlet and triplet SC gap causes asymmetry in the spin space. The predicted edge spin current in the $d+s^{\rm odd}$ wave state is a useful signal for detecting the "hidden" odd-frequency SC gap function. We also verified that the Hermite relationship (Eq. (77)) is the correct relation for the odd-frequency gap function because imaginary spin current emerges in the non-Hermite relationship. In addition, to analyze the behavior of the odd-f SC below $T_{cs^{\rm odd}}$, we solved the gap equation without linearization. We found that the non-zero odd-f SC gap emerges when $\lambda \lesssim 1$. This unconventional behavior is caused by the minus sign in the coefficient of the free energy due to the odd-frequency dependence. Finally, we evaluate the free energy based on the Luttinger-Ward theory, and confirmed that the edge-induced odd-frequency state is stable in the strongly correlated system. The analysis including the magnetic field is an important problem because the para-Meissner effect induces a magnetic field and it may contribute to the free energy greatly.

7 Nematic state of FeSe

7.1 Introduction

In strongly correlated electron systems, the nematic order, which is the rotational symmetry braking from C_4 to C_2 in the electron system attracts a lot of attention. In iron-based superconductors, various materials such as $BaFe_2As_2$ [158], NaFeAs [159], and FeSe [39, 160–167] have the nematic phase. The development of nematic fluctuations at T_s is observed by the softening of the shear modulus C_{66} [22,168–170], and Raman spectroscopy [171–173], and in-plane resistivity anisotropy $\Delta\rho$ [174].

In iron-based superconductor FeSe, the nematic transition is realized below $T = T_s \approx 90K$ without magnetic phase, while other iron-based superconductors have magnetic phase. Thus, FeSe is a favorable system for examining the relation between superconductivity and the nematic phase. The nematic state of FeSe is examined by various experiments. Recently, in the ARPES experiments, the transformation of the hole pocket at Γ point and absence of Y electron pocket are observed. The absence of Y electron pocket is also suggested by observation of Shubnikov-de Haas oscillations [177].

Theoretically, to explain the mechanism of the nematic state, spin-nematic scenario [178–183] and orbital order scenario [22, 184–189] are studied by many theorists. In the orbital order scenario, the order parameter is called "form factor", which is the C_2 component in the self-energy. In the C_4 state, the levels of d_{xz} and d_{yz} orbitals are degenerate. On the other hand, in the nematic state, form factor yields the difference in the levels of d_{xz} and d_{yz} orbitals, and the occupation numbers of d_{xz} and d_{yz} orbitals become non-equivalent. The form factor has been analyzed by Density-wave (DW) equation. The DW-equation includes higher-order many-body effects beyond the mean-field theory. For example, Aslamazov-Larkin (AL)-term in the DW-equation corresponds to the interference effect between two spin fluctuations. By the analysis of the DW-equation for d_{xz} and d_{yz} orbitals [30], modulation of Fermi pockets at Γ and X points are reproduced. However, electron pocket at Y point does not vanish in contrast to the experiments, because the form factor for d_{xy} orbital is not considered.

The absence of Y electron pocket is related to the level of d-orbitals at Y point [164]. In this study, E_{xz} and E_{xy} denote the level of d_{xz} and d_{xy} orbitals, respectively. In Figure 37, d_{yz} and d_{xy} band at Y point are shown. A band gap opens at Y point when $E_{xy} > E_{xz}$. It can be understood by the discussion of parity of each orbitals. However, for $E_{xy} < E_{xz}$, band gap does not open. Therefore, if $E_{xy} > E_{xz}$ and $E_{xy} > 0$ are realized, Y electron pocket vanishes.

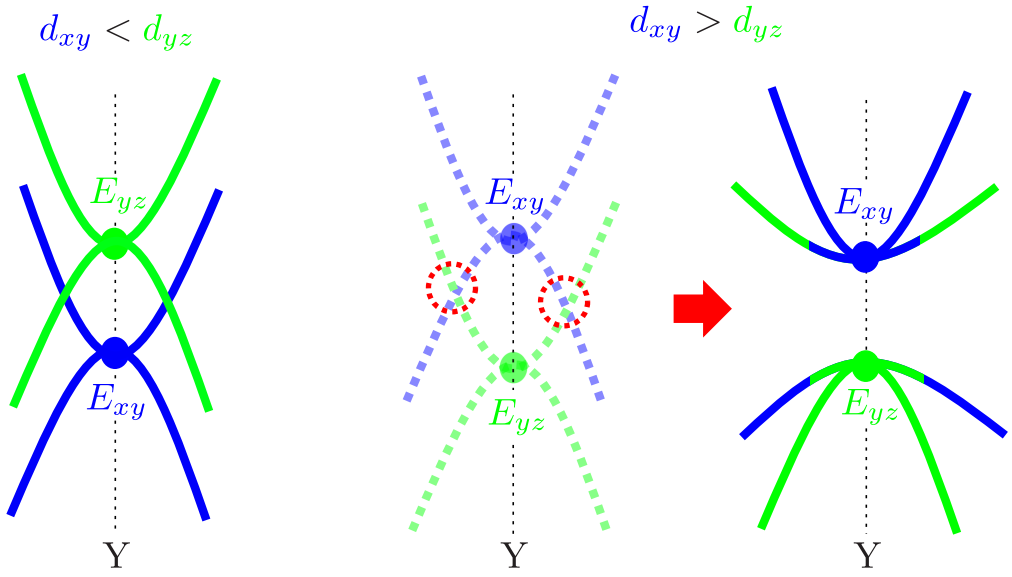

Figure 37: Schematic diagram of d_{xz} and d_{xy} band at Y point. (a) For $E_{yz} < E_{xy}$. (b) For $E_{yz} > E_{xy}$. A band gap opens at the intersection of d_{xz} and d_{xy} band, and the left figure is realized.

In this study, we analyze the DW-equation for d_{xz}, d_{yx}, and d_{xy} orbitals without linearization. We confirm that the form factor for d_{xz} and d_{yz} orbitals correspond to experimental results. The obtained form factor for d_{xy} orbital is d-wave bond order. At Y points, the band gap opens and the Fermi pocket vanishes. In addition, we calculate the T-dependence of the Form factor, and second order transition at T_s is verified. Relative phase between form factors of d_{xz} and d_{xy} are analyzed by Luttinger-Ward free energy. The relative phase is determined to decrease the free energy. In addition, we analyzed the linearized DW equation based on the FLEX approximation. λ reaches unity at $T \approx 0.007$. Therefore, we confirm that the nematic order in FeSe is driven by the quantum interference effect. Furthermore, to elucidate the self-energy effect, we solve the 3-orbital DW-equation including FLEX self-energy without linearization. We also obtain the orbital polarization and bond order, and the absence of the Y electron pocket is reproduced even if FLEX self-energy is taken into account.

7.2 Model

In this study, we use the 5-orbital Hubbard model.

$$\mathcal{H} = H_M + rH_M^U \tag{85}$$

H_M is 8-orbital Hubbard model. rH_M^U is the Coulomb interaction obtained by the first principle calculation. r is a parameter to adjust the size of Coulomb interaction.

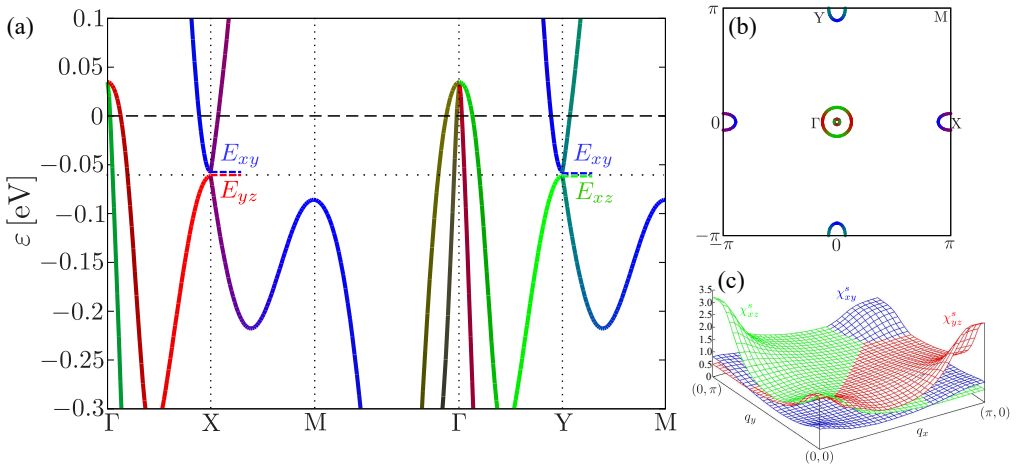

Figure 38: (a) Band of this study near the fermi level. (b) Fermi surface in the normal state (with rotational symmetry). (c) Spin susceptibilities χ^s_{xz}, χ^s_{yz}, and χ^s_{xy} calculated by RPA.

Figure 38(a) shows the band near the fermi level in this model. The level of d_{xz}, d_{yz}, and d_{xy} orbitals are represented by E_{xz}, E_{yz}, and E_{xy}, respectively. We set $E_{xz} \approx E_{xy} \approx -0.07$ which corresponds to experiments by considering the renormalization factor $z \approx 2.5$. We set the ratio of the renormalization factor $z_{xy}/z_{xz} = 1.6$. Fig. 38(b) is the Fermi surface in the normal state. In the normal state, the system has C_4 symmetry. Fig. 38(c) is the spin susceptibilities calculated by the RPA. Anti-ferromagnetic fluctuations at $q = (0, \pi)$ and $(\pi, 0)$ develops. It corresponds to experiments.

In this study, we analyze DW-equation without linearization. DW-equation can treat the rotational symmetry braking component $\Delta\hat{\Sigma}$ emerging in the FLEX self-energy $\hat{\Sigma}^{\rm FLEX}$. In this analysis, Green function is represented by a matrix of orbitals and it is given by

$$\hat{G}(k) = (\hat{z}^{-1} i\varepsilon_n + \mu - \hat{h}^0_M(\mathbf{k}) - \Delta\hat{\Sigma}(k))^{-1}, \tag{86}$$

where $\varepsilon_n = (2n+1)\pi T$ is Matsubara frequency. $k = (k_x, k_y, i\varepsilon_n) = (\mathbf{k}, i\varepsilon_n)$. z^{-1} is the renormalization factor. The spin (charge) susceptibility $\hat{\chi}^{s(c)}(q)$ is given by

$$\hat{\chi}^{s(c)}(q) = \hat{\chi}^0(q)[1 - \hat{\Gamma}^{s(c)}\hat{\chi}^0(q]^{-1}, \tag{87}$$

$$(\hat{\Gamma}^s)_{l_1,l_2,l_3,l_4} = \begin{cases} U_{l_1,l_1} & l_1 = l_2 = l_3 = l4 \\ U'_{l_1,l_2} & l_1 = l_3 \neq l_2 = l4 \\ J_{l_1,l_3} & l_1 = l_2 \neq l_3 = l4 \\ J_{l_1,l_2} & l_1 = l_4 \neq l_2 = l3 \\ 0 & \text{otherwise.} \end{cases} \tag{88}$$

$$(\hat{\Gamma}^c)_{l_1,l_2,l_3,l_4} = \begin{cases} -U_{l_1,l_1} & l_1 = l_2 = l_3 = l4 \\ U'_{l_1,l_2} - 2J_{l_1,l_2} & l_1 = l_3 \neq l_2 = l4 \\ -2U'_{l_1,l_3} + J_{l_1,l_3} & l_1 = l_2 \neq l_3 = l4 \\ -J_{l_1,l_2} & l_1 = l_4 \neq l_2 = l3 \\ 0 & \text{otherwise.} \end{cases} \tag{89}$$

where $\hat{\chi}^0(q)$ is the irreducible susceptibility. We assume $J = J'$ and $U = U + 2J$. Next, we calculate $\Sigma^{\rm FLEX}$ as follows:

$$\Sigma^{\rm FLEX} = \Sigma^H_{l,l'} + T \sum_{q,m,m'} V_{l,m;l'm'}(q) G_{m,m'}(k-q), \tag{90}$$

$$\begin{aligned} V_{l,m;l'm'}(q) &= \frac{3}{2}\hat{\Gamma}^s \hat{\chi}^s(q) \hat{\Gamma}^s + \frac{1}{2}\hat{\Gamma}^c \hat{\chi}^c(q) \hat{\Gamma}^c \\ &\quad -\frac{1}{2}\left[\hat{\Gamma}^c \hat{\chi}^0(q) \hat{\Gamma}^c + \hat{\Gamma}^s \hat{\chi}^0(q) \hat{\Gamma}^s - \frac{1}{4}\left(\hat{\Gamma}^s + \hat{\Gamma}^c\right) \hat{\chi}^0(q) \left(\hat{\Gamma}^s + \hat{\Gamma}^c\right)\right] \end{aligned} \tag{91}$$

where $\Sigma^H_{l,l'}$ is the Hartree term. $\hat{\Gamma}^{s(c)}$ is the Coulomb interaction for spin (charge) channel. To obtain C_2 component in self-energy, we subtract $\Sigma^{A_{1g}}$ from $\Sigma^{\rm FLEX}$. $\Sigma^{A_{1g}}$ represents the A_{1g} component in the self-energy, which has C_4 rotational symmetry.

$$\Delta\hat{\Sigma} = \hat{\Sigma}^{\rm FLEX} - \hat{\Sigma}^{A_{1g}} \tag{92}$$

where $\mathbf{k}' = (k_y, k_x)$. We solve (86)–(92) self-consistently by performing iteration.

In this numerical analysis, k-mesh is $N_x \times N_y = 64 \times 64$, the number of Matsubara frequencies is 512. We set the size of Coulomb interaction as $r = 0.27$. Here, the unit of energy is $|t|$, which corresponds to ~ 0.1eV in FeSe.

7.3 Numerical Results of DW equation

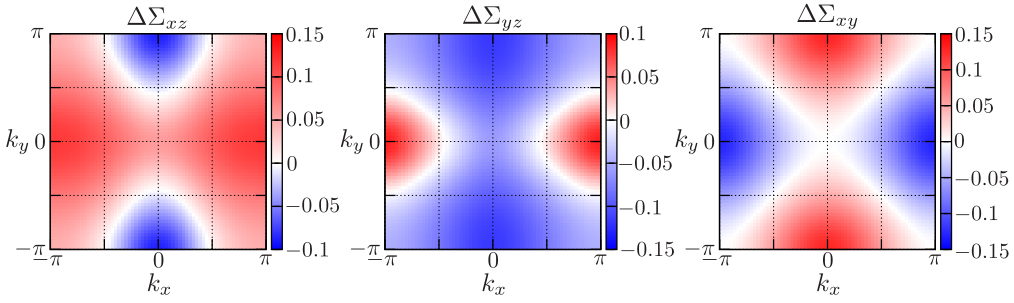

Figure 39: k-dependence of form factors $\Delta\Sigma$ obtained by the DW equation without linearization. $\Delta\Sigma_{xz}$ and $\Delta\Sigma_{yz}$ cause the orbital polarization. $\Delta\Sigma_{xy}$ corresponds to the d-wave bond order.

Figure 39 shows the solution of the DW-equation. Form factor gives the shift of the level of each orbital. $\Delta\Sigma_{xz}$ lowers the level of d_{xz} orbitals at Y point. On the other hand, $\Delta\Sigma_{yz}$ raises the level of d_{yz} orbitals at X point. They correspond to the orbital order. The hole pocket at Γ point extends in y-direction because $\Delta\Sigma_{xz}$ and $\Delta\Sigma_{yz}$ have opposite sign at the Γ point. The obtained $\Delta\Sigma_{xy}$ is proportional to $\cos k_x - \cos k_y$. It is the d-wave bond order, which yields modulation in the hopping integrals between d_{xy} orbitals in the different sites.

Figure 40 shows its physical explanation. The hopping integral in y-direction increases by δ, while it decreases in x-direction by δ.

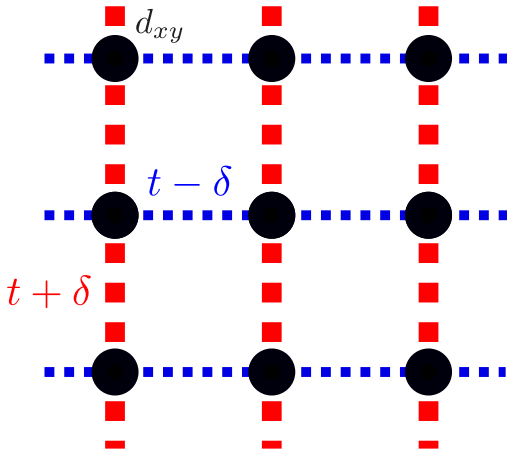

Figure 40: Modulation in the hopping integrals by the d-wave bond order. In the y (x) direction, hopping integral increases (decreases) by δ.

Figure 41 (a) shows the band in the nematic state based on the obtained form factor $\Delta\Sigma$. At X point, due to the form factor $\Delta\Sigma$ level of d_{yz} and d_{xy} move upward and downward, respectively. In this case, $E_{yz} > E_{xy}$ holds, and gap does not open. On the other hand, at X point, level of d_{xz} and d_{xy} move downward and upward, respectively. In this case, $E_{xz} < E_{xy}$ holds, and gap opens. If $E_{xy} > 0$, Fermi pocket at Y point vanishes as shown in Fig. 41 (b).

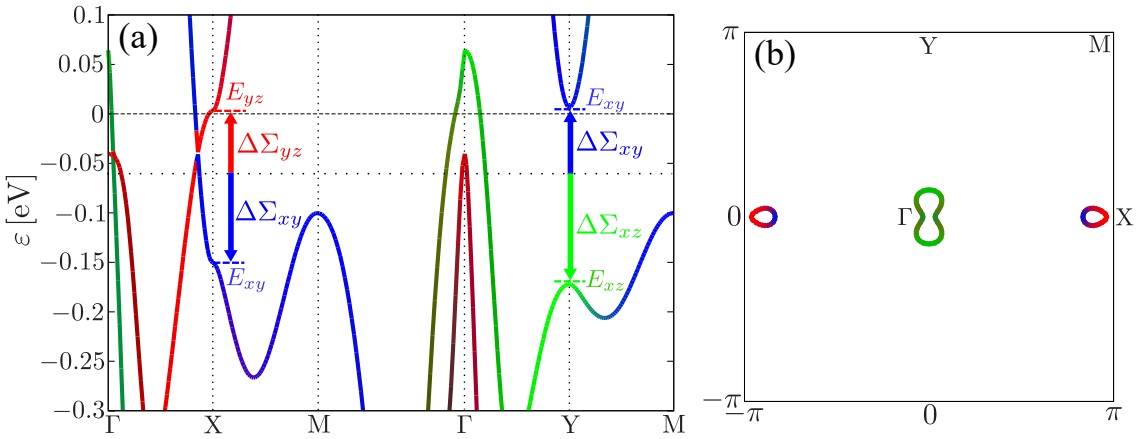

Figure 41: (a) Band in the nematic state. Form factor $\Delta\Sigma$ is taken into account. (b) Fermi surface in the nematic state.

7.4 Temperature dependence

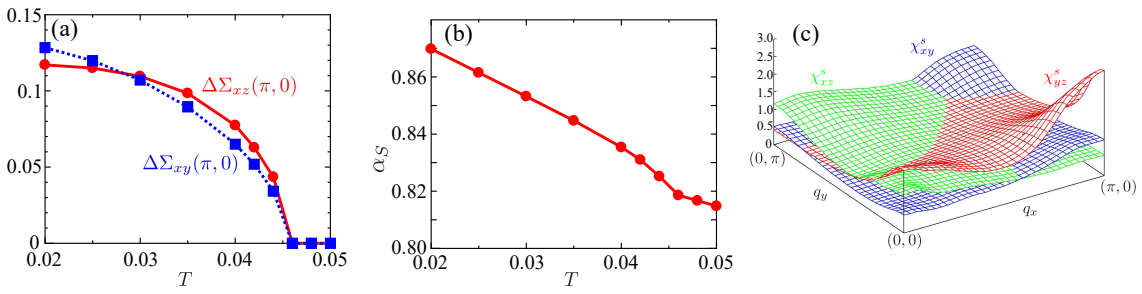

Figure 42: T-dependence of the form factors obtained by the DW equation without linearization.

In this study, we analyze the DW-equation without linearization. Thus, we can obtain the size of the form factor. Figure 42 (a) shows the temperature dependence of form factor. Nematic transition is second order transition, and realized at $T_s \approx 0.045$. In Fig. 42 (b), Stoner factor α_S increases below T_s because the spin fluctuation at $q = (0, \pi)$ is enhanced as shown in 42 (b) in the nematic state. This behavior is consistent with the experiments.

7.5 Physical meaning of Relative Phase between $\Delta\Sigma_{22}$ and $\Delta\Sigma_{44}$

In this study, the obtained form factor $\Delta\Sigma_{22}$ and $\Delta\Sigma_{44}$ satisfy following relation:

$$\Delta\Sigma_{xz}(0,\pi)\Delta\Sigma_{xy}(0,\pi) < 0. \tag{93}$$

This relative phase is important for vanishing of Y electron pocket. If relative phase satisfies $\Delta\Sigma_{xz}(0,\pi)\Delta\Sigma_{xy}(0,\pi) > 0$ E_{xz} and E_{xy} shift same direction. Thus, $E_{xz} < E_{xy}$ is not realized.

In this section, we discuss the reason for obtained relative phase from the viewpoint of free energy. We evaluate the free energy based on Luttinger-Ward theory, which can treat the strongly correlated system.

$$\Omega = \Omega_F + \Phi \tag{94}$$

$$\Delta\Sigma = \begin{pmatrix} \Delta\Sigma_{xz} \\ \Delta\Sigma_{yz} \\ r\Delta\Sigma_{xy} \end{pmatrix} \tag{95}$$

$$\Omega_F = -T\sum_{k_x,n} \log\left(\frac{\det \hat{G}(k_x, i\varepsilon_n)}{\det \hat{G}^0(k_x, i\varepsilon_n)}\right) - T\sum_{k_x,n} \mathrm{Tr}\hat{G}(k_x, i\varepsilon_n)\Delta\hat{\Sigma}(k_x, i\varepsilon_n) \tag{96}$$

$$\Phi = T\sum_{q,n}\mathrm{Tr}\left\{\frac{3}{2}\log\left(1-\hat{\Gamma}^s\hat{\chi}^0(q,i\omega_n)\right)\right\}+T\sum_{q,n}\mathrm{Tr}\left\{\log\left(1+\hat{\Gamma}^c\hat{\chi}^0(q,i\omega_n)\right)\right\}$$
$$+T\sum_{q,n}\frac{1}{4}(\hat{\Gamma}^s\hat{\chi}^0(q,i\omega_n))^2+T\sum_{q,n}\left\{\hat{\Gamma}^s\frac{3}{2}\hat{\chi}^0(q,i\omega_n)-\frac{1}{2}\hat{\Gamma}\hat{\chi}^0(q_x,i\omega_n)\right\} \quad (97)$$

Here, we introduce r as a parameter to modulate the size of the form factor and the relative phase. $r>0$ corresponds to the correct relative phase. If $r<0$, the relative phase is opposite.

Figure 43 (a) shows obtained free energy. Total free energy Ω_{total} has a minimum in the range of $r>0$. When $r>0$, the relative phase corresponds to the solution of DW-equation and the Y electron pocket is absent as shown in Fig 43 (b). On the other hand, Ω_{total} increases in the range of $r<0$. In this case, the relative phase is opposite from the solution of DW-equation, and Y electron pocket does not vanish as shown in Fig 43 (c). The contribution from Ω_0 is dominant. Therefore, the relative phase is determined to decrease the free energy by opening the band gap.

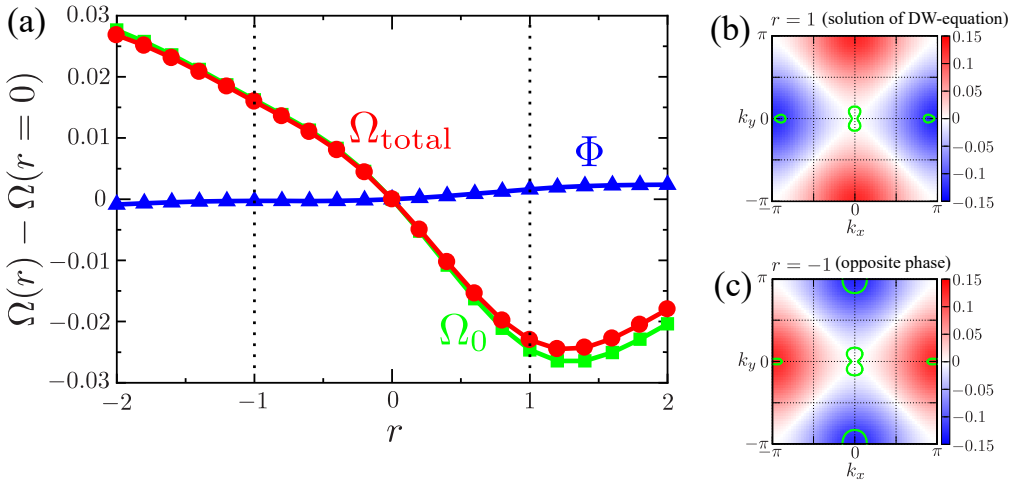

Figure 43: (a) r dependence of Free energy. (b) $r\Delta_{xy}$ for $r=1$. Green curve represents the Fermi surface for $r=1$. (c) $r\Delta_{xy}$ for $r=-1$ Green curve represents the Fermi surface for $r=-1$.

7.6 Linearized DW equation based on FLEX approximation

We analyzed linearized DW-equation based on FLEX approximation to consider the effect of self-energy. The diagram of linearized DW-equation is shown in figure 44. AL terms include two spin fluctuations. Thus they correspond to interference between spin fluctuations. The linearized DW-equation is derived by expanding the FLEX self-energy by $\Delta\Sigma$ and considering only the first order terms. λ is the eigenvalue of DW-equation. By solving the linearized DW equation, we can obtain the form factor $\Delta\Sigma$ and eigenvalue λ. If $\lambda>1$ is realized, the nematic order corresponding to $\Delta\Sigma$ emerges. In this calculation, we set the size of Coulomb interaction as $r=0.4$.

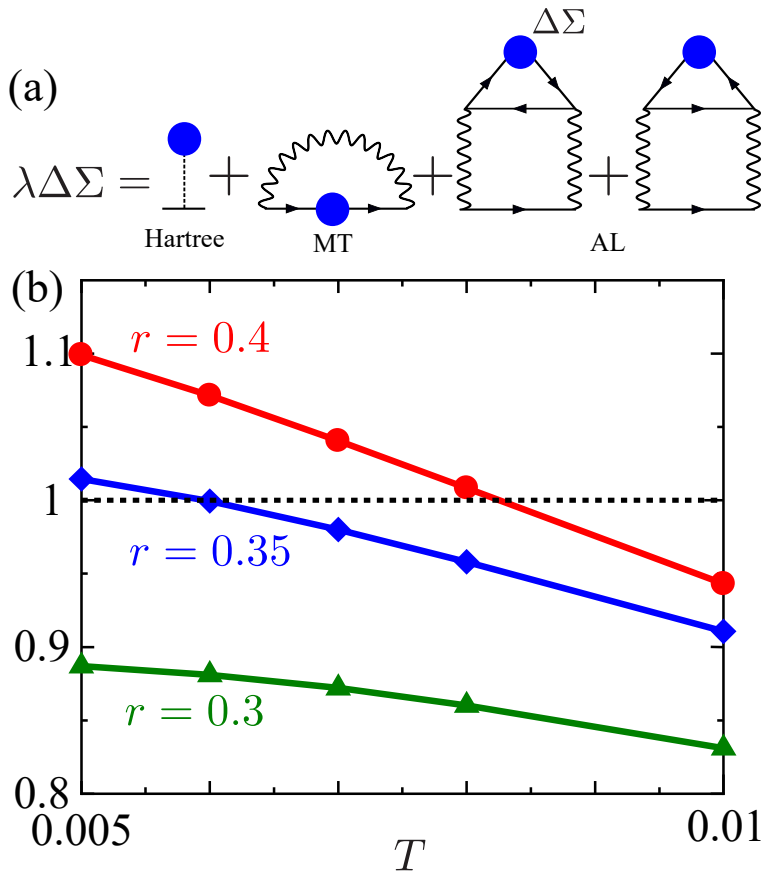

Figure 44: (a) Diagram of linearized DW-equation. The arrow represents the Green function G. The wavy line corresponds to the spin fluctuations. The blue circle is the form factor. (b) Temperature dependence of eigenvalue of DW equation.

The eigenvalue λ reaches unity at $T \approx 0.008$. Due to the self-energy effect, T_s is lower than Fig 42 based on RPA. It means that the nematic order is realized if we consider the self-energy effect. In addition, we verify that the origin of the nematic order is quantum interference of spin fluctuations.

7.7 DW equation based on FLEX approximation

In this section, we analyze the DW-equation including $\Sigma^{\rm FLEX}$ without linearization, while we did not consider $\Sigma^{\rm FLEX}$ in the previous section. Green function in this analysis is given by

$$\hat{G}(k) = (\hat{z}^{-1} i\varepsilon_n + \mu - \hat{h}^0_M(\mathbf{k}) - \Sigma^{\rm FLEX}(k) - \Delta\hat{\Sigma}(k))^{-1}. \tag{98}$$

We first perform the conventional FLEX calculation, and obtain self-energy in C_4-symmetry system $\Sigma^{\rm FLEX}$. Then, we fix $\Sigma^{\rm FLEX}$, and calculate C_2-symmetry part $\Delta\hat{\Sigma}$ self-consistently. Figure 45(a)–(c) shows the renormalized form factor $\Delta\Sigma^*$ obtained by this analysis. The renormalization factor is evaluated by FLEX self-energy. k-dependence of Form factor is qualitatively the same as that based on the RPA.

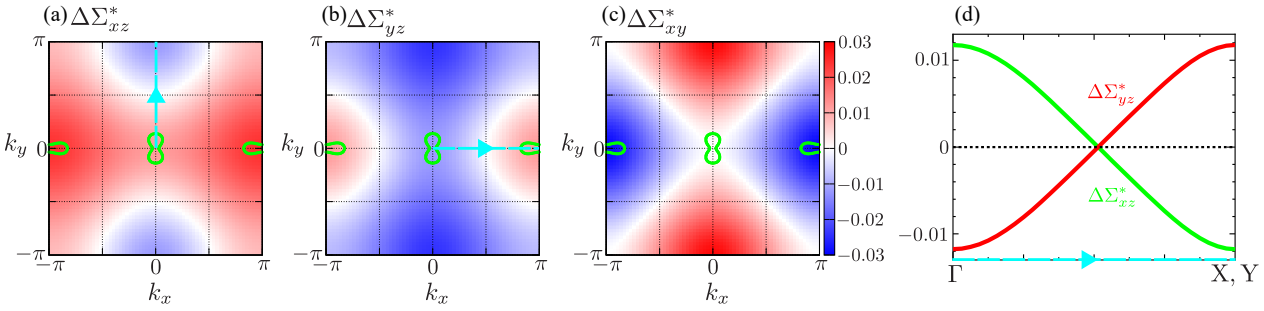

Figure 45: Renormalized form factors obtained by DW equation without linearization including $\Sigma^{\rm FLEX}$. Green curves are the Fermi surface in the obtained nematic state.

Figure 45 (d) shows the $\mathbf{k}$-dependence of $\Delta\Sigma^*_{xz}$ and $\Delta\Sigma^*_{yz}$ along with the blue arrows illustrated in Figure 45 (a), (b). Sign change between Γ and X point is consistent with the experiments [164, 165].

Figure 46 (a) shows the band in the nematic state. We confirmed that the Y electron pocket vanishes also considering the FLEX self-energyas shown in Fig. 46 (b)

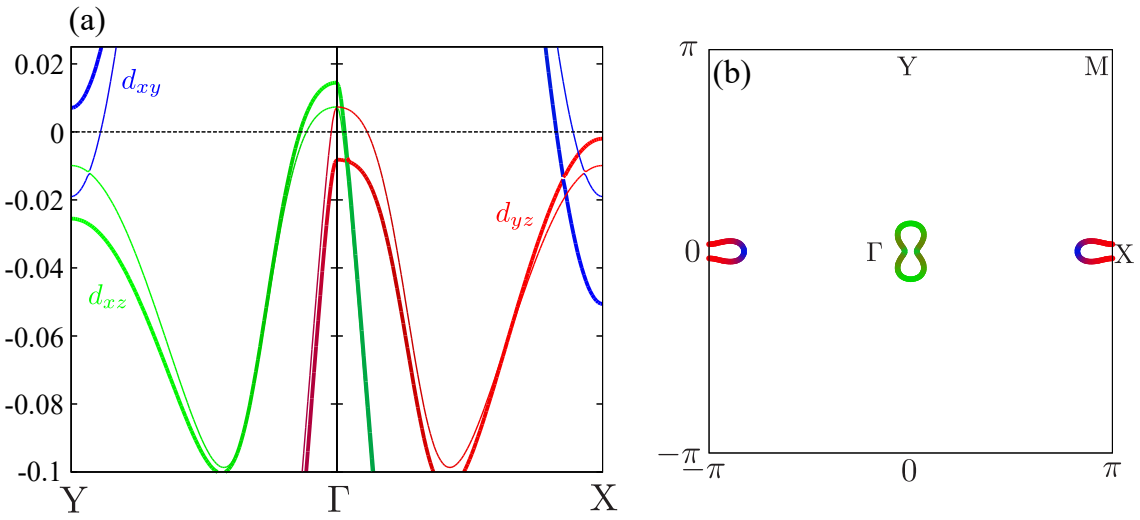

Figure 46: Band structure and Fermi surface in the nematic state obtained by the analysis including the FLEX self-energy. (a) Band structure. The bold curves are the band in the nematic state. The thin curves are the band in the normal state. (b) Fermi surface in the nematic state.

Figure 47 shows the temperature dependence of the renormalized form factor $\Delta\Sigma^* = z^{-1}\Delta\Sigma$. z^{-1} for each orbitals are obtained from FLEX self-energy $\Sigma^{\rm FLEX}(0,\pi)$. The obtained values are $z^{-1}_{xz} = z^{-1}_{yz} \approx 0.27$ and $z^{-1}_{xy} \approx 0.17$. The nematic transition is realized at $T_s \approx 0.0081$ by the second order transition. In the previous subsection, we analyze the linearized DW equation based on the FLEX, and obtained $T_s \approx 0.08$ for $r = 0.4$. It is consistent with the result of the full DW equation.

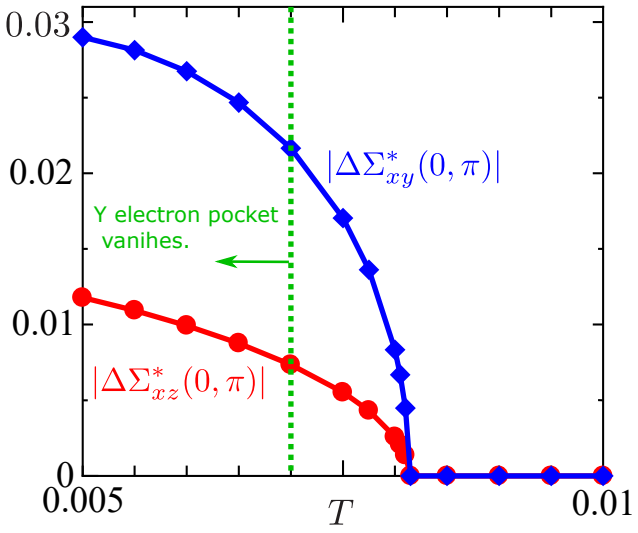

Figure 47: Temperature dependence of renormalized form factors. We set $r = 0.4$ in the FLEX calculation. Transition temperature is $T_s \approx 0.0081$.

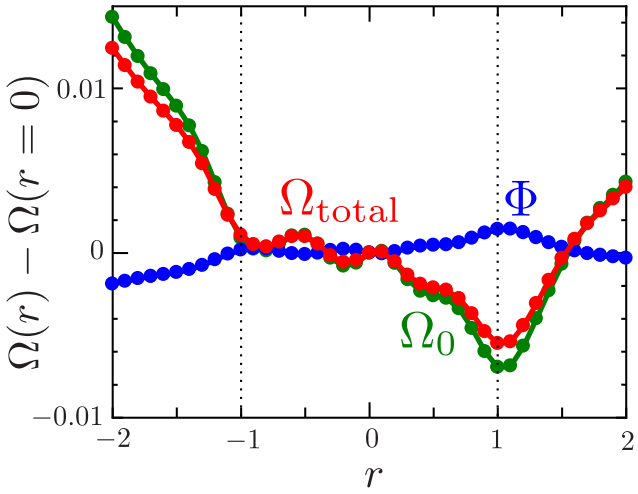

Figure 48: r dependence of Free energy including the FLEX self-energy. The red line is the total free energy $\Omega_{\rm total}$. The green and blue line are Ω_0 and Φ, respectively.

Finally, we evaluate the free energy by Luttinger-Ward theory. To include FLEX self-energy, we substitute following $\Sigma_{\rm total}$ instead of $\Delta\Sigma$ in eq (95).

$$\Sigma_{\rm total} = \Sigma^{A_{1g}} + \begin{pmatrix} \Delta\Sigma_{xz} \\ \Delta\Sigma_{yz} \\ r\Delta\Sigma_{xy} \end{pmatrix}. \tag{99}$$

We adjust the size of $\Delta\Sigma$ by using parameter r. The size of $\Sigma^{A_{1g}}$ is fixed in this analysis. Figure 48 shows the obtained free energy. When $r < 0$, the relative phase is opposite to

that of the obtained solution. When $r > 0$, the relative phase corresponds to the obtained solution. $\Omega_{\rm total}$ has a minimum at $r \approx 1$ because the DW equation is derived from the minimum condition of free energy. Therefore, we confirmed that the relative phase between $\Delta\Sigma_{xz}$ and $\Delta\Sigma_{xy}$ is determined to open the band gap also including the FLEX self-energy.

7.8 Summary

In this study, we discussed the nematic state of FeSe by analyzing the DW-equation for d_{xz}, d_{yz}, and d_{xy} orbitals without linearization. The form factor of d_{xz} and d_{yz} orbitals corresponds to orbital order. Sign change between Γ and Y(X) point is consistent with the experimental band shift. For d_{xy} orbital, d-wave bond order is realized. It shits the level of d_{xy} orbital upward at Y point. Then, the band gap opens, and the Y electron pocket vanishes. We also obtained the T-dependence of form factor because we analyzed DW-equation without linearization. We confirmed that the nematic transition is second order transition. The Stoner factor α_S increases in below T_s because spin susceptibility at $q = (\pi, 0)$ grows in the nematic state. In addition, we discussed the relative phase between $\Delta\Sigma_{xz}$ and $\Delta\Sigma_{xy}$ from the viewpoint of free energy based on Luttinger-Ward theory. We verified that the correct relative phase reduces the free energy and minimum yields $r \approx 0.5$, while the free energy increases for the wrong relative phase. Finally, we analyzed the linearized DW-equation based on the FLEX approximation to consider the effect of self-energy. We confirmed that λ reaches unity even if the self-energy effect is included. Therefore, the nematic transition is driven by the quantum interference effect represented by the AL term.

8 Summary

In section 3, we studied the effect of edge on the strongly correlated electron systems in the normal state. Due to the Friedel oscillation by the edge, the spin fluctuations are enhanced near the edge. In the FLEX, the site-dependent mass-enhancement factor Z_x and quasiparticle damping γ_y have large value near the open edge. Thus, we proposed the edge-induced quantum critical phenomena in the normal state.

In section 4, we studied the drastic development of the FM fluctuations at the $(1,1)$ edge of the d-wave superconductor. By detailed analysis, we found that the ABS induces the strong FM correlation mainly through the increase of irreducible susceptibility $\hat{\varphi}^0$. Furthermore, we examined the temperature dependence, and predicted the drastic increase of Stoner factor $\alpha_S$just below the bulk d-wave T_c. Finally, we verified that the enhancement in FM fluctuations are still prominent under the conditions $2\Delta_{\max}/T_{cd} \gtrsim 6$ and $\xi_d \ll 10$, which are satisfied in cuprate superconductors. Therefore, the ABS-induced FM order or strong FM fluctuations is expected to appear in real cuprate superconductors.

In section 5, we discussed the emergence of the even-frequency spin-triplet gap function at the $(1,1)$ edge of the d-wave superconductors. We revealed that the edge-localized p-wave SC is mediated by the strong FM fluctuations caused by the ABS. The bulk d-wave gap and the edge p-wave gap are coexistent as the time-reversal symmetry braking $d \pm ip$-wave SC state by choosing the relative phase as $\pi/2$ in the $\boldsymbol{k}$-space. Next, we explain the T-dependence of the eigenvalue λ for the edge-induced triplet SC state. Below the bulk d-wave transition temperature T_{cd}, λ increases drastically as T decreases, and reaches unity at $T = T_{cp}$. Therefore, the $d \pm ip$-wave SC state is realized at $T_{cp} \lesssim T_{cd}$. By the calculation of the edge current, we found that no spontaneous edge current emerges in the $d \pm ip$-wave SC state although the time-reversal symmetry is broken.

In section 6, we discussed the emergence of the odd-frequency spin-triplet s wave gap function due to the ABS-driven strong FM fluctuations. We analyzed the linearized triplet gap equation including the frequency-dependence of the triplet gap in the cluster Hubbard model with bulk d wave gap. The predicted odd-frequency s wave gap function is expected to be robust against randomness. The obtained solution is odd-frequency s wave gap function, which is expected to be robust against impurities. The obtained SC state preserves the TRS, and the spontaneous edge spin current flows along the edge. We can experimentally detect the "hidden" odd-frequency SC gap function if this spontaneous spin current is observed. We also verified that the Hermite relationship (Eq. (77)) is the correct relation of the odd-frequency gap function. In addition, we solve the gap equation without linearization. We found that the odd-frequency gap is non-zero for $\lambda \lesssim 1$. This behavior is originated from the sign of the coefficient of free energy. Finally, we evaluated the free energy based on the Luttinger-Ward theory, which includes contributions from the electron correlation, and confirmed realization of the edge-induced odd-frequency SC state.

In section 7, we analyzed the nematic state of FeSe. We analyzed the DW-equation for d_{xz}, d_{yz}, and d_{xy} orbitals without linearization. For d_{xy} orbital, d-wave bond order is obtained. It shits the level of d_{xy} orbital upward at Y point. Then, the band gap opens and the Y electron pocket vanishes. By the non-linearized analysis, the T-dependence of form

factor is obtained, and the nematic transition is second order transition. In addition, the relative phase between $\Delta\Sigma_{xz}$ and $\Delta\Sigma_{xy}$ is determined to minimize the free energy. Next, we analyzed the DW-equation including the FLEX self-energy, and confirmed that the emergence of nematic order and the absence of the Y Fermi pocket. By the analysis of the linearized DW-equation, we confirmed that the nematic transition is driven by the quantum interference effect represented by the AL term.

In this study, we examined the effect of real space structure on the strongly correlated electron systems by constructing the real space formalism. In the normal state, Friedel oscillation due to the edge induced the strong correlation state near the edge. In the bulk d-wave SC state, the Andreev bound state enhances edge ferromagnetic fluctuations strongly. Then, ferromagnetic fluctuations induce even-frequency spin-triplet p-wave or odd-frequency spin-triplet s-wave. Therefore, the real space structure can induce various interesting phenomena, which can not be realized in the bulk. We exhibited that the "edge induced superconductivity" can be a valuable method to realize exotic superconductivity. Finally, we analyzed the nematic state in FeSe by the DW equation. We found that the interference effect of spin fluctuations can induce nematic order, and the experimental Fermi surface is reproduced.

As a future work, to examine the nematic order induced by the real space structure is an important problem. If we analyze the DW-equation in the open edge Hubbard model, edge-induced nematic order of fluctuations may be obtained. In addition, the time-reversal symmetry breaking SC at the boundary of nematic order in FeSe is also an interesting problem [80]. The site-dependence analysis developed in this study should be a useful method to analyze the boundary-induced SC based on the microscopic pairing interaction.

9 Acknowledgement

I would like to express my great appreciation to my advisor Professor Hiroshi Kontani. His precise advice and daily discussion encouraged me to carry out this study. In the process of this study, I learned a lot of things not only about physics but also how to deal with a difficult problem. 5 years in this laboratory is a treasure of my life. I would like to express thanks to him for recommending me to go to the doctoral course. I would like to thank gratitude for Professor Seiichiro Onari for his kind advice in the study on FeSe. I would like to thank Dr. Youichi Yamakawa. Without his advice, I could not perform the site-dependent numerical calculation. I would like to sincere gratitude to Professor Yukio Tanaka for his fruitful advice and discussion in the collaborative research on odd-frequency superconductivity.

Besides my supervisor, I would like to thank all members of Sc laboratory. My phD study has been supported by KAKENHI (No.JP19H05825) from the Japan Society for the Promotion of Science (JSPS).

Finally, I would like to express my deepest thanks to my family.

A Filling dependence in the normal state

A.1 Filling dependence in LSCO TB model

In the main text, we fix the electron filling at $n = 0.95$, which corresponds to under-doped region of hole-doping compounds. Interesting edge-induced quantum critical phenomena are realized in both LSCO TB and YBCO TB cluster Hubbard models. In this Appendix, we present the numerical results for $n = 0.90 \sim 1.10$ in order to understand the origin of the edge-induced quantum criticality. We find the realization condition of the prominent edge-induced quantum criticality.

First, we explain the numerical results for the LSCO TB model. We set $T = 0.02$ and $U = 1.78$ in unit eV, for $n = 0.90$, 0.95, 1.05 and 1.10. Figure 49 presents the (a) $\chi^s_{x,x}(q_y)$ and (b) quasiparticle damping γ^*_x, mass-enhancement factor Z_x, and the bare local density of states (LDOS) at the Fermi level $D_x(0)$. The obtained spin Stoner factors are shown in Fig. 49 (a). The oscillation in $D_x(0)$ is understood as the Friedel oscillation caused by the open edge.

In the $(1, 1)$ edge model, the edge-induced quantum criticality is prominent in both hole-doped case ($n < 1$) and electron-doped case ($n > 1$). $\chi^s_{x,x}(q_y)$ is strongly enlarged at $x = 1$ and $q_y = 0$. By reflecting this fact, both γ^*_x and Z_x are strongly enlarged in both hole- and electron-doped cases. In the $(1, 0)$ edge model, the edge-induced quantum criticality is moderate. In electron-doped case, $\chi^s_{x,x}(q_y)$ takes the maximum at $x = 1$ and $q_y = \pi$. In hole-doped case, in contrast, $\chi^s_{x,x}(q_y = \pi)$ is moderately enlarged at $x \geq 2$. Both γ^*_x and Z_x show similar x-dependences to $D_x(0)$.

The obtained nontrivial n-dependences for both $(1, 1)$ and $(1, 0)$ edge models are well understood in terms of the LDOS without interaction shown in Fig. 49 (b). In the $(1, 0)$ edge model, the LDOS at $x = 1$ is strongly suppressed in hole-doped case. Due to this fact, the edge electronic states deviate from the quantum criticality. In electron-doped case, the LDOS at $x = 1$ is larger than the balk DOS, so the edge effect becomes moderate. In the $(1, 1)$ edge model, the x-dependence of the LDOS is essentially n-independent. For this reason, the edge electronic states approach the quantum criticality in both hole-doped and electron-doped cases.

A.2 Filling dependence in YBCO TB model

Next, we explain the numerical results for the YBCO TB model for $n = 0.90$, 0.95, 1.05 and 1.10. The obtained $\chi^s_{x,x}(q_y)$, γ^*_x, Z_x, and $D_x(0)$ are shown in Fig. 50. The YBCO TB model with $n > 1$ corresponds to the electron-doped cuprate superconductors, NCCO and PCCO. The obtained spin Stoner factors are shown in Fig. 50 (a).

In both $(1, 0)$ and $(1, 1)$ edge models, the obtained n-dependences are qualitatively similar to those obtained in the LSCO TB model. In the $(1, 1)$ edge model, $\chi^s_{x,x}(q_y = 0)$, are strongly enlarged at $x \approx 1$. Thus, the edge electronic states approach to the quantum criticality. This result originates from the large LDOS on the $(1, 1)$ edge in YBCO model, shown in Fig. 50 (b). In the $(1, 0)$ edge model, the edge-induced quantum criticality is moderate. For both

$n > 1$ and $n < 1$ cases, $\chi^s_{x,x}(q_y = \pi)$ takes the maximum at $x = 1$. In hole-doped case, in contrast $\chi^s_{x,x}(q_y = \pi)$ is moderately enlarged at $x \geq 2$. Both γ^*_x and Z_x show similar x-dependences.

To summarize, prominent edge-induced quantum criticality is realized when the edge LDOS is large. This result is a useful principle to control the quantum criticality driven by real-space structure because it is easy to calculate the LDOS in non-interacting systems. The YBCO TB model with $n > 1$ corresponds to NCCO and PCCO. In the YBCO TB model, very large quasiparticle damping rate γ^*_x is obtained in the (1,1) open edge. This result may lead to the pseudo-gap formation in the LDOS in the (1,1) open edge in YBCO, NCCO, and PCCO cuprate superconductors.

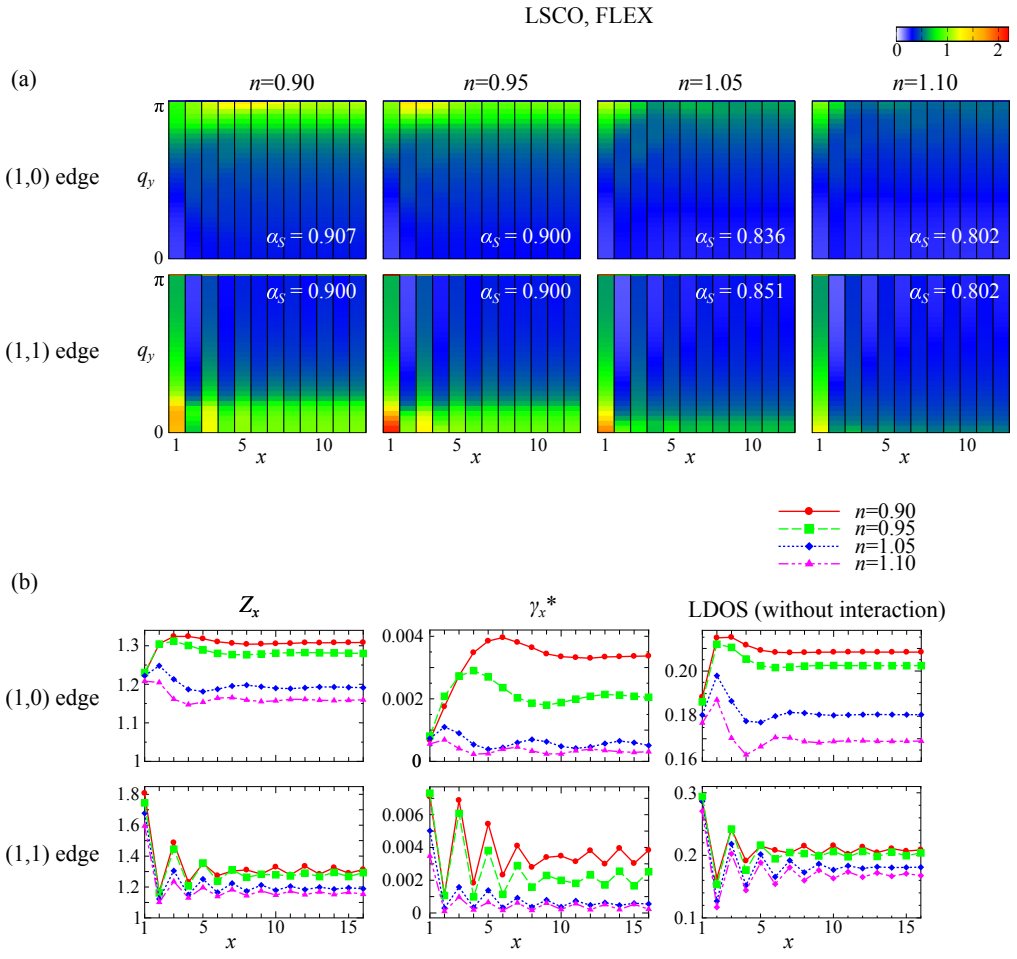

Figure 49: (a) Obtained $\chi^s_{x,x}(q_y)$ in LSCO TB model with $(1,1)$ open edge and $(1,0)$ open edge, respectively. The results for $n = 0.90$, 0.95, 1.05, and 1.10 are shown. (b) Obtained filling-dependences of the mass-enhancement factor Z_x and quasiparticle damping γ^*_x, and LDOS at the Fermi level $D_x(0)$ in the LSCO TB model ($n = 0.90 \sim 1.10$).

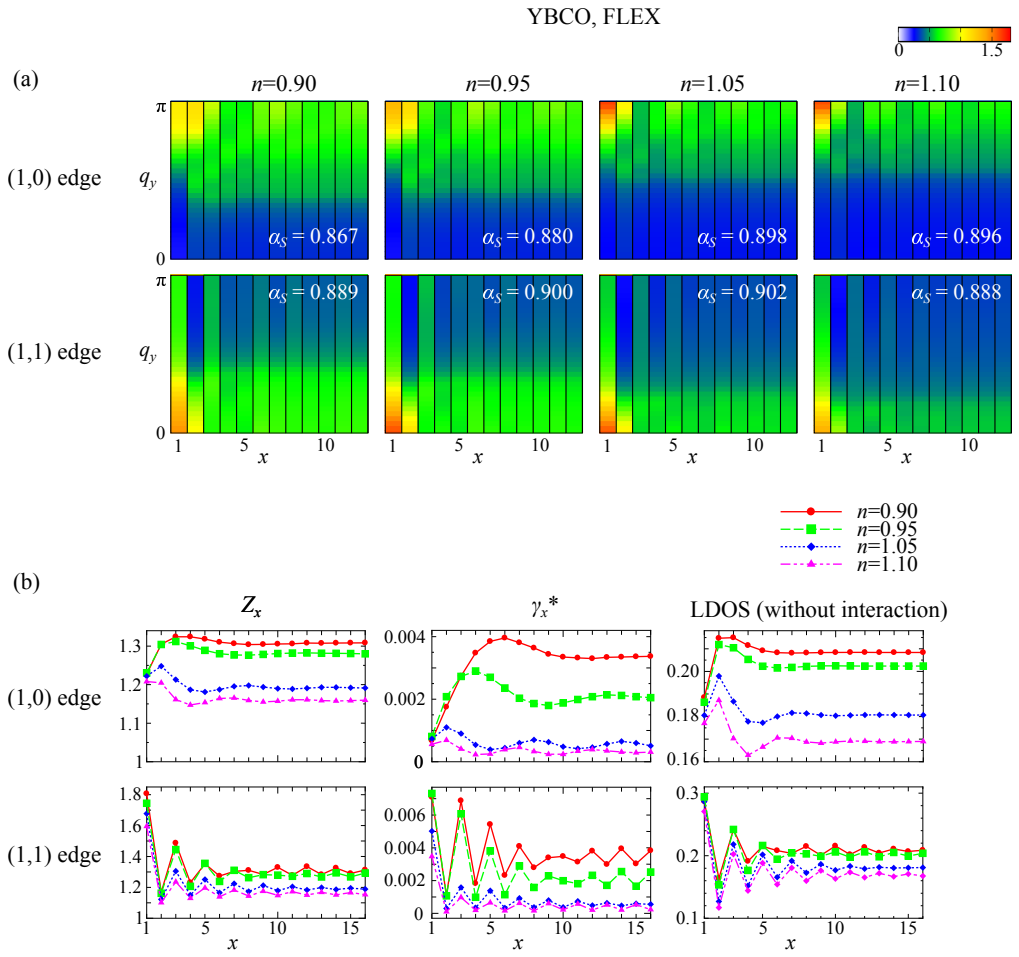

Figure 50: (a) Obtained $\chi^s_{x,x}(q_y)$ in YBCO TB model with $(1,1)$ open edge and $(1,0)$ open edge, respectively. The results for $n = 0.90$, 0.95, 1.05, and 1.10 are shown. (b) Obtained filling-dependences of the mass-enhancement factor Z_x and quasiparticle damping γ^*_x, and LDOS at the Fermi level $D_x(0)$ in the YBCO TB model ($n = 0.90 \sim 1.10$).

B The origin of the minor peak in the LDOS

In this appendix, we explain the origin of the secondary minor peak of the edge LDOS at $\varepsilon = 0.1$ shown in Fig. 10. For this purpose, we calculate the energy spectra of the d-wave SC cluster model with the $(1,1)$ edge. Figure 51 (a) shows the obtained energy spectra for $\Delta^d = 0.09$ ($\Delta_{\rm max} = 0.158$) We can see the surface ABS as the flat band at Fermi level. Moreover, two isolated curves separated from the bulk band are formed in the range of $3\pi/4 \lesssim k_x \lesssim 5\pi/4$. The LDOS at $y = 1$ ($y = 2$) is exhibited in Figure 51 (b). In layer $y = 1$ ($y = 2$), the minor peak appears at $\varepsilon = 0.1$ ($\varepsilon = -0.1$), which corresponds to the energy of the isolated curve. Therefore, we confirm that the energies of the minor peaks are originated from these finite-energy surface states.

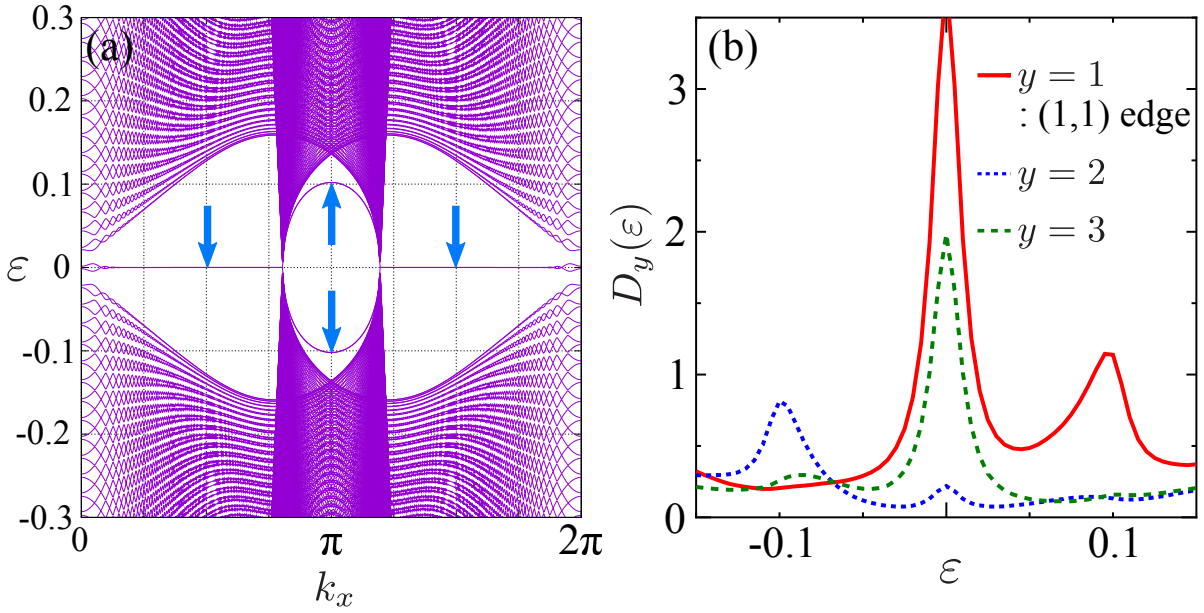

Figure 51: (a)Band structure of the d-wave SC cluster model with the $(1,1)$ edge. The flat dispersion at $\varepsilon = 0$ corresponds to the ABS. There are two surface states separated from the bulk states in the range of $3\pi/4 \lesssim k_x \lesssim 5\pi/4$. These surface states are pointed out by arrows. (b) LDOS near the $(1,1)$ edge in the bulk d-wave SC state. The minor peaks at $\varepsilon = \pm 0.1$ correspond to the edge states in (a).

C Relation between enhanced FM fluctuations and odd-frequency superconductivity

In this Appendix, we consider the detail mechanism of the development of $\hat{\varphi}^0$ near the $(1,1)$. First, we analyze the anomalous Green function, by which $\hat{\varphi}^0$ is composed. Figure 52 (a) shows the ε_n-dependence of $\mathrm{Re}F_{y,y}(\pi/4, \varepsilon_n)$. In the bulk, $\mathrm{Re}F_{y,y}(\pi/4, \varepsilon_n) = 0$ because the d wave gap has a line node in x-direction in the bulk. Interestingly, $\mathrm{Re}F_{1,1}(\pi/4, \varepsilon_n)$ is non-zero, and its frequency-dependence is an odd function. This odd-frequency component can be understood as another physical picture of the ABS as pointed out in Refs. [91,119]. Figure 52 (b) shows the k_x-dependence of $\mathrm{Re}F_{y,y}(k_x, i\pi T)$. At the edge, $\mathrm{Re}F_{1,1}(k_x, i\pi T)$ has peaks at $k_x \approx 4\pi/5$ and $k_x \approx 6\pi/5$, whereas $\mathrm{Re}F_{y,y}(k_x, i\pi T) = 0$ in the bulk. These peaks give rise to the enhancement of $\varphi^0_{1,1}$ at $q_x = 0$ because the convolution integral about F becomes largest for $q_x = 0$ Therefore, we can explain the enhancement of the FM fluctuations as the direct effect of the odd-frequency nature, which is another interpretation of the ABS.

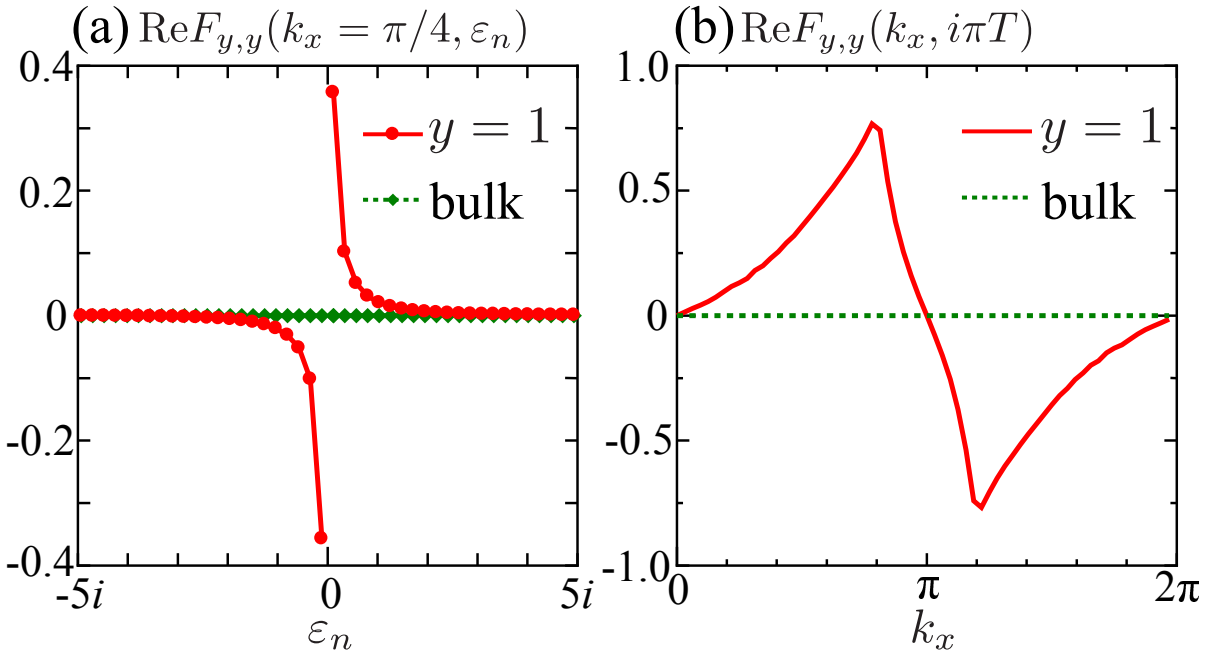

Figure 52: Anomalous Green function calculated for $\Delta_0^d = 0.09$ at $T = 0.0365$. (a) ε_n-dependence of $\mathrm{Re}F_{y,y}(k_x = \pi/4, \varepsilon_n)$. The red and green points represent the component in the edge ($y = 1$) and bulk (periodic system), respectively. (b) k_x-dependence of $\mathrm{Re}F_{y,y}(k_x, i\pi T)$. The red solid line and the green dotted line represents the component in the edge and bulk, respectively.

Next, we explain how the large odd-frequency component emerges near the edge by using the atomic picture, assuming that t is the small parameter. Here, the zeroth-order Green function at the same site i in the normal state is

$$G_{i,i}^0(\varepsilon_n) = \frac{1}{\varepsilon_n - E}, \tag{100}$$

where E is the atomic energy level. The Green function between the nearest neighbor sites i and j is represented by the first-order perturbation of hopping integral t as follows:

$$\begin{aligned} G_{i,j}^0(\varepsilon_n) &= \frac{1}{\varepsilon_n - E} t \frac{1}{\varepsilon_n - E} \\ &= \frac{t}{(\varepsilon_n - E)^2}. \end{aligned} \tag{101}$$

In figure 53, we exhibit the the lowest order contributions to the anomalous Green function $F_{1,2}$ visually. They are represented as follows:

$$\begin{aligned} F_{1,2}(\varepsilon_n) =& - G_{1,1}^0(\varepsilon_n)\Delta_{1,3}^d G_{2,3}^0(-\varepsilon_n) \\ & - G_{1,3}^0(\varepsilon_n)\Delta_{3,2}^d G_{2,2}^0(-\varepsilon_n) \\ =& - \frac{2\Delta_{1,3}^d t\varepsilon_n}{(E^2 - \varepsilon_n^2)^2}. \end{aligned} \tag{102}$$

In the second equal sign, we use $\Delta^d_{1,3} = -\Delta^d_{3,2}$. The obtained $F_{1,2}(\varepsilon_n)$ is proportional to ε_n, and therefore the odd-frequency component emerges at the edge of d-wave superconductor. In contrast, F is absent in the bulk due to the perfect cancellation of contributions via site 4 and those via site 3.

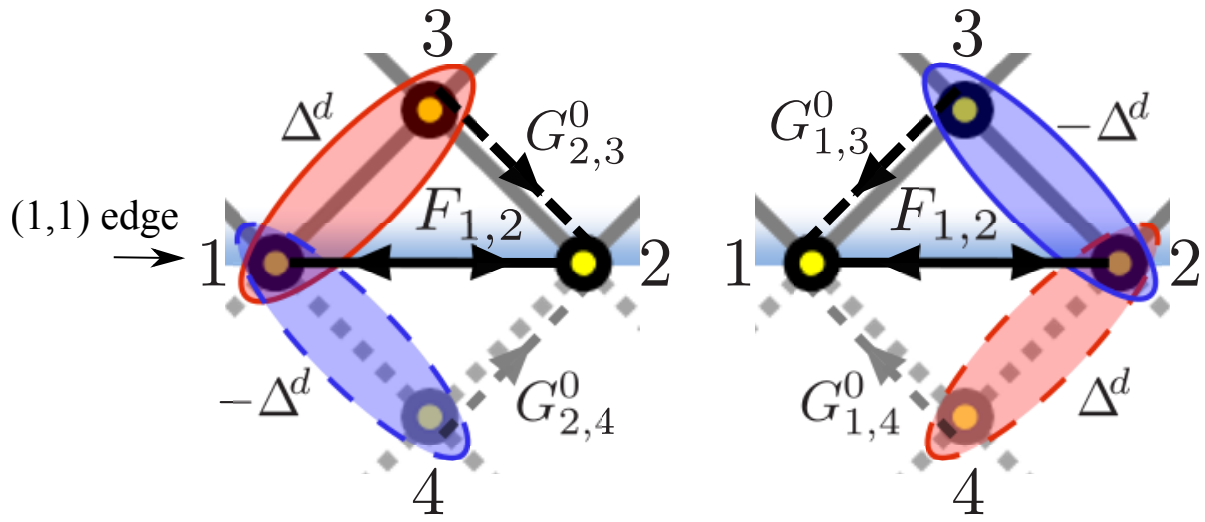

Figure 53: Contributions to the anomalous Green function at the $(1,1)$ edge, $F_{1,2}$. The solid line with two arrows represents $F_{1,2}$. The red and blue circles show the d-wave SC gap between the nearest neighbor sites. The dotted line with an arrow is the Green function in the normal state, G^0. At the edge, $F_{1,2}$ is finite because the contributions through site 4 are dropped.

D LDOS in the $d \pm ip$-wave SC state

In this Appendix, we calculate the LDOS in the $d+ip$-wave SC state. For simplicity, we can set the d-vector of the p-wave gap as z-direction, because we ignore the spin-orbit interaction in this study. We use the p-wave gap obtained by the numerical analysis. In the numerical calculation, we use the p-wave gap obtained as the solution of the linearized gap equation. The LDOS is obtained by Green function as follows:

$$D_y(\epsilon) = \frac{1}{\pi} \sum_{k_x,\sigma} \mathrm{Im} \mathcal{G}^{\sigma,\sigma}_{y,y}(k_x, \epsilon - i\delta). \tag{103}$$

We set $\delta = 0.01$ in the numerical calculation.

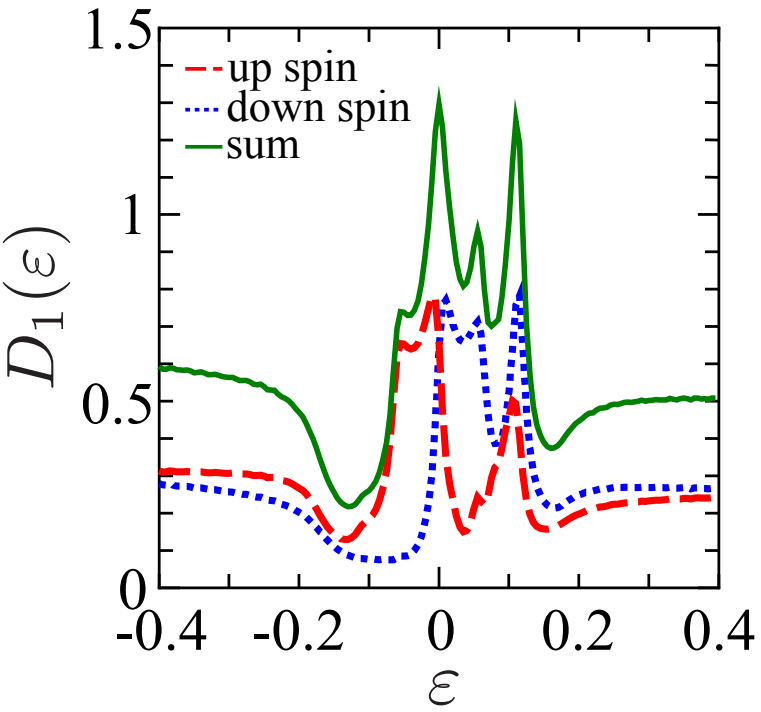

Figure 54: ε-dependence of the LDOS at the $(1,1)$ edge in the $d+ip$-wave SC state. We set $\Delta_0 = 0.09$ and $\max_{i,j}|\phi_{i,j}| = 0.05$. The red dashed line and blue doted line represent the LDOS for up and down spin, respectively. The green solid line is the sum of spins.

Figure 54 shows the obtained LDOS at the edge. The emergence of edge p-wave SC makes a difference between up and down spins in the LDOS because the $d \pm ip$-wave SC state breaks the time-reversal symmetry.

E k_x-dependence of $s^{\rm odd}$ gap

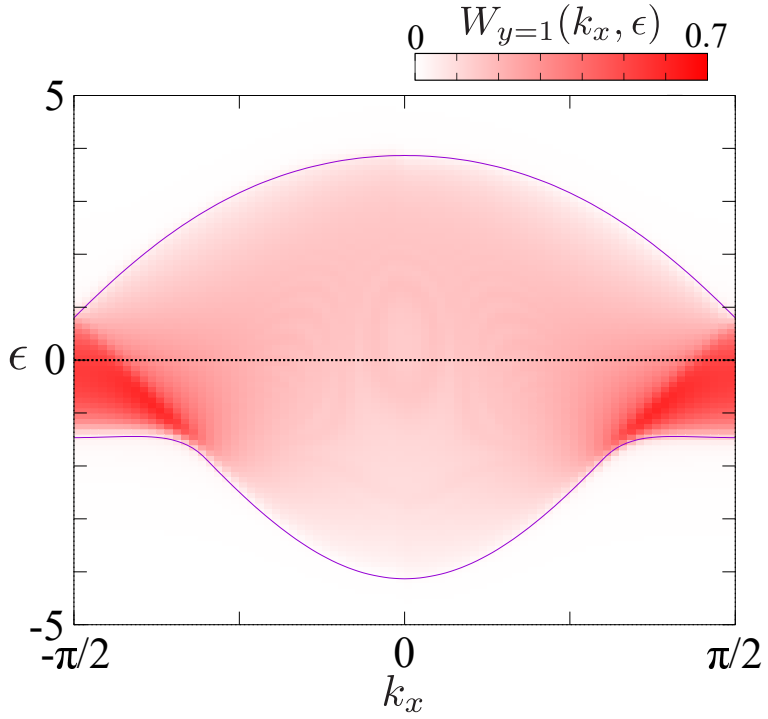

Figure 55: Weight of the edge layer state in the normal state; $W_{y=1}(k_x,\epsilon)$.

In this Appendix, we explain the reason for the obtained k_x-dependence of s^{odd} wave gap. To explain this, we calculate the weight of the edge layer state $W_{y=1}(k_x,\epsilon)$ in the whole band of the present cluster tight-binding model without Δ^d. We evaluate it by $W_y(k_x,\epsilon) = \sum_b \delta(E_{b,k_x}-\epsilon)|U(y,b,k_x)|^2$, where E_{b,k_x} is the b-th band energy at k_x measured from μ and $U(y,b,k_x)$ is the Unitary matrix. Note that $W_y(k_x,\epsilon)$ is associated with the LDOS $D_y(\epsilon)$ by the relation $D_y(\epsilon) = \sum_{k_x} W_y(k_x,\epsilon)$. Figure 55 shows the obtained weight of the edge layer state ($y=1$). Because the edge weight is large for $|k_x| \sim \pi/2$, the magnitude of the $s^{\rm odd}$ wave gap function in Fig. 2 (a) is large for $|k_x| \sim \pi/2$.

F Analysis by modified FLEX approximation

In section 6, site-dependent pairing interaction $V_{y,y'}(k_x, i\omega_n)$ is obtained by using the site-dependent RPA theory. In this Appendix, we estimate $V_{y,y'}(k_x, i\omega_n)$ using the modified FLEX approximation, and solve the linearized triplet gap equation to study the effect of the self-energy effect We set $U = 2.8$ in this Appendix.

Figures 56 (a) and (b) represent the q_x- and ω_n-dependences of the obtained odd-frequency $s^{\rm odd}$ wave gap at $T = 0.05$, respectively. Due to the self-energy in the FLEX approximation,

the d wave gap is renormalized as $\Delta_0^{d*} = 0.17$ (0.14) for $\Delta_0^d = 0.24$ (0.20). We obtain the similar result to those in Fig. 30 (a) and (b) based on the RPA without self-energy effect.

Figures 56 (c) and (d) exhibit the obtained spin Stoner factor α_S and the eigenvalue $\lambda^{\rm edge}$ as functions of T, respectively. Without bulk d-wave gap ($\Delta_0^{d*} = 0$), α_S exhibits moderate increase at low temperatures. In contrast, $\lambda^{\rm edge}$ decreases at low T because the pairing interaction for the odd-frequency SC gap is proportional to $T\chi^s(\boldsymbol{q}_x, 0)$. On the other hand, in the presence of the d wave gap Δ_0^{d*}, α_S rapidly increases due to the huge zero-energy surface-Andreev-bound-state (SABS) peak. Therefore, $\lambda^{\rm edge}$ rapidly increases owing to the SABS-induced magnetic criticality [133]. These results are also similar to those in Fig. 30 (c) and (d) in the main text. Thus, we conclude that the SABS-driven odd-frequency SC state is naturally induced at the edge of d wave superconductors, even if the negative feedback effect of the self-energy is taken into consideration by using the modified FLEX theory.

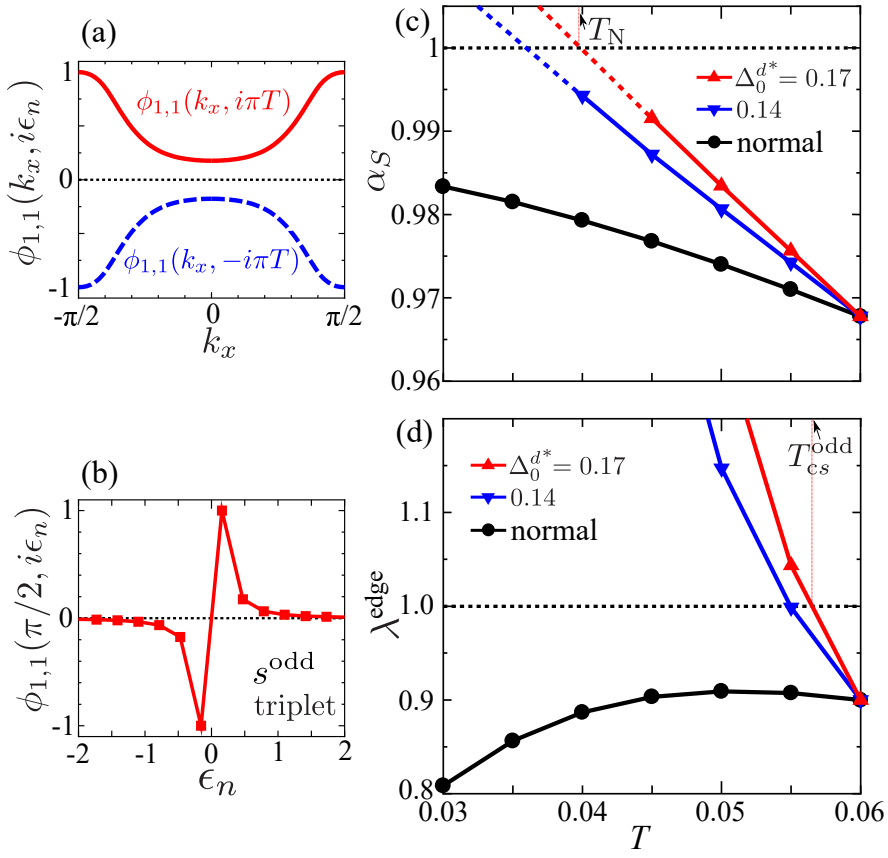

Figure 56: Odd-frequency gap functions obtained by the modified FLEX theory for $U = 2.8$. (a)(b) Obtained $s^{\rm odd}$ wave triplet gap at edge: (a) $\phi_{1,1}(k_x, \pm i\pi T)$ and (b) $\phi_{1,1}(k_x = \pi/2, i\epsilon_n)$ in case of $\Delta_0^{d*} = 0.17$ at $T = 0.05$. (c)(d) T-dependences of (c) the Stoner factor α_S and (d) the eigenvalue $\lambda^{\rm edge}$ for the $s^{\rm odd}$ wave state. Here, the bulk d wave SC gap appears at $T_{cd} = 0.06$. $2\Delta_0^{d*}/T_{cd} = 4.7$ and 5.6 for $\Delta_0^{d*} = 0.14$ and 0.17, respectively. The edge $s^{\rm odd}$ wave gap is obtained for $\alpha_S \gtrsim 0.968$ at $T = T_{cd}$.

References

[1] N. E. Bickers and S. R. White, Phys. Rev. B **43** 8044 (1991).

[2] P. Monthoux and D. J. Scalapino, Phys. Rev. Lett. **72** 1874 (1994).

[3] S. Koikegami, S. Fujimoto, and K. Yamada, J. Phy. Soc. Jpn. **66** 1438 (1997).

[4] T. Takimoto and T. Moriya, J. Phy. Soc. Jpn. **66** 2459 (1997).

[5] T. Dahm, D. Manske, and L. Tewordt, Europhys. Lett. **55** 93 (2001).

[6] D. Manske, I. Eremin, and K. H. Bennemann, Phys. Rev. B **67** 134520 (2003).

[7] T. Yoshida, X. J. Zhou, T. Sasagawa, W. L. Yang, P. V. Bogdanov, A. Lanzara, Z. Hussain, T. Mizokawa, A. Fujimori, H. Eisaki, Z.-X. Shen, T. Kakeshita, and S. Uchida, Phys. Rev. Lett. 91, 027001 (2003).

[8] T. Yoshida, M. Hashimoto, I. M. Vishik, Z.-X. Shen, and A. Fujimori, J. Phys. Soc. Jpn. 81, 011006 (2012).

[9] A. Kanigel, M. R. Norman, M. Randeria, U. Chatterjee, S. Souma, A. Kaminski, H. M. Fretwell, S. Rosenkranz, M. Shi, T. Sato, T. Takahashi, Z. Z. Li, H. Raffy, K. Kadowaki, D. Hinks, L. Ozyuzer, and J. C. Campuzano, Nat. Phys. 2, 447 (2006).

[10] T. Kondo, Y. Hamaya, A. D. Palczewski, T. Takeuchi, J. S. Wen, Z. J. Xu, G. Gu, J. Schmalian, and A. Kaminski, Nat. Phys. 7, 21 (2011).

[11] T. Moriya and K. Ueda, Rep. Prog. Phys. **66** 1299 (2003).

[12] T. Moriya and K. Ueda: Adv. Phys. **49** (2000) 555.

[13] P. Monthoux and D. Pines: Phys. Rev. B **47** (1993) 6069.

[14] H. Kontani, Rep. Prog. Phys. **71** (2008) 026501.

[15] H. Kontani, K. Kanki, and K. Ueda, Phys. Rev. B **59** 14723 (1999).

[16] H. Kontani, J. Phys. Soc.Jpn, **70** 2840 (2001); H. Kontani, Phys. Rev. Lett. **89** 237003 (2002).

[17] H. Kontani, Phys. Rev. B. **64** 054413 (2001).

[18] G. Ghiringhelli, M. L. Tacon, M. Minola, S. Blanco-Canosa, C. Mazzoli, N. B. Brookes, G. M. D. Luca, A. Frano, D. G. Hawthorn, F. He, T. Loew, M. M. Sala, D. C. Peets, M. Salluzzo, E. Schierle, R. Sutarto, G. A. Sawatzky, E. Weschke, B. Keimer, and L. Braicovich, Science **337**, 821 (2012).

[19] J. Chang, E. Blackburn, A. T. Holmes, N. B. Christensen, J. Larsen, J. Mesot, R. Liang, D. A. Bonn, W. N. Hardy, A. Watenphul, M. von Zimmermann, E. M. Forgan, and S. M. Hayden, Nat. Phys. **8**, 871 (2012).

[20] K. Fujita, M. H. Hamidian, S. D. Edkins, C. K. Kim, Y. Kohsaka, M. Azuma, M. Takano, H. Takagi, H. Eisaki, S. Uchida, A. Allais, M. J. Lawler, E. A. Kim, S. Sachdev, and J. C. Davis, Proc. Natl. Acad. Sci. U.S.A. **111**, E3026 (2014).

[21] Y. Sato, S. Kasahara, H. Murayama, Y. Kasahara, E.-G. Moon, T. Nishizaki, T. Loew, J. Porras, B. Keimer, T. Shibauchi, and Y. Matsuda, Nat. Phys. **13**, 1074 (2017).

[22] S. Onari and H. Kontani, Phys. Rev. Lett. **109**, 137001 (2012).

[23] M. Tsuchiizu, Y. Ohno, S. Onari, and H. Kontani, Phys. Rev. Lett. **111**, 057003 (2013).

[24] M. Tsuchiizu, Y. Yamakawa, and H. Kontani, Phys. Rev. B **93**, 155148 (2016).

[25] M.A. Metlitski and S. Sachdev, New J. Phys. **12**, 105007 (2010); S. Sachdev and R. La Placa, Phys. Rev. Lett. **111**, 027202 (2013).

[26] C. Husemann and W. Metzner, Phys. Rev. B **86**, 085113 (2012); T. Holder and W. Metzner, Phys. Rev. B **85**, 165130 (2012).

[27] Y. Wang and A.V. Chubukov, Phys. Rev. B **90**, 035149 (2014).

[28] J. C. S. Davis and D.-H. Lee, Proc. Natl. Acad. Sci. USA, **110**, 17623 (2013).

[29] E. Berg, E. Fradkin, S. A. Kivelson, and J. M. Tranquada, New J. Phys. **11**, 115004 (2009)

[30] S. Onari, Y. Yamakawa and H. Kontani, Rev. Lett. **116**, 227001 (2016).

[31] Y. Yamakawa, S. Onari and H. Kontani, Phys. Rev. X **6**, 021032 (2016).

[32] Y. Yamakawa and H. Kontani, Phys. Rev. Lett. **114**, 257001 (2015).

[33] K. Kawaguchi, Y. Yamakawa, M. Tsuchiizu, and H. Kontani, J. Phys. Soc. Jpn. **86**, 063707 (2017).

[34] Y. Kamihara, T. Watanabe, M. Hirano, and H. Hosono, J. Am. Chem. Soc. **130**, 3296 (2008).

[35] T. Iye, Y. Nakai, S. Kitagawa, K. Ishida, S. Kasahara, T. Shibauchi, Y. Matsuda, and T Terashima, J. Phys. Soc. Jpn. **81**, 033701 (2012).

[36] M. Hiraishi, S. Iimura, K. M. Kojima, J. Yamaura, H. Hiraka, K. Ikeda, P. Miao, Y. Ishikawa, S. Torii, M. Miyazaki, I. Yamauchi, A. Koda, K. Ishii, M. Yoshida, J. Mizuki, R. Kadono, R. Kumai, T. Kamiyama, T. Otomo, Y. Murakami, S. Matsuishi and H. Hosono, Nature Phys. **10**, 300 (2014).

[37] J.-H. Chu, J. G. Analytis, C. Kucharczyk, and I. R. Fisher, Phys. Rev. B **79**, 014506 (2009).

[38] A. F. Wang, X. G. Luo, Y. J. Yan, J. J. Ying, Z. J. Xiang, G. J. Ye, P. Cheng, Z. Y. Li, W. J. Hu, and X. H. Chen, Phys. Rev. B **85**, 224521 (2012).

[39] M. D. Watson, T. K. Kim, A. A. Haghighirad, S. F. Blake, N. R. Davies, M. Hoesch, T. Wolf, and A. I. Coldea, Phys. Rev. B **92**, 121108(R) (2015)

[40] K. Kuroki, S. Onari, R. Arita, H. Usui, Y. Tanaka, H. Kontani, and H. Aoki, Phys. Rev. Lett. **101**, 087004 (2008).

[41] I. I. Mazin, D. J. Singh, M. D. Johannes, and M. H. Du, Phys. Rev. Lett. **101**, 057003 (2008).

[42] A. V. Chubukov, D. V. Efremov, and I. Eremin, Phys. Rev. B **78**, 134512 (2008).

[43] S. Graser, G. R. Boyd, C. Cao, H.-P. Cheng, P. J. Hirschfeld, and D. J. Scalapino, Phys. Rev. B **77**, 180514(R) (2008).

[44] H. Kontani and S. Onari, Phys. Rev. Lett. **104**, 157001 (2010).

[45] P. Mendels, J. Bobroff, G. Collin, H. Alloul, M. Gabay, J.F. Marucco, N. Blanchard and B. Grenier: Europhys. Lett. **46** (1999) 678.

[46] J. Bobroff, W. A. MacFarlane, H. Alloul, P. Mendels, N. Blanchard, G. Collin, aPhys. Rev. Lett. **83** (1999) 4381.

[47] K. Ishida, Y. Kitaoka, K. Yamazoe, K. Asayama, and Y. Yamada: Phys. Rev. Lett. **76** (1996) 531.

[48] A. V. Mahajan, H. Alloul, G. Collin, and J. F. Marucco: Phys. Rev. Lett. **72** (1994) 3100.

[49] W. A. MacFarlane, J. Bobroff, H. Alloul, P. Mendels, N. Blanchard, G. Collin, and J.-F. Marucco: Phys. Rev. Lett. **85** (2000) 1108.

[50] A. V. Mahajan, H. Alloul, G. Collin, J. F.Marucco, Eur. Phys. J. **B** 13 (2000) 457.

[51] T. Kimura, S. Miyasaka, H. Takagi, K. Tamasaku, H. Eisaki, S. Uchida, K. Kitazawa, M. Hiroi, M. Sera, and N. Kobayashi: Phys. Rev. B **53** (1996) 8733.

[52] D.Jaccard, E. Vargoz, K. Alami-Yadri, H. Wilhelm: Rev. High Pressure Sci. Technol. **7**, 412 (1998).

[53] J. Flouquet, P. Haen, F. Lapierre, C. Fierz, A. Amato and D. Jaccard: J. Magn. Magn. Mat. **76&77** (1988) 285.

[54] H. Kontani and M. Ohno, Phys. Rev. B **74**, 014406 (2006); H. Kontani and M. Ohno, J. Magn. Magn. Mat. **310**, 483 (2007).

[55] W. Ziegler, D. Poilblanc, R. Preuss, W. Hanke, and D. J. Scalapino: Phys. Rev. B **53** (1996) 8704

[56] D. Poilblanc, D.J. Scalapino, and W. Hanke: Phys. Rev. Lett. **72** (1994) 884.

[57] N. Bulut, D. Hone, D.J. Scalapino, and E.Y. Loh: Phys. Rev. Lett. **62** (1989) 2192.

[58] A.W. Sandvik, E. Dagotto, and D.J. Scalapino: Phys. Rev. B **56** (1997) 11701.

[59] N. Bulut: Physica C **363** (2001) 260.

[60] N. Bulut: Phys. Rev. B **61** (2000) 9051.

[61] Y. Ohashi: J. Phys. Soc. Jpn. **70** (2001) 2054.

[62] M.Fujita, K.Wakabayashi, K.Nakada, and K.Kusakabe, J. Phys. Soc. Jpn. **65** (1996) 1920

[63] H. Kumazaki and D. S. Hirashima, J. Phys. Soc. Jpn. **76**, 064713 (2007).

[64] C. R. Hu, Phys. Rev. Lett. **72**, 1526 (1994).

[65] Y. Tanaka and S. Kashiwaya, Phys. Rev. Lett. **74**, 3451 (1995).

[66] S. Kashiwaya, Y. Tanaka, M. Koyanagi, K. Kajimura, Phys. Rev. B **53**, 2667 (1996).

[67] M. Matsumoto and H. Shiba, J. Phys. Soc. Jpn. **64**, 1703 (1995).

[68] Y. Nagato and K. Nagai, Phys. Rev. B **51**, 16254 (1995).

[69] S. Kashiwaya and Y. Tanaka, Rep. Prog. Phys. **63**, 1641 (2000).

[70] M. Sato, Y. Tanaka, K. Yada, and T. Yokoyama, Phys. Rev. B **83**, 224511 (2011).

[71] S. Kashiwaya, Y. Tanaka, M. Koyanagi, H. Takashima, and K. Kajimura, Phys. Rev. B **51**, 1350 (1995).

[72] I. Iguchi, W. Wang, M. Yamazaki, Y. Tanaka, and S. Kashiwaya, Phys. Rev. B **62**, R6131 (2000).

[73] J. Y. T. Wei, N. -C. Yeh, D. F. Garrigus, and M. Strasik, Phys. Rev. Lett. **81**, 2542 (1998).

[74] J. Geerk, X. X. Xi, and G. Linker, Z. Phys. B **73**, 2542 (1988).

[75] L. Alff, H. Takashima, S. Kashiwaya, N. Terada, H. Ihara, Y. Tanaka, M. Koyanagi, and K. Kajimura, Phys. Rev. B **55**, R14757 (1997).

[76] M. Matsumoto and H. Shiba, J. Phys. Soc. Jpn. **64**, 3384 (1995).

[77] M. Matsumoto and H. Shiba, J. Phys. Soc. Jpn. **64**, 4867 (1995).

[78] M. Matsumoto and H. Shiba, J. Phys. Soc. Jpn. **65**, 2194 (1995).

[79] K. Kuboki and M. Sigrist, J. Phys. Soc. Jpn. **67**, 2873 (1998).

[80] T. Watashige, Y. Tsutsumi, T. Hanaguri, Y. Kohsaka, S. Kasahara, A. Furusaki, M. Sigrist, C. Meingast, T. Wolf, H. v. Löhneysen, T. Shibauchi, and Y. Matsuda, Phys. Rev. X **5** 031022 (2015).

[81] D. J. Scalapino, E. Loh, Jr., and J. E. Hirsch Phys. Rev. B **34**, 8190(R) (1986).

[82] D. Fay and J. Appel, Phys. Rev. B **22**, 3173 (1980).

[83] P. Monthoux and G. G. Lonzarich,Phys. Rev. B **59**, 14598 (1999).

[84] Z. Wang, W. Mao, and K. Bedell, Phys. Rev. Lett. **87**, 257001 (2001).

[85] R. Roussev and A. J. Millis, Phys. Rev. B **63**, 140504(R) (2001).

[86] S. Fujimoto, J. Phys. Soc. Jpn. **73**, 2061 (2004).

[87] V. L. Berezinskii, JETP Lett. **20**, 287 (1974).

[88] T. R. Kirkpatrick and D. Belitz, Phys. Rev. Lett. **66**, 1533 (1991); D. Belitz and T. R. Kirkpatrick, Phys. Rev. B **60**, 3485 (1999).

[89] E. Abrahams, A. Balatsky, D. J. Scalapino, and J. R. Schrieffer, Phys. Rev. B **52**, 1271 (1995).

[90] P. Coleman, E. Miranda and A. Tsvelik, Phys. Rev. Lett. **70**, 2960 (1993).

[91] Y. Tanaka, M. Sato, and N. Nagaosa, J. Phys. Soc. Jpn. **81**, 011013 (2012).

[92] J. Linder and A. V. Balatsky, Rev. Mod. Phys. **91**, 045005 (2019).

[93] M. Matsumoto, M. Koga, and H. Kusunose, J. Phys. Soc. Jpn. **82**, 034708 (2013).

[94] Y. V. Fominov, Y. Tanaka, Y. Asano, and M.Eschrig, Phys. Rev. B **91**, 144514 (2015).

[95] S. Hoshino, K. Yada, and Y. Tanaka, Phys. Rev. B **93**, 224511 (2016).

[96] Y. Fuseya, H. Kohno, and K. Miyake, J. Phys. Soc. Jpn. **72**, 2914 (2003).

[97] D. Solenov, I. Martin, and D. Mozyrsky, Phys. Rev. B **79**, 132502 (2009).

[98] H. Kusunose, Y. Fuseya, and K. Miyake, J. Phys. Soc. Jpn. **80**, 054702 (2011).

[99] H. Kusunose, M. Matsumoto, and M. Koga, Phys. Rev. B **85**, 174528 (2012).

[100] N. Bulut, D. J. Scalapino and S. R. White, Phys. Rev. B **47** 14599 (1993).

[101] M. Vojta and E. Dagotto, Phys. Rev. B **59**, R713 (1999).

[102] T. Hotta, J. Phys. Soc. Jpn. **78**, 123710 (2009).

[103] K. Shigeta, S. Onari, K. Yada and Y. Tanaka, Phys. Rev. B **79**, 174507 (2009).

[104] Y. Yanagi, Y. Yamashita, and K. Ueda, J. Phys. Soc. Jpn. **81**, (2012) 123701.

[105] R. Heid, Z. Phys. B Condens. Matter **99**, 15 (1995).

[106] S. Hoshino, Phys. Rev. B **90**, 115154 (2014).

[107] F. S. Bergeret, A. F. Volkov, and K. B. Efetov, Phys. Rev. Lett. **86**, 4096 (2001); F. S. Bergeret, A. F. Volkov, and K. B. Efetov Phys. Rev. B **64**, 134506 (2001).

[108] F. S. Bergeret, A. F. Volkov, and K. B. Efetov, Rev. Mod. Phys. **77**, 1321 (2005).

[109] A. A. Golubov, Ya. V. Fominov, N. M. Chtchelkatchev, and A. A. Golubov Phys. Rev. B **66**, 014507 (2002).

[110] T. Yokoyama, Y. Tanaka, and A. A. Golubov Phys. Rev. B **75**, 134510 (2007).

[111] A. I. Buzdin, Rev. Mod. Phys. **77**, 935 (2005).

[112] A. I. Buzdin, A. S. Mel ' nikov, and N. G. Pugach Phys. Rev. B **83**, 144515 (2011).

[113] S. Mironov, A. Mel ' nikov, and A. Buzdin Phys. Rev. Lett. **109**, 237002 (2012).

[114] Jacob Linder, Takehito Yokoyama, Asle Sudbø, and Matthias Eschrig Phys. Rev. Lett. **102**, 107008 (2009).

[115] Mohammad Alidoust, Klaus Halterman, and Jacob Linder Phys. Rev. B **89**, 054508 (2014).

[116] M. Eschrig, J. Kopu, J. C. Cuevas, and G. Sch¨ on, Phys. Rev. Lett. 90, 137003 (2003).

[117] Y. Asano, Y. Tanaka, and A. A. Golubov, Phys. Rev. Lett. **98**, 107002 (2007).

[118] Cayao, C. Triola, and A. M. Black-Schaffer, Eur. Phys. J. Special Topics **229**, 545 (2020).

[119] Y. Tanaka and A. A. Golubov, Phys. Rev. Lett. **98**, 037003 (2007).

[120] S. Tamura, S. Hoshino, and Y. Tanaka, Phys. Rev. B **99**, 184512 (2019).

[121] Y. Tanaka, A. A. Golubov, S. Kashiwaya, and M. Ueda. Phys. Rev. Lett. **99**, 037005 (2007).

[122] Y. Tanaka, Y. Tanuma, and A. A. Golubov. Phys. Rev. B **76**, 054522 (2007).

[123] Y. Tanaka and S. Kashiwaya: Phys. Rev. B **70** 012507 (2004).

[124] S. Higashitani, Y. Nagato, and K. Nagai, Journal of Low Temperature Physics 155, 83 (2009).

[125] S. Higashitani: J. Phys. Soc. Jpn. **66** 2556 (1997).

[126] Y. Tanaka, Y. Asano, A. Golubov, and S. Kashiwaya: Phys. Rev. B **72** 140503(R) (2005).

[127] S. Suzuki and Y. Asano, Phys. Rev. B **89**, 184508 (2014).

[128] S. Suzuki and Y. Asano, Phys. Rev. B **91**, 214510 (2015).

[129] A. Di Bernardo, Z. Salman, X. L. Wang, M. Amado, M. Egilmez, M. G. Flokstra, A. Suter, S. L. Lee, J. H. Zhao, T. Prokscha, E. Morenzoni, M. G. Blamire, J. Linder, and J. W. A. Robinson, Phys. Rev. X 5, 041021 (2015).

[130] J. A. Krieger, A. Pertsova, S. R. Giblin, M. Döbeli, T. Prokscha, C. W. Schneider, A. Suter, T. Hesjedal, A. V. Balatsky, and Z. Salman, Phys. Rev. Lett. 125, 026802 (2020).

[131] S. Matsubara, Y. Yamakawa, and H. Kontani, J. Phys. Soc. Jpn. **87**, 073705 (2018).

[132] S. Matsubara and H. Kontani, Phys. Rev. B **101**, 075114 (2020).

[133] S. Matsubara and H. Kontani, Phys. Rev. B **101**, 235103 (2020).

[134] Y. Matsuda, T. Hirai, S. Komiyama, T. Terashima, Y. Bando, K. Iijima, K. Yamamoto, and K. Hirata Phys. Rev. B **40**, 5176 (1989).

[135] K. Semba, A. Matsuda, and T. Ishii Phys. Rev. B **49**, 10043 (1994).

[136] K. Tomimoto, I. Terasaki, and A. I. Rykov, T. Mimura, and S. Tajima Phys. Rev. B **60**, 114 (1999).

[137] F. Izumi, H. Asano, T. Ishigaki, A. Ono, and F. P. Okamura Jpn. J. Appl. Phys. **26**, L611 (1987).

[138] D. S. Inosov, J. T. Park, A. Charnukha, Yuan Li, A. V. Boris, B. Keimer, and V. Hinkov Phys. Rev. B **83**, 214520 (2011).

[139] Øystein Fischer, Martin Kugler, Ivan Maggio-Aprile, Christophe Berthod, and Christoph Renner Rev. Mod. Phys. **79**, 353 (2007).

[140] J. W. Harter, B. M. Andersen, J. Bobroff, M. Gabay, and P. J. Hirschfeld Phys. Rev. B **75**, 054520 (2007).

[141] Brian M. Andersen, Ashot Melikyan, Tamara S. Nunner, and P. J. Hirschfeld Phys. Rev. Lett. **96**, 097004 (2006).

[142] S. Kashiwaya, Y. Tanaka, M. Koyanagi, H. Takashima, and K. Kajimura, J. Phys. Chem. Solids **56**, 1721 (1995).

[143] Y. Tanuma, Y. Tanaka, M. Ogata, and S. Kashiwaya, Phys. Rev. B **60**, 9817 (1999).

[144] Y. Tanaka, Y. Tanuma, and S. Kashiwaya, Phys. Rev. B **64**, 054510 (2001).

[145] Y. Tanuma, Y. Tanaka, and S. Kashiwaya, Phys. Rev. B **64**, 214519 (2001).

[146] K. Kuboki and M. Sigrist, J. Phys. Soc. Jpn. **65**, 361 (1995).

[147] K. Kuboki and M. Sigrist, J. Phys. Soc. Jpn. **67**, 2873 (1998).

[148] M. Hakansson, T. Löfwander, and M. Fogelström, Nat. Phys. **11**, 755 (2015).

[149] P. Holmvall, A.B. Vorontsov, M. Fogelström, and T. Löfwander, Nat. Commun. **9**, 2190 (2018).

[150] A. C. Durst and P. A. Lee Phys. Rev. B **62**, 1270 (2000).

[151] A. Y. Kitaev, Phys. Usp. **44**, 131 (2001).

[152] S. Nakosai, Y. Tanaka, and N. Nagaosa, Phys. Rev. B **88**, 180503 (2013).

[153] W. Chen and A. P. Schnyder Phys. Rev. B **92**, 214502 (2015).

[154] Y. Chen and C. S. Ting, Phys. Rev. Lett. **92**, 077203 (2004).

[155] H. Kashiwaya, S. Kashiwaya, B. Prijamboedi, A. Sawa, I. Kurosawa, Y. Tanaka, and I. Iguchi Phys. Rev. B 70, 094501 (2004)

[156] S. Bouscher, Z. Kang, K. Balasubramanian, D. Panna, P. Yu, X. Chen, and A. Hayat, 32, 475502 (2020).

[157] H. Saadaoui, Z. Salman, T. Prokscha, A. Suter, H. Huhtinen, P. Paturi, and E. Morenzoni, Phys. Rev. B **88**, 180501(R) (2013).

[158] M. Yi, D. Lu, J.-H. Chu, J. G. Analytis, A. P. Sorini, A. F. Kemper, B. Moritz, S.-K. Mo, R. G. Moore, M. Hashimoto, W.-S. Lee, Z. Hussain, T. P. Devereaux, I. R. Fisher, and Z.-X. Shen, Proc. Natl. Acad. Sci. U.S.A. **108**, 6878 (2011).

[159] J. Maletz, V. B. Zabolotnyy, D. V. Evtushinsky, S. Thirupathaiah, A. U. B. Wolter, L. Harnagea, A. N. Yaresko, A. N. Vasiliev, D. A. Chareev, A. E. Böhmer, F. Hardy, T. Wolf, C. Meingast, E. D. L. Rienks, B. Büchner, and S. V. Borisenko, Phys. Rev. B **89**, 220506(R) (2014).

[160] K. Nakayama, Y. Miyata, G. N. Phan, T. Sato, Y. Tanabe, T. Urata, K. Tanigaki, and T. Takahashi, Phys. Rev. Lett. **113**, 237001 (2014).

[161] M. D. Watson, T. K. Kim, A. A. Haghighirad, N. R. Davies, A. McCollam, A. Narayanan, S. F. Blake, Y. L. Chen, S. Ghannadzadeh, A. J. Schofield, M. Hoesch, C. Meingast, T. Wolf, and A. I. Coldea, Phys. Rev. B **91**, 155106 (2015).

[162] T. Shimojima, Y. Suzuki, T. Sonobe, A. Nakamura, M. Sakano, J. Omachi, K. Yoshioka, M. Kuwata-Gonokami, K. Ono, H. Kumigashira, A. E. Böhmer, F. Hardy, T. Wolf, C. Meingast, H. v. Löhneysen, H. Ikeda, and K. Ishizaka, Phys. Rev. B **90**, 121111(R) (2014).

[163] P. Zhang, T. Qian, P. Richard, X. P. Wang, H. Miao, B. Q. Lv, B. B. Fu, T. Wolf, C. Meingast, X. X. Wu, Z. Q. Wang, J. P. Hu, and H. Ding, Phys. Rev. B **91**, 214503 (2015).

[164] Y. Zhang, M. Yi, Z.-K. Liu, W. Li, J. J. Lee, R. G. Moore, M. Hashimoto, M. Nakajima, H. Eisaki, S.-K. Mo, Z. Hussain, T. P. Devereaux, Z.-X. Shen, and D. H. Lu Phys. Rev. B **94**, 115153 (2016).

[165] Y. Suzuki, T. Shimojima, T. Sonobe, A. Nakamura, M. Sakano, H. Tsuji, J. Omachi, K. Yoshioka, M. Kuwata-Gonokami, T. Watashige, R. Kobayashi, S. Kasahara, T. Shibauchi, Y. Matsuda, Y. Yamakawa, H. Kontani, and K. Ishizaka, Phys. Rev. B **92**, 205117 (2015).

[166] M. D. Watson, T. K. Kim, A. A. Haghighirad, S. F. Blake, N. R. Davies, M. Hoesch, T. Wolf, and A. I. Coldea, Phys. Rev. B 92, 121108 (2015).

[167] S. Y. Tan, Y. Fang, D. H. Xie, W. Feng, C. H. P. Wen, Q. Song, Q. Y. Chen, W. Zhang, Y. Zhang, L. Z. Luo, B. P. Xie, X. C. Lai, and D. L. Feng, Phys. Rev. B 93, 104513 (2016).

[168] R. M. Fernandes, L. H. VanBebber, S. Bhattacharya, P. Chandra, V. Keppens, D. Mandrus, M. A. McGuire, B. C. Sales, A. S. Sefat, and J. Schmalian, Phys. Rev. Lett. **105**, 157003 (2010).

[169] M. Yoshizawa, D. Kimura, T. Chiba, S. Simayi, Y. Nakanishi, K. Kihou, C.-H. Lee, A. Iyo, H. Eisaki, M. Nakajima, and S. Uchida, J. Phys. Soc. Jpn. **81**, 024604 (2012).

[170] A. E. Böhmer, P. Burger, F. Hardy, T. Wolf, P. Schweiss, R. Fromknecht, M. Reinecker, W. Schranz, and C. Meingast, Phys. Rev. Lett. **112**, 047001 (2014).

[171] Y. Gallais, R. M. Fernandes, I. Paul, L. Chauviere, Y.-X. Yang, M.-A. Measson, M. Cazayous, A. Sacuto, D. Colson, and A. Forget, Phys. Rev. Lett. **111**, 267001 (2013).

[172] H. Kontani and Y. Yamakawa, Phys. Rev. Lett. **113**, 047001 (2014).

[173] M. Khodas and A. Levchenko, Phys. Rev. B **91**, 235119 (2015).

[174] J.-H. Chu, H.-H. Kuo, J. G. Analytis, and I. R. Fisher, Science **337**, 710 (2012).

[175] R. Yu, Q. Si, D.-H. Lee, Pengcheng Dai, Z.-X. Shen, D.H. Lu, and R.J. Birgeneau Phys. Rev. X **9**, 041049 (2019).

[176] S. S. Huh, J. J. Seo, B. S. Kim, S. H. Cho, J. K. Jung, S. Kim, C. I. Kwon, Jun Sung Kim, Y. Y. Koh, W. S. Kyung, J. D. Denlinger, Y. H. Kim, B. N. Chae, N. D. Kim, Y. K. Kim, and C. Kim, Commun Phys **3**, 52 (2020).

[177] Taichi Terashima, Naoki Kikugawa, Andhika Kiswandhi, Eun-Sang Choi, James S. Brooks, Shigeru Kasahara, Tatsuya Watashige, Hiroaki Ikeda, Takasada Shibauchi, Yuji Matsuda, Thomas Wolf, Anna E. Böhmer, Frédéric Hardy, Christoph Meingast, Hilbert v. Löhneysen, Michi-To Suzuki, Ryotaro Arita, and Shinya Uji, Phys. Rev. B **90**, 144517 (2014).

[178] R. M. Fernandes, L. H. VanBebber, S. Bhattacharya, P. Chandra, V. Keppens, D. Mandrus, M. A. McGuire, B. C. Sales, A. S. Sefat, and J. Schmalian, Phys. Rev. Lett. **105**, 157003 (2010).

[179] F. Wang, S. A. Kivelson, and D.-H. Lee, Nat. Phys. **11**, 959 (2015).

[180] A. V. Chubukov, R. M. Fernandes, and J. Schmalian, Phys. Rev. B **91**, 201105 (2015).

[181] R. Yu and Q. Si, Phys. Rev. Lett. **115**, 116401 (2015).

[182] J. K. Glasbrenner, I. I. Mazin, H. O. Jeschke, P. J. Hirschfeld, and R. Valenti, Nat. Phys. **11**, 953 (2015).

[183] L. Fanfarillo, A. Cortijo, and B. Valenzuela, Phys. Rev. B **91**, 214515 (2015).

[184] F. Krüger, S. Kumar, J. Zaanen, and J. van den Brink, Phys. Rev. B **79**, 054504 (2009).

[185] W. Lv, J. Wu, and P. Phillips, Phys. Rev. B **80**, 224506 (2009).

[186] C.-C. Lee, W.-G. Yin, and W. Ku, Phys. Rev. Lett. **103**, 267001 (2009).

[187] S. Onari, Y. Yamakawa, and H. Kontani, Phys. Rev. Lett. **112**, 187001 (2014).

[188] S. Onari and H. Kontani, in Iron-Based Superconductivity, edited by P. D. Johnson, G. Xu, and W.-G. Yin (SpringerVerlag Berlin, 2015).

[189] K. Jiang, J. P. Hu, H. Ding, and Z. Wang, Phys. Rev. B **93**, 115138 (2016).